AD NUMBER

AD291819

LIMITATION CHANGES

TO:

Approved for public release; distribution is unlimited.

FROM:

**Distribution authorized to U.S. Gov't. agencies and their contractors;
Administrative/Operational Use; OCT 1962. Other requests shall be referred to Aeronautical Systems Division, Wright-Patterson AFB, OH 45433.**

AUTHORITY

AFFDL ltr, Nov 1968

SUPERSONIC TURBULENT BOUNDARY LAYER GROWTH OVER COOLED WALLS IN ADVERSE PRESSURE GRADIENTS

TECHNICAL DOCUMENTARY REPORT NO ASD TDR 62-87

October 1962

Flight Dynamics Laboratory
Aeronautical Systems Division
Air Force Systems Command
Wright-Patterson Air Force Base, Ohio

Project No. 1366, Task No. 136605

(Prepared under Contract No. AF 33(616)-6800
by United Aircraft Corporation
Research Laboratories
East Hartford 8, Connecticut
Author: C. E. Kepler and R. L. O'Brien)

NOTICES

When Government drawings, specifications, or other data are used for any purpose other than in connection with a definitely related Government procurement operation, the United States Government thereby incurs no responsibility nor any obligation whatsoever; and the fact that the Government may have formulated, furnished, or in any way supplied the said drawings, specifications, or other data, is not to be regarded by implication or otherwise as in any manner licensing the holder or any other person or corporation, or conveying any rights or permission to manufacture, use, or sell any patented invention that may in any way be related thereto.

ASTIA release to OTS not authorized.

Qualified requesters may obtain copies of this report from the Armed Services Technical Information Agency, (ASTIA), Arlington Hall Station, Arlington 12, Virginia.

Copies of this report should not be returned to the Aeronautical Systems Division unless return is required by security considerations, contractual obligations, or notice on a specific document.

D

13-304M, 200, 12-13-62

Aeronautical Systems Division, Dir/Aeromechanics, Flight Dynamics Laboratory, Wright-Patterson Air Force Base, Ohio. Rpt No. ASD-TDR-62-87, SUPERSONIC TURBULENT BOUNDARY LAYER GROWTH OVER COOLED WALLS IN ADVERSE PRESSURE GRADIENTS. Final report, Oct 1962, 94p incl illus., 39 refs.

Unclassified Report

The characteristics of supersonic turbulent boundary layers on cooled surfaces having adverse pressure gradients were investigated to provide design information for hypersonic inlets. Tests were conducted at Mach numbers of 3 and 6 with values of wall temperature as low as 30% of the adiabatic recovery temperature. Velocity and temperature profiles through the boundary layer were obtained and the integral boundary layer parameters were evaluated along the surface. An analytical investigation was also conducted to provide a basis for evaluating the experimental results.
It was found that cooled, turbulent boundary layers in adverse pressure gradients are thinner and less distorted than uncooled boundary layers, that the ratio of Stanton number to skin-friction coefficient is higher than the flat-plate value, and that the total amount of heat removed is greater than that predicted by integrating local heat transfer rates based on flat-plate conditions along the surface.

(over)

1. Turbulent boundary layer
2. Heat transfer
   I. AFSC Project 1366 Task 136605
   II. Contract AF33 (616)-6800
   III. United Aircraft Corp, Research Laboratories, East Hartford, Conn.
   IV. C. E. Kepler R. L. O'Brien
   V. Not aval fr OTS
   VI. In ASTIA collection

Aeronautical Systems Division, Dir/Aeromechanics, Flight Dynamics Laboratory, Wright-Patterson Air Force Base, Ohio. Rpt No. ASD-TDR-62-87, SUPERSONIC TURBULENT BOUNDARY LAYER GROWTH OVER COOLED WALLS IN ADVERSE PRESSURE GRADIENTS. Final report, Oct 1962, 94p incl illus., 39 refs.

Unclassified Report

The characteristics of supersonic turbulent boundary layers on cooled surfaces having adverse pressure gradients were investigated to provide design information for hypersonic inlets. Tests were conducted at Mach numbers of 3 and 6 with values of wall temperature as low as 30% of the adiabatic recovery temperature. Velocity and temperature profiles through the boundary layer were obtained and the integral boundary layer parameters were evaluated along the surface. An analytical investigation was also conducted to provide a basis for evaluating the experimental results.
It was found that cooled, turbulent boundary layers in adverse pressure gradients are thinner and less distorted than uncooled boundary layers, that the ratio of Stanton number to skin-friction coefficient is higher than the flat-plate value, and that the total amount of heat removed is greater than that predicted by integrating local heat transfer rates based on flat-plate conditions along the surface.

(over)

1. Turbulent boundary layer
2. Heat transfer
   I. AFSC Project 1366 Task 136605
   II. Contract AF33 (616)-6800
   III. United Aircraft Corp, Research Laboratories, East Hartford, Conn.
   IV. C. E. Kepler R. L. O'Brien
   V. Not aval fr OTS
   VI. In ASTIA collection

Aeronautical Systems Division, Dir/Aeromechanics, Flight Dynamics Laboratory, Wright-Patterson Air Force Base, Ohio. Rpt No. ASD-TDR-62-87, SUPERSONIC TURBULENT BOUNDARY LAYER GROWTH OVER COOLED WALLS IN ADVERSE PRESSURE GRADIENTS, Final report, Oct 1962, 94p incl illus., 39 refs.

Unclassified Report

The characteristics of supersonic turbulent boundary layers on cooled surfaces having adverse pressure gradients were investigated to provide design information for hypersonic inlets. Tests were conducted at Mach numbers of 3 and 6 with values of wall temperature as low as 30% of the adiabatic recovery

(over)

temperature. Velocity and temperature profiles through the boundary layer were obtained and the integral boundary layer parameters were evaluated along the surface. An analytical investigation was also conducted to provide a basis for evaluating the experimental results.

It was found that cooled, turbulent boundary layers in adverse pressure gradients are thinner and less distorted than uncooled boundary layers, that the ratio of Stanton number to skin-friction coefficient is higher than the flat-plate value, and that the total amount of heat removed is greater than that predicted by integrating local heat transfer rates based on flat-plate conditions along the surface.

1. Turbulent boundary layer
2. Heat transfer
   I. AFSC Project 1366 Task 136605
   II. Contract AF33 (616)-6800
   III. United Aircraft Corp, Research Laboratories, East Hartford, Conn.
   IV. C. E. Kepler R. L. O'Brien
   V. Not avail fr OTS
   VI. In ASTIA collection

Aeronautical Systems Division, Dir/Aeromechanics, Flight Dynamics Laboratory, Wright-Patterson Air Force Base, Ohio. Rpt No. ASD-TDR-62-87, SUPERSONIC TURBULENT BOUNDARY LAYER GROWTH OVER COOLED WALLS IN ADVERSE PRESSURE GRADIENTS, Final report, Oct 1962, 94p incl illus., 39 refs.

Unclassified Report

The characteristics of supersonic turbulent boundary layers on cooled surfaces having adverse pressure gradients were investigated to provide design information for hypersonic inlets. Tests were conducted at Mach numbers of 3 and 6 with values of wall temperature as low as 30% of the adiabatic recovery

(over)

temperature. Velocity and temperature profiles through the boundary layer were obtained and the integral boundary layer parameters were evaluated along the surface. An analytical investigation was also conducted to provide a basis for evaluating the experimental results.

It was found that cooled, turbulent boundary layers in adverse pressure gradients are thinner and less distorted than uncooled boundary layers, that the ratio of Stanton number to skin-friction coefficient is higher than the flat-plate value, and that the total amount of heat removed is greater than that predicted by integrating local heat transfer rates based on flat-plate conditions along the surface.

1. Turbulent boundary layer
2. Heat transfer
   I. AFSC Project 1366 Task 136605
   II. Contract AF33 (616)-6800
   III. United Aircraft Corp, Research Laboratories, East Hartford, Conn.
   IV. C. E. Kepler R. L. O'Brien
   V. Not avail fr OTS
   VI. In ASTIA collection

FOREWORD

This work was performed by the UAC Research Laboratories for the Aeronautical Systems Division, Wright-Patterson Air Force Base, under Contract AF 33(616)-6800, Project No. 1366, Task No. 136605. This Project and Task is a part of the Air Force Systems Command's Applied Research Program 750A, "Mechanics of Flight." This contract was issued to the UAC Research Laboratories on the basis of their response to Purchase Request No. 65496 and work was initiated under the contract on April 4, 1960.

Included among those who co-operated in the research and preparation of the report were: Mr. M. Schweiger, Head, Propulsion Section, Mr. C. E. Kepler, Supervisor, Inlet Group, and Mr. R. L. O'Brien, Project Engineer. The work was monitored by Mr. P. H. Kutschenreuter of the Flight Dynamics Laboratory, ASD.

ABSTRACT

The characteristics of supersonic turbulent boundary layers on cooled surfaces having adverse pressure gradients were investigated to provide design information for hypersonic inlets. Tests were conducted at Mach numbers of 3 and 6 with values of wall temperature as low as 30% of the adiabatic recovery temperature. The adverse pressure gradients were generated by two-dimensional models including a circular-arc surface, an isentropic-compression surface, and an oblique shock generator. Velocity and temperature profiles through the boundary layer were obtained and the integral boundary layer parameters were evaluated along the surface. An analytical investigation was also conducted to provide a basis for evaluating the experimental results.

It was found that cooled, turbulent boundary layers in adverse pressure gradients are thinner and less distorted than uncooled boundary layers, that the ratio of Stanton number to skin-friction coefficient is higher than the flat-plate value, and that the total amount of heat removed is greater than that predicted by integrating local heat-transfer rates based on flat-plate conditions along the surface.

PUBLICATION REVIEW

This report has been reviewed and is approved.

FOR THE COMMANDER:

PHILIP P. ANTONATOS
Chief, Flight Branch
Flight Dynamics Laboratory

TABLE OF CONTENTS

TABLE OF CONTENTS
(Cont.)

LIST OF FIGURES

LIST OF FIGURES
(Cont.)

LIST OF FIGURES
(Cont.)

LIST OF FIGURES
(Cont.)

LIST OF FIGURES
(Cont.)

LIST OF SYMBOLS

A_1, A_2, A_3, A''	Effective Flow Areas in Eqs. 16, 17, and 18
B, B', B''	Constants used in evaluating probe temperature error
c_p	Specific heat at constant pressure
C_f	Local skin-friction coefficient
C_1, C_2	Constants in Eq. 11
G	Reduced boundary layer shape parameter, $H/H'_{1/7}$
h_T	Local total enthalpy
h_{T_0}	Free-stream total enthalpy
H	Boundary layer shape parameter, δ''/θ
H_i	Incompressible shape parameter
$H_{1/5}$	Boundary layer shape parameter for 1/5-power velocity profile from Ref. 33
$H_{1/7}$	Boundary layer shape parameter for 1/7-power velocity profile from Ref. 33
$H'_{1/7}$	Boundary layer shape parameter for 1/7-power velocity profile having constant total temperature
k	Coefficient of thermal conductivity
ℓ_2	Effective length in Eq. 17
L	Length

LIST OF SYMBOLS
(Cont.)

$\overline{m}$	Mass flow function tabulated in Ref. 39
M	Mach number
M_w	Mach number determined from P_{S_w}/P_{T_0}
M_0	Nominal free-stream Mach number
n	Value of exponent in power law for velocity profiles, $\frac{u}{u_0} = \left(\frac{y}{\delta}\right)^{\frac{1}{n}}$
P_M	Measured probe pressure
P_p	Local pitot pressure
Pr	Prandtl number
P_S	Static pressure
P_{S_w}	Wall static pressure
P_{S_δ}	Calculated static pressure at edge of boundary layer
P_{T_0}	Tunnel stagnation pressure
q	Dynamic pressure determined from wall conditions, $\frac{1}{2}\cdot\rho'_w u'^2_w$
$\dot{q}$	Local heat-transfer rate
Q	Total heat removed, $\rho_0 u_0 h_{T_0} \phi_c$

LIST OF SYMBOLS
(Cont.)

Re_θ	Reynolds number based on momentum thickness
St	Stanton number, heat-transfer coefficient
T	Temperature
T_M	Measured probe temperature
T_P	Temperature measured by probe at zero probe weight flow
T_R	Recovery temperature
T_{REF}	Reference temperature
T_S	Local static temperature
T_{S_0}	Free-stream static temperature
T_T	Local total temperature
T_{T_0}	Tunnel stagnation temperature
T_W	Wall temperature
T'_W	Effective wall temperature - see Fig. 34 and Eq. 38
u	Local velocity determined from local P_S, P_P, T_T
u'	Local ideal velocity determined from P_S, P_{T_0}, T_{T_0}
u'_W	Ideal velocity determined from P_{S_W}, P_{T_0}, T_{T_0}

LIST OF SYMBOLS
(Cont.)

u_o	Nominal free-stream velocity
W_B	Probe bleed flow
W_o	Probe capture flow, ideal capture flow which can pass through capture area of probe at free-stream conditions
x	Distance; reference station, $x = 0$, is 34.7 in. from nozzle throat
x_s	Distance to inviscid shock reflection point
x_o	Initial value of x at start of integration
y	Distance normal to the surface of the model
y_k	Distance normal to the surface at match point
α	Angle of attack of shock generator
β	Local surface angle on circular-arc and isentropic models
γ	Ratio of specific heats
δ	Boundary layer thickness - see Fig. 6
δ^*	Boundary layer displacement thickness - see Fig. 6
η_R	Recovery factor
θ	Boundary layer momentum thickness - see Fig. 6

LIST OF SYMBOLS
(Cont.)

θ_o	Boundary layer momentum thickness at start of cooled surface
μ	Coefficient of viscosity
μ_o	Coefficient of viscosity evaluated at local free-stream conditions
ρ	Local density obtained from P_S, P_P, and T_T
ρ'	Density determined from P_S, P_{T_o}, and T_T
ρ'_w	Density determined from P_{S_w}, P_{T_o}, and T_{T_o}
ρ_o	Density determined from P_{S_o}, P_{T_o}, and T_{T_o}
τ_w	Wall-shearing stress
ϕ	Boundary layer total enthalpy thickness - see Fig. 6 and Eq. 5
ϕ_c	Corrected boundary layer total enthalpy thickness, $\frac{\rho'_w u'_w}{\rho_o u_o}\phi$
ϕ'_{c_o}	Corrected boundary layer total enthalpy thickness at start of compression surface
ϕ'_{c_ℓ}	Theoretical lower probable limit of corrected total enthalpy thickness
ϕ'_{c_u}	Theoretical upper probable limit of corrected total enthalpy thickness

LIST OF SYMBOLS
(Cont.)

ϕ_0	Boundary layer total enthalpy thickness at start of cooled surface
ψ	Total deflection angle

Subscripts

w	Conditions evaluated at the wall
1	Conditions on upstream segment of wall
2	Conditions on downstream segment of wall

Superscripts

$\bar{}$	Bar denotes average conditions
*	Star denotes sonic conditions

CONCLUSIONS

1. The shape of a supersonic turbulent boundary layer in an adverse (positive) pressure gradient created by a curved compression surface is improved by the application of wall cooling and a significant reduction in boundary layer thickness is obtained. Calculation of hypersonic inlet performance by methods which would properly account for these changes in the boundary layer characteristics with wall cooling (for example, the method of Ref. 2) would indicate that wall cooling will improve the total pressure recovery of hypersonic inlets. The increase in pressure recovery is a result of two factors; the boundary layer with wall cooling can negotiate a higher pressure rise without separating, and the reduction of boundary layer thickness with cooling allows higher maximum inlet contraction ratios to be obtained.

2. The ratio of Stanton number to skin-friction coefficient for a supersonic turbulent boundary layer on a cooled flat plate is independent of Mach number in the range from 3 to 6. For the configuration tested (a flat plate downstream of a streamwise step in wall temperature distribution), this ratio is higher than that predicted on the basis of the Reynolds-Colburn analogy.

3. The ratio of Stanton number to skin-friction coefficient for a supersonic turbulent boundary layer in an adverse pressure gradient is larger than that on a flat plate and the deviation from the flat-plate value increases with the magnitude of the gradient.

4. The total amount of heat removed from a supersonic turbulent boundary layer on a cooled surface having an adverse pressure gradient is greater than that predicted by integrating local heat-transfer rates based on flat-plate conditions along the surface.

Manuscript released by the authors November 1961 for publication as an ASD Technical Report

RECOMMENDATIONS

1. Additional investigations of supersonic turbulent boundary layers on cooled surfaces having adverse pressure gradients should be conducted to provide more detailed experimental data for use in the development of generalized procedures for predicting boundary layer characteristics in hypersonic inlets, since the results of this study (see CONCLUSION 1) indicate that wall cooling should have a significant favorable effect on the performance of hypersonic inlets. Specifically, the following characteristics should be investigated:

   a. The effect of Reynolds number on the shape parameter for boundary layers on cooled walls.

   b. The effect of wall cooling on boundary layer separation criteria.

   c. The effect of wall cooling on duct flows comprised entirely of boundary layer.

2. Investigations should be conducted to determine the characteristics of supersonic laminar boundary layers on cooled walls having pressure gradients which simulate those of hypersonic inlets designed for supersonic-burning ramjets.

3. Improved experimental techniques should be developed for measuring boundary layer total temperature profiles adjacent to cooled walls so that more accurate data can be obtained in future studies. Techniques for measuring wall temperature differences accurately should also be developed so that direct measurements of wall heat-transfer rates can be obtained.

4. Future hypersonic inlet investigations should be conducted with wall cooling to provide proper simulation of the boundary layer characteristics in such inlets.

INTRODUCTION

The boundary layer development on the walls of supersonic and hypersonic inlets has a large influence on the performance of high Mach number, air-breathing propulsion systems. The boundary layer characteristics limit the amount of supersonic compression and, for systems employing subsonic combustion, influence the pressure recovery through the normal shock. Although detailed boundary layer growth characteristics having direct application to the design of supersonic inlets with uncooled walls were obtained in a previous investigation at the UAC Research Laboratories (Ref. 1), these data are not generally applicable to hypersonic inlets where wall cooling will be required. Recent studies of hypersonic inlets at UAC (Ref. 2) have shown that wall cooling has a significant effect on the performance of hypersonic inlets. This is to be expected since boundary layer growth and separation phenomena play a large role in determining the performance of hypersonic inlets. In such inlets, the boundary layer constitutes the major portion of the flow at the throat.

The objective of the investigation described herein was to obtain detailed information on supersonic turbulent boundary layer growth over cooled walls in adverse pressure gradients to provide a more rational basis for the design of hypersonic inlets.

RESUME OF PREVIOUS WORK

The only available experimental data on supersonic turbulent boundary layer characteristics over cooled or heated walls in adverse pressure gradients is contained in Ref. 3. This work was limited to a single case of a strong oblique shock interaction on a wall which was only moderately cooled or heated ($0.93 < T_w/T_R < 1.26$), and the data consisted primarily of wall static pressure distributions. From this data the author deduced that a small increase of the separation pressure ratio was obtained with cooling. A prior survey of the literature (Ref. 4) contains data for subsonic cooled turbulent boundary layers in adverse pressure gradients but no comparable results for supersonic flow. Because of this lack of experimental data, theoretical calculation procedures for cooled supersonic boundary layers in adverse pressure gradients, such as that of Ref. 5, are extensions of the procedures developed for incompressible flow, e.g., Ref. 6.

Limited data exist for turbulent boundary layers on cooled flat plates (zero pressure gradient) at high supersonic Mach numbers, see Refs. 7 through 10. These data are not in complete agreement with existing theories (see, for example, Refs. 5, 11, and 12); the data indicate a trend of decreasing skin friction with wall cooling, whereas the theories all predict an increase.

Supersonic turbulent boundary layer growth over insulated walls in adverse pressure gradients has been investigated quite extensively for the case of the severe adverse pressure gradients caused by oblique or normal shocks (see, for example, Refs. 13 through 23). For this class of gradients, the mixing of flow from the free stream into the boundary layer has little effect on the shape of the boundary layer over the short length of pressure rise, and several theories (Refs. 24 through 28) have been developed to determine the maximum pressure rise that can be obtained without separation. The only known data on supersonic boundary layers in adverse pressure gradients not created by shocks are contained in Refs. 1, 29, and 30. The theory presented in Ref. 5 is applicable for very mild pressure gradients of this type; however, for large gradients, the theory severely underestimates the pressure rise which can be obtained without separation of the boundary layer. This discrepancy between theory and experiment (see Ref. 1 for detailed discussion) occurs because the theory does not account for increased mixing of the freestream flow into the boundary layer. The effect of this increased mixing is included in the "lag-length procedure" developed in Ref. 1 for calculating supersonic turbulent boundary layer growth in adverse pressure gradients. This theory, which is based on experimental data obtained from tests in which the wall temperature was in equilibrium for zero heat transfer (adiabatic wall), is modified in the following section to account for wall cooling.

ANALYTICAL INVESTIGATION

Prediction of Boundary Layer Growth and Heat Transfer on a Flat Plate

The theoretical methods for predicting turbulent boundary layer growth and heat-transfer characteristics on a flat plate employed in this report were derived from the skin-friction coefficient relationship obtained from Ref. 5. In this reference the incompressible Ludwieg-Tillmann skin-friction equation (Ref. 31) is modified for compressibility by using the Eckert reference enthalpy method of Ref. 32. The relationship for skin-friction coefficient used in Ref. 5 can be rewritten in the following form:

$$C_f = 0.246e^{-1.561H_i}\left(\frac{\rho_0 u_0 \theta}{\mu_0}\right)^{-0.268}\left(\frac{T_{S_0}}{T_{REF}}\right)^{0.796} \qquad (1)$$

where H_i is the incompressible shape parameter and T_{REF} is the reference temperature as defined in Ref. 32. In this derivation the power law for viscosity, $\mu \sim T^{0.76}$, has been used. After integrating the von Kármán boundary layer momentum equation (employing Eq. 1 to evaluate C_f), the boundary layer momentum thickness, θ, may be evaluated by the following expression:

$$\theta = 0.231e^{-1.232H_i}\left(\frac{\rho_0 u_0}{\mu_0}\right)^{-0.212}\left(\frac{T_{S_0}}{T_{REF}}\right)^{0.628}(x)^{0.788} \qquad (2)$$

where the boundary conditions are $\theta = 0$ at $x = 0$.

The boundary layer displacement thickness, δ^*, was evaluated from the theoretical value of θ and the theoretical value of $H = \delta^*/\theta$ for a cooled 1/7-power profile as tabulated in Ref. 33. This reference employed a modification of the Crocco energy integral to relate total temperature and velocity for evaluating the integral boundary layer parameters.

The equation relating heat-transfer rate, $\dot{q}$, to the total heat removed, Q, is

$$\dot{q} = \frac{dQ}{dx} = St\rho_0 u_0 c_p (T_R - T_W) \tag{3}$$

The total heat removed, Q, is related to the total enthalpy thickness, ϕ, by the following relation

$$Q = \rho_0 u_0 h_{T_0} \phi \tag{4}$$

where ϕ is defined by

$$\phi = \int_0^\delta \frac{\rho u}{\rho_0 u_0} \left(1 - \frac{h_T}{h_{T_0}}\right) dy \tag{5}$$

Thus, for a flat plate, ϕ is directly proportional to the total heat removed from the boundary layer. If the ratio of the Stanton number (heat-transfer coefficient) to skin-friction coefficient, St/C_f, is a constant, Eq. 3 may be integrated directly to evaluate the total enthalpy thickness as a function of distance along the surface. The resulting expression is

$$\phi = \phi_0 + 2\frac{St}{C_f}\left(\frac{T_R}{T_{T_0}} - \frac{T_W}{T_{T_0}}\right)(\theta - \theta_0) \tag{6}$$

where the boundary conditions are $\phi = \phi_0$ at $\theta = \theta_0$. The ratio of Stanton number to skin-friction coefficient given by the Reynolds-Colburn analogy is equal to 0.635 for a Prandtl number of 0.70.

Prediction of Boundary Layer Growth and Heat Transfer in an Adverse Pressure Gradient

The method used in this report to predict boundary layer growth in an adverse pressure gradient is based on the von Kármán momentum integral equation for compressible flow (Ref. 34):

$$d\theta = \frac{C_f}{2}\,dx - \theta\left(\frac{dq}{q} + H\,\frac{du'_w}{u'_w}\right) \qquad (7)$$

where u'_w is the velocity based on the wall static pressure and the free-stream total pressure. The use of this equation is justified in Ref. 1 where it is concluded that the momentum thickness of a turbulent boundary layer in adverse pressure gradients where there is a component of the pressure gradient normal to the wall (i.e., in the pressure field generated by a curved compression surface in supersonic flow) can be calculated from the von Kármán momentum integral equation. The form factor, H, in this equation was evaluated by a modification of the "lag length" procedure developed in Ref. 1. This procedure is based on the experimental observation that mixing of external flow into the boundary layer in an adverse pressure gradient "lags" the mixing that would be required to maintain a flat-plate profile. In employing this procedure, the mass flow within the boundary layer is assumed to increase at the flat-plate value over the initial portion of the adverse pressure gradient; but after a distance called the lag length, the rate of mass flow into the boundary layer increases rapidly. Reference 1 shows that the lag length is a function of the Reynolds number but independent of Mach number.

The boundary layer shape parameter employed in Ref. 1 was divided by the form factor for a 1/7-power profile, and a new reduced shape parameter, $G = H/H'_{1/7}$ was defined; the values of $H'_{1/7}$ were obtained from Ref. 35. For an uncooled boundary layer, a G of unity implies a profile having integral characteristics which are similar to those of a flat-plate profile and a value of $G>1$ implies a distorted profile.

In the present analysis of turbulent boundary layer growth over a cooled surface in an adverse pressure gradient, the value for G was first computed for the insulated-wall case using the lag-length procedure as developed in Ref. 1. The effect of cooling on G was then introduced by correcting the insulated-wall value by the ratio of the cooled to adiabatic flat-plate reduced form factors.

$$G_{COOLED} = (G_{ADIABATIC}) \left(\frac{G_{COOLED\ FLAT\ PLATE}}{G_{ADIABATIC\ FLAT\ PLATE}} \right) \qquad (8)$$

Here the assumption is made that the ratio of the shape parameter on the cooled surface to the shape parameter on the adiabatic (insulated) surface is the same for the distorted profile (resulting from the adverse pressure gradient) as it is for a flat plate profile. For the theoretical shape parameters tabulated in Ref. 33 for various power law profiles, calculations of the ratio of the shape parameter on a cooled surface to the shape parameter on an adiabatic surface at given values of Mach number and wall temperature indicate that the value of this ratio is approximately constant for power-law exponents ranging from 1/5 to 1/11. This assumption is investigated further in APPENDIX III where an attempt is made to evaluate the validity of Eq. 8 by an analysis of the data obtained in this investigation.

The value of G for a cooled flat plate was obtained from the experimental data for the flat-plate studies described in a later section of this report.

The skin-friction coefficient was computed from Eq. 1 which includes the effects of a distorted profile in the incompressible shape parameter, H_i. The momentum thickness was then computed by a step-by-step integration of Eq. 7 and the displacement thickness was computed from θ using the value of G from Eq. 8.

Two reference values of heat transfer were computed for comparison with the experimental data. The first value, herein termed the "lower probable limit" of total heat transfer, was computed by assuming that the local heat-transfer rate at each point on the surface is the same as that for a flat-plate profile at the same wall temperature, Mach number, and Reynolds number based on momentum thickness. This is the method suggested in Ref. 5 and is commonly used in boundary layer and heat transfer calculation procedures. The second reference value, herein termed the "upper probable limit" of total heat transfer, was computed by assuming that the total heat removed up to a given station in an adverse pressure gradient is equal to the value that would have been removed from the flat-plate profile having the same θ, assuming that the boundary layer developed over a flat plate having constant values of the wall temperature and Mach number equal to those at the given

station. In all cases calculations show that this second value of total heat removed is much larger than the first value. Thus the second method (higher total heat removed) would result in a lower average total temperature of the air within the boundary layer than the first method (lower total heat removed). If it is assumed that the rate at which heat is transferred from a boundary layer to a wall is a function of the difference between the average temperature of the air within the boundary layer and the wall temperature, then the heat-transfer rate for the actual boundary layer must be greater than the value used in evaluating the lower probable limit (first method) and less than the value required to establish the upper probable limit (second method).

The total heat removed at any station along the surface was computed in terms of the corrected total enthalpy thickness, $\phi_c = \frac{\rho'_w u'_w}{\rho_o u_o} \phi$ using the following equations:

For the lower probable limit, $\phi_c = \phi'_{c_\ell}$

$$\phi'_{c_\ell} = \phi'_{c_o} + \int_{x_o}^{x} St \frac{\rho'_w u'_w}{\rho_o u_o} \left(\frac{T_R}{T_{T_o}} - \frac{T_w}{T_{T_o}} \right) dx \qquad (9)$$

where St is evaluated for the flat-plate value as determined by Re_θ, M_w, and T_w/T_{T_o}.

For the upper probable limit, $\phi_c = \phi'_{c_u}$

$$\phi'_{c_u} = \phi'_{c_o} + 2 \frac{St}{C_f} \left(\frac{T_R}{T_{T_o}} - \frac{T_w}{T_{T_o}} \right) \left(\frac{\rho'_w u'_w}{\rho_o u_o} \theta - \theta_o \right) \qquad (10)$$

where $St/C_f = 0.5\ Pr^{-2/3} = 0.635$.

The method for predicting the turbulent boundary layer growth and heat-transfer characteristics developed in this section were employed to calculate the theoretical values presented with the data in subsequent sections.

The method for calculating turbulent boundary layer growth over a cooled compression surface presented in Ref. 5 was also employed for the case of the flow over an isentropic compression surface at Mach 6 (one of the configurations tested). The results indicate that the boundary layer would separate at a total turning angle of 18 deg, whereas the method described above did not predict separation at any point on the surface having a total turning angle of 34 deg. Schlieren photographs of the flow-over model, presented in Fig. 26, give no indication of boundary layer separation at any point on the surface of the model. A brief description of the lag-length method which was employed for predicting boundary layer separation and a comparison of this method with Ref. 5, has been presented in the RESUMÉ OF PREVIOUS WORK.

EXPERIMENTAL INVESTIGATION

Description of Test Equipment

Tunnel

Tests to determine turbulent boundary layer growth over cooled walls in adverse pressure gradients were conducted in the UAC Research Laboratories 4.5-x 3.5-in. continuous-flow supersonic wind tunnel. Dry air is supplied to this tunnel at a total temperature of approximately 400 F and at stagnation pressures up to 400 psig and is exhausted to vacuum pumps. The tunnel is equipped with interchangeable single supersonic nozzle blocks (Mach 3 or Mach 6) and a centerline block on which

the boundary layer approaching the models develops naturally. The Reynolds numbers in the tunnel test section were 0.32×10^6 per in. at Mach 3 and 0.59×10^6 per in. at Mach 6.

Models

Three models were employed for the tests: a flat plate, a compression surface having a constant radius of curvature and a total turning angle of 26 deg (the circular-arc model), and a Mach 6 isentropic compression surface having a total turning angle of 34 deg (the isentropic-surface model). The inviscid isentropic compression contour was corrected for boundary layer displacement effects using the method outlined in the ANALYTICAL INVESTIGATION to arrive at the theoretical displacement thickness. For one series of tests, a shock generator which could be oriented at various angles of attack ($0 < \alpha < 10$ deg) with respect to the free stream was employed to create a shock-reflection interaction on the flat plate. Photographs of the models installed in the tunnel are presented in Figs. 1, 2, and 3. The model surfaces were fabricated from copper to provide good heat-transfer characteristics between the measured boundary layer on the upper surface of the models and the coolant (liquid N_2) on the lower surface. The models were attached to a triple-pass heat exchanger as shown in Fig. 4. The liquid nitrogen from a throttled 125 psig supply was first passed between the copper models and the closely spaced inner plates to create high coolant velocities; then the coolant flow made a double pass beneath the models to minimize heat conduction from the hot walls of the tunnel to the cold model. The spacing between the copper models and the inner plate and the thickness distributions of the copper models were designed so that a constant wall temperature could be maintained on the air side of the models. The heat-transfer rates employed in these calculations were based on the lower probable limit of heat transfer as defined in the ANALYTICAL INVESTIGATION.

The sides of the compression-surface models were cut back from the walls of the tunnel in order to minimize the effect of tunnel side-wall boundary layer on the flow over the models. This design was found to be necessary for similar tests reported in Ref. 1. The models were

instrumented at various stations with both surface thermocouples and static pressure orifices for measuring wall temperature and static pressure distributions.

Probe

The probe employed to measure the boundary layer (see Figs. 1, 2, or 3) was driven by a mechanism which allowed the probe to traverse at any angle in the longitudinal vertical plane so that the survey could be made normal to the model surface. The probe position was measured to an accuracy of 0.002 in. The probe head permitted simultaneous measurement of pitot pressure and temperature. A sketch of the probe is presented in Fig. 5. An iron-constantan thermocouple junction was located inside the probe head (which had an opening 0.010 in. high), and a small fraction of the flow was bled through the probe to provide airflow past the thermocouple junction. The method of evaluating the local total temperature from the measured temperature is discussed in APPENDIX I.

The effect of the small amount of bleed flow through the probe on the measured pitot pressure was evaluated on the basis of normal shock inlet data. Typical pressure-recovery, weight-flow data for a normal shock inlet at Mach numbers of 1.6 and 2.5 are shown in Fig. 5. The size of the bleed hole in the probe was selected to pass a maximum of 15 to 20% of the ideal weight flow through the probe. Over this range of weight flows, the measured pressure recovery of a normal shock inlet is identical to the dead-ended pitot pressure. An experimental verification of this characteristic was performed by surveying the boundary layer on a flat plate with both a conventional pitot probe and the combination pressure-temperature probe. The measured pressures were identical.

Data Reduction Procedure

Conventional data reduction procedures employed in the evaluation

of boundary layer parameters on flat plates cannot be used for boundary layers on curved surfaces because of the large static pressure gradients normal to the surface. These gradients provide the centripetal force necessary to turn the flow. Although the wall static pressure was measured, the static pressure distribution through the boundary layer could not be measured accurately by a static pressure probe because of flow angularity. Consequently, the method of estimating the static pressure distribution developed in Ref. 1 was employed. The essential features of this method are as follows: A typical pitot pressure profile normal to a curved surface increases as the distance from the wall, y , increases, reaches a maximum, and then decreases as the probe traverses into the free stream where there is also a static pressure and Mach number gradient. The edge of the boundary layer is usually 10 to 20% beyond the y value for the peak pitot pressure. The static pressures just outside the boundary layer were evaluated from the measured pitot and free-stream total pressures. The shape of the static pressure distribution through the boundary layer was obtained by fairing a curve which matched the value and slope of the free-stream static pressure distribution and the value and slope at the wall. The slope at the wall was assumed zero on the basis of a zero velocity and the point in the free stream at which the static pressure curves were matched was usually 20-30% beyond the y value for the peak pitot pressure. The estimated static pressure variation, the measured pitot pressures, and the measured total temperature could then be employed to determine all the other local flow properties.

Three integral boundary layer parameters were evaluated to describe the boundary layer characteristics: the mass parameter or displacement thickness, δ^* ; the momentum parameter or momentum thickness, θ ; and the energy parameter or total enthalpy thickness, ϕ . The first two are the conventional parameters; the third is a measure of the total heat removed by cooling prior to the station at which the profile is evaluated. This parameter was employed to estimate the heat-transfer rates since measurements of the temperature gradient across the cooled copper wall and heat rise in the coolant could not be determined accurately. The method

of evaluating these integrals is presented pictorially in Fig. 6. In all cases the parameters are based on the ideal conditions (primed quantities) that would exist at the wall (subscripted w) as determined from the measured wall static pressure, free-stream total pressure, and free-stream total temperature. These ideal wall conditions were used rather than the conditions at the edge of the boundary layer because the large variation of the conditions outside the boundary layer do not provide a convenient set of reference conditions. It can be seen from Fig. 6 that δ^* and θ as defined in this report reduce to the standard definitions of these quantities for the case of a zero pressure gradient normal to the surface. For the cases considered herein the existence of a normal pressure gradient introduces additional terms into the von Kármán momentum integral equation. Due to the complexity of these terms and the uncertainty introduced into the data reduction procedure by the necessity of estimating the static pressure distribution through the boundary layer, the magnitude of this effect is difficult to evaluate. This term was neglected on the basis of the conclusions of Ref. 1 where it was shown for a sizeable data sample that the von Kármán momentum integral equation in the form of Eq. 7 predicted the boundary layer growth characteristics on curved surfaces. The magnitude of these terms is zero for the case of a zero normal pressure gradient. The definition of ϕ , however, allows an exact calculation of the total heat removed (using Eq. 9), when St is known exactly.

Discussion of Experimental Results

Mach 3 Studies

Flat Plate

Tests were conducted at Mach 3 with the flat-plate model installed to establish the initial flow conditions for subsequent tests. Three coolant rates were employed: zero, the maximum, and one intermediate value. The conditions which correspond to these three coolant flow

rates are hereafter referred to as "uncooled", "maximum cooling", and "intermediate cooling". The maximum coolant flow rate was established as the rate for which liquid nitrogen was exhausted from the heat exchanger; increasing the coolant flow rate beyond this value provided little decrease in the wall temperature ratio. Figure 7 shows the distributions of the wall Mach number and wall temperature for each of the three coolant conditions. It can be seen that the Mach numbers and wall temperatures were uniform over the three survey stations, and that the values of wall temperature for the uncooled tests are significantly lower than the recovery temperature, T_R, for a turbulent boundary layer at Mach 3. This characteristic is due to heat losses from the tunnel to the surrounding room and, as a result, the data obtained with zero coolant flow had significant heat-transfer rates.

Typical velocity and total temperature profiles are shown in Fig. 8. From these profiles it can be seen that wall cooling had little or no effect on the shape of the flat-plate velocity profiles which were approximately a 1/6-power profile. The total temperature profiles are similar at the outer edge of the boundary layer and only near the wall do they show the effect of cooling. The theoretical total temperature profile for the maximum cooling condition is also shown in the lower figure. The theoretical value was determined from the experimental velocity profiles making use of the Crocco energy integral which formulates a linear relationship between total temperature and velocity. The data for the maximum cooling condition exhibit higher total temperatures than the theory. This discrepancy probably occurs, in part, because the measured profile did not develop over an isothermal surface. The initial 24 in. of flat-plate surface was not cooled ($T_W/T_{T_0} \approx 0.85 < T_R/T_{T_0}$), and a sudden drop in the wall temperature occurred at the start of the cooled flat plate (7 in. upstream of the first survey station). As a consequence, the temperatures in a portion of the boundary layer away from the wall would be expected to be higher than the values for a flat-plate profile which developed over a uniformly cooled surface. The theoretical curve corresponding to the data obtained with no coolant flow is not

shown in Fig. 8 as it would fall along the line faired through the uncooled data points.

Experimentally determined variations of momentum thickness, displacement thickness, and total enthalpy thickness are shown in Fig. 9 for each of the three cooling conditions. The effect of wall cooling on the integral parameters can be seen for δ^* and ϕ; however, there is no consistent variation of the boundary layer momentum thickness with cooling. At the upstream station, the data exhibit an increase in θ with increased cooling, at the middle station the data show little effect of cooling, and at the downstream station the data show an opposite trend. The accuracy in the measurements of θ is estimated to be on the order of 3 to 5%. Hence no significant effect of cooling on momentum thickness can be deduced from the data presented in Fig. 9.

The theoretical variations of θ, δ^*, and ϕ are shown on Fig. 9 for two values of the wall temperature ratio. The method of calculation is discussed under ANALYTICAL INVESTIGATION. The values of momentum thickness (0.018 in.) and total enthalpy thickness (0.004 in.) at the start of the cooled portion of the wall were estimated by extrapolating the data to the start of the cooled surface making use of the theoretical slope to obtain a best fit. For a wall temperature ratio of 0.85 (uncooled), the theoretical and experimental variations of momentum thickness with x are in agreement. The theoretical increase of the momentum thickness due to cooling at the last survey station is about 9%.

The theoretical values for the displacement thicknesses were obtained from the theoretical momentum thickness and the theoretical shape parameter, $H_{1/7}$, for a 1/7-power profile as tabulated in Ref. 33. The displacement thickness data are in good agreement with theory at a wall temperature ratio of 0.85; however, the decrease in displacement thickness with wall cooling is not as great as that predicted by Ref. 33. As shown in Fig. 8, the experimental total temperatures for the maximum cooling condition are greater than the theoretical values obtained by

employing the Crocco energy integral. The total temperatures used in evaluating the parameters tabulated in Ref. 33 were computed by a modification of the Crocco energy integral which results in even lower total temperatures than would be computed from a linear total temperature-velocity relationship. This difference between the theoretical and experimental values of total temperature is the primary reason for the large discrepancy between the theoretical and measured values of δ^* for the intermediate and maximum cooling conditions. The data for total enthalpy thickness show the same trends as the theory; however, the values are not in quantitative agreement. One reason for this lack of agreement can be attributed to the accuracy of the ϕ integration. Small errors in the measurement of total temperature near the edge of the boundary layer, where the mass flow is large, can result in large errors in the calculated values of total enthalpy thickness.

Figure 10 shows the experimental values of the shape parameter, H, and the reduced shape parameter, G, for the flat plate at Mach 3. The theoretical values of the shape parameter for a boundary layer with constant total temperature ($H'_{1/7}$, see Ref. 35) and for a boundary layer with a total temperature profile determined by a modification of the Crocco integral ($H_{1/7}$, see Ref. 33) are also shown in this figure. Although the experimental shape parameter is reduced with cooling, the reduction is not as great as that predicted by Ref. 33. This departure from theory can also be seen in the measured displacement thicknesses discussed previously.

Shock Generator

The shock-generator model (see Fig. 1) was employed to obtain boundary layer profile data immediately downstream of the shock reflection on a cooled flat plate for generator angles of attack of 0, 4, 8, and 10 deg. Figure 11 contains a schlieren photograph and a sketch of the shock-reflection interaction region showing the incident shock wave, the reflected shock wave (an initial compression followed by an

expansion and then recompression), and the expansion fan originating at the base of the shock generator wedge. The inviscid shock-reflection point, x_s , and the probe station are also shown on this figure. The location of the surface of the flat plate in the schlieren photograph was obscured by scratches in the tunnel window and is therefore indicated by the white line.

The measured wall static pressure and wall temperature distributions are given in Fig. 12 for each of the generator angles for both zero and maximum coolant flow rates, hereafter referred to as "uncooled" and "cooled". The location of the inviscid shock-reflection point varied from $x_s = 3.3$ in. for the 10-deg shock to $x_s = 3.6$ in. for the 0-deg wave. The probe station was at $x = 4.0$ in. for all profiles. For all generator angles of attack, the interaction started farther downstream with wall cooling then without, and the static pressure rose to a higher value at the probe station. This is in agreement with the trends shown by the data of Ref. 3. At a generator setting of 0 deg, a weak wave was observed in the schlieren even though the net flow deflection was very small. A slight rise in wall static pressure can be seen at this generator setting. The pressure ratios at the probe station were less than the theoretical values for angles of 8 and 10 deg because the expansion fan from the wedge intersected the boundary layer before the pressure rise was completed.

Figures 13 and 14 present the velocity and total temperature profiles at the probe station for tests with both cooled and uncooled walls. In Fig. 13 the velocities are ratioed to the nominal tunnel velocity, and therefore do not necessarily approach unity at the edge of the boundary layer. At zero angle of attack the velocity profiles were similar (no significant change in the velocity profile would be expected since the flat-plate profiles showed no significant change with cooling); at 4 deg the velocity profile was much fuller for the maximum cooling condition; at 8 deg the profiles were similar; and at

10 deg the velocity profile was fuller for the uncooled tests. This reversal of cooling effect with increasing angle of attack can be attributed to two opposing factors: (1) for a given pressure rise cooling tends to improve the boundary layer profile since upstream of the interaction the cooled profile has higher Mach numbers through the boundary layer and is able to negotiate the pressure rise with less reduction in velocity and hence less distortion than the uncooled profile, and (2) for a given incident shock strength cooling tends to (a) reduce the length of the interaction (i.e., larger adverse pressure gradient) and (b) shift the interaction downstream, effectively shifting the probe station forward into the highly distorted portion of the interaction region. These factors tend to increase the distortion measured at the probe station. From the data, it appears that the first of these factors predominates at low angles of attack, while at higher angles of attack, the second of these factors was more pronounced.

The boundary layer momentum and displacement thicknesses and the reduced shape parameters for these profiles are presented in Fig. 15. The figure shows the expected trend with increasing angle of attack, i.e., the values of θ, δ^*, and G generally increase with increasing shock strength. The increase in G between 0- and 10-deg angles of attack is greater for the data with maximum coolant flow than for the data with zero coolant flow. This is due to the same factors which produced the reversal in trend in the velocity profiles. No consistent trend could be established for the corrected total enthalpy thickness data obtained with the shock generator and, consequently, these data are not presented.

Circular Arc

Boundary layer profile data were obtained at five stations on the circular-arc model for three rates of coolant flow which corresponded to wall temperature ratios of approximately 0.85, 0.60, and 0.45 (the uncooled, intermediate cooling, and maximum cooling conditions, respectively). Schlieren photographs of the flow over the circular-arc model with each of these cooling rates are shown in Fig. 16. Figure 17

shows the measured and theoretical values of wall static pressure, P_{s_w}, the calculated static pressure at the edge of the boundary layer, P_{s_δ}, and the measured wall temperature, T_w, as a function of distance along the surface. The stations at which surveys were obtained are noted on the figure. The wall temperature ratio did not vary significantly over the portion of the model covered by the survey stations, as shown by the lower portion of the figure.

The velocity profiles obtained on the circular-arc model are shown in Fig. 18. The velocity profiles upstream of the tangent point show no significant change with cooling, as would be expected from the flat-plate data, whereas the velocity profiles on the curved portion of the surface do show a substantial improvement in shape and a decrease in boundary layer height with cooling. This trend with increased coolant flow is observed at all stations except at the 12-deg station where the velocity profile with maximum cooling shows negligible change from the profile obtained at the intermediate cooling rate. Analysis of the data at this station indicates that there was an error in the probe position data due to backlash in the probe drive mechanism. An attempt has been made to correct the data but the magnitude of the correction (Δy = 0.015 in.) could not be accurately determined. The total-temperature profiles (Fig. 19) on the upstream portion of the curved surface show a change with cooling over the lower third of the profile as was the case with the flat-plate profiles (see Fig. 8). On the downstream portion of the surface, however, the profiles show no change with cooling except in the immediate vicinity of the wall. There is a strong possibility that the profiles at the downstream station could be seriously affected by probe conduction error due to the low bleed flow through the probe in the distorted profiles at these stations. For a given height within the boundary layer at the 24-deg station, boundary layer mass flow calculations indicate that there is approximately 30% more mass flow for the maximum cooling rate than there is for the uncooled profile. This is an important consideration in the diffusion of a supersonic boundary layer (e.g., such as encountered in high-performance internal-compression inlets) since this increase in mass

flow in the boundary layer will permit the use of higher inlet contraction ratios with cooled walls than without.

Figure 20 shows the experimental variations of displacement thickness and reduced shape parameter. The change of displacement thickness along the surface was less with wall cooling than without, and the data for reduced shape parameter show that cooling produces a significant reduction (i.e., improvement) in the shape parameter. Figure 21 shows the variation of boundary layer momentum thickness and corrected total enthalpy thickness computed from the measured profiles. The corrected total enthalpy thickness, ϕ_c , is defined as the local ϕ times the ratio of the mass flow computed from the local wall static pressure ratio to the mass flow at the nominal free-stream conditions. This parameter is more useful than ϕ since it is directly proportional to the total heat removed from the boundary layer, i.e., $Q = \rho_0 u_0 h_{T_0} \phi_c$. The rate of increase of momentum thickness, θ , (top half of Fig. 21) over the upstream portion of the surface is the same for the three cooling conditions. Over the downstream portion of the surface, the rate of increase of θ is significantly reduced with wall cooling as would be expected on the basis of the improved velocity profiles shown in Fig. 18. The corrected total enthalpy thickness increases with cooling at each station, but there is a lack of consistency in the variation with distance over the downstream portion of the plate. This may also be attributed to probe conduction error since such an error would tend to increase ϕ_c for the case without cooling and reduce ϕ_c for the case with cooling.

Theoretical values for displacement thickness, reduced shape parameter, momentum thickness, and corrected total enthalpy thickness are also shown with the experimental data in Figs. 20 and 21. The theoretical values are based on the methods discussed in a previous section (ANALYTICAL INVESTIGATION). For each value of wall temperature ratio, the initial value of G on the circular arc was determined from the Mach 3 flat-plate studies (see Fig. 10). The theoretical values of G (see Fig. 20) are in general agreement with the experimental data except in the uncooled case where the theoretical values are a maximum of 10% lower

than the experimental data. However, the theoretical values of momentum thickness (see Fig. 21) and displacement thickness (see Fig. 20) are lower than the experimental data. The largest differences between theory and experiment are for the uncooled case where the differences at the last survey station are 30 and 35% of the experimental values of θ and δ^*, respectively. The best agreement between theory and experiment might be expected for the uncooled case since the lag-length theory employed to evaluate the theoretical values was based on experimental data obtained from uncooled tests. In Ref. 1 a statistical analysis of the differences between lag-length theory and experiment was performed. The results for many cases showed that the maximum difference between theory and experiment was random and that most of the data fell within 35% (two standard deviations) of the theoretical values. The magnitude of the differences shown in Figs. 20 and 21 are within these expected limits of accuracy for the lag-length calculation procedure. As can be seen from Fig. 20, the deviations between the theoretical and experimental values of the shape parameter, G, are of the order of the experimental accuracy ($\approx 3\%$) at all points except the two points obtained without cooling at the 12-and 18-deg stations. The uncooled data were expected to show the best agreement with theory since the lag-length theory was originally developed for the adiabatic wall case. As shown in APPENDIX III, the maximum errors introduced by Eq. 8 are of the order of 10 to 15% depending on the method of analysis chosen. The deviations between experimental and the theoretical values computed from the lag-length procedure and the use of Eq. 8 are of the same order as those resulting from the use of the lag-length procedure alone (see Ref. 1).

The lower portion of Fig. 21 shows the theoretical values for the upper and lower probable limits of heat transfer, ϕ'_{c_u} and ϕ'_{c_ℓ}. Virtually all the data lie between the two limits established for each cooling rate. The only point which lies above the upper probable limit is at the 24-deg station with zero coolant flow. As noted before, all of the points at the 24-deg, and possibly 18-deg stations, could be seriously affected by probe conduction error. A statistical analysis of the data indicated that the value of total heat transfer is greater

than the lower probable limit by an amount which is approximately 30% of the difference between the upper and lower probable limits.

Mach 6 Studies

Flat Plate

Tests were conducted at Mach 6 with the flat-plate model installed. The wall Mach number and wall temperature distributions for zero coolant flow rate (uncooled) and maximum coolant flow rate (cooled) are shown in Fig. 22. The Mach number varied from a value of 6.02 at the upstream survey station to a value of 5.85 at the downstream station; the wall temperature was uniform over the three survey stations. As with the Mach 3 data, the wall temperature for the uncooled tests was lower than the turbulent recovery temperature; with maximum cooling, however, the wall temperatures were lower than for the Mach 3 tests. Typical velocity and total temperature profiles for the two cooling rates are shown in Fig. 23. The velocity profiles were similar (approximately a 1/5-power profile); the cooled profile was a little fuller near the wall. As in the Mach 3 studies, the total temperatures near the edge of the boundary layer were the same and the effect of cooling was evident in the lower portion of the boundary layer. The theoretical total temperature distribution for a linear temperature-velocity relationship as formulated by the Crocco energy integral is shown for the profile obtained with the maximum coolant flow rate. Again, the experimental total temperatures are significantly different from the theoretical values (see Mach 3 flat-plate results); a characteristic which may be attributed to the stepwise temperature distribution on the surface over which the boundary layer developed. As in the case of the Mach 3.0 flat plate data, the theoretical total temperature profile with no cooling agrees with the total temperature data points. The theoretical and experimental total temperature distributions are in agreement for the cases with no cooling because there is no stepwise temperature gradient along the surface.

The experimentally obtained variations of boundary layer momentum thickness, displacement thickness, and total enthalpy thickness are shown in Fig. 24 together with the theoretical values for these para-

meters. The data show a larger momentum thickness, a smaller displacement thickness, and a larger total enthalpy thickness for the cooled profiles than for the uncooled profiles. The direction of all these trends is in general agreement with theory. The values of momentum thickness (0.030 in.) and total enthalpy thickness (0.010 in.) at the start of the cooled portion of the surface were estimated by extrapolating the data to the start of the cooled surface. The momentum thickness data are in general agreement with the theoretical values; the maximum deviation is of the order of the repeatability of the measurements as indicated by the two points for the uncooled tests at the middle survey station. The change in momentum thickness from the uncooled case to the cooled case is in good agreement with theory but is of the same order of magnitude as the accuracy of the data; hence no significant conclusion may be drawn from this. The data show higher displacement thicknesses than predicted by theory and, similar to the Mach 3 data, the reduction in displacement thickness with cooling is not as great as that predicted by theory. The data for total enthalpy thickness are in fair agreement with the theoretical values with maximum cooling, but the data obtained on the uncooled surface do not agree with theory. As was pointed out for the Mach 3 studies, the probable source of error is in the measurement of total temperature near the edge of the boundary layer which can result in large errors in total enthalpy thickness due to the high mass flow rates at the edge of the boundary layer.

The variation of the boundary layer shape parameters with wall temperature ratio is shown in Fig. 25. The theoretical values of the shape parameters for cooled 1/5- and 1/7-power profiles were obtained from Ref. 33. The experimental values of the shape parameters are reduced by wall cooling, but the reduction is not as great as that predicted by the temperature-velocity relationship for the modified Crocco integral as tabulated in Ref. 33.

Isentropic Surface

Boundary layer surveys were obtained at five stations on the

isentropic-surface model for zero and maximum coolant flow rates. The wall temperature ratios were approximately 0.82 (uncooled) and 0.45 (cooled). Schlieren photographs of the flow over the isentropic-surface model at each of these temperature ratios are shown in Fig. 26. Measured and theoretical distributions of wall static pressure, measured wall temperature, and the calculated distribution of static pressure at the edge of the boundary layer are shown in Fig. 27. Good agreement was obtained between the measured and theoretical values of wall static pressure. There was no significant change in wall temperature along the surface of the model for the data obtained with the uncooled wall, but the data for the cooled wall show a fairly large longitudinal temperature gradient. The data for this case are reported at an average temperature ratio of 0.45 (0.36 at the upstream survey station and 0.57 at the last survey station). The survey stations and values of local surface angles are shown in the lower portion of the figure. Although the model had a total turning angle of 34 deg, the total turning angle at the last station at which surveys were obtained was 26.5 deg. Downstream of this station the flow was influenced by the expansion originating at the end of the curved surface. On this portion of the surface, the turning angle increases from 26.5 to 34.0 deg in a distance of 0.31 in. whereas the boundary layer thickness was 0.4 in.

Velocity and total temperature profiles are shown in Figs. 28 and 29. The velocity profiles at the 1-deg station show no significant change with cooling, whereas the velocity profiles at the downstream stations show a substantial improvement in shape and a decrease in boundary layer height with cooling. The total temperature profiles at the 1-deg station appear to be much the same as the flat-plate total temperature profiles with almost all of the change due to cooling occurring over the lower quarter of the profile. Downstream, the profiles differ farther away from the wall and, at the 12.8-deg station, the difference is seen over half of the profile. For the last two stations on the surface the measured total temperature profiles for the cooled case are higher than those for the uncooled case in the middle third of the profile. In spite of this apparent discrepancy, the total temperature for the cooled case is always less than or equal

to the total temperature for the uncooled case when total temperature is plotted as a function of the integrated mass flow since the cooled profiles have more mass flow near the wall than the uncooled profiles. Calculations of the mass flow in the boundary layer show that the profiles at the 24-deg station for the cooled case have 50% more mass flow than the uncooled profiles. As was the case for Mach 3, this increased mass flow within a given height implies that supersonic diffusers having cooled walls could operate with higher area contraction ratios and hence higher total pressure recoveries than uncooled inlets.

The data for displacement thickness and reduced shape parameter are presented in Fig. 30. The large decrease in δ^* for both cases is due to the large compression of the boundary layer over the length of the surface. Cooling caused an additional decrease in the displacement thickness at the downstream stations. At all stations, cooling caused a significant reduction (improvement) in the shape parameter. Figure 31 shows the variation of momentum thickness and corrected total enthalpy thickness with distance along the surface. The difference in initial level of the two curves is of the same order of magnitude as the accuracy of the data and hence is not significant; however, the over-all reduction in θ for the cooled surface is greater than that for the uncooled case as would be expected on the basis of the improved velocity profiles shown in Fig. 28. The corrected total enthalpy thickness data show a consistent increase with wall cooling.

The theoretical predictions of displacement thickness, reduced shape parameter, momentum thickness, and the upper and lower probable limits of corrected total enthalpy thickness, are also shown in Figs. 30 and 31. These predictions are based on the methods outlined in a previous section (see ANALYTICAL INVESTIGATION). The theoretical values of the reduced shape parameter (Fig. 30) show the same trends as the data, but the quantitative agreement is not as good as it was for Mach 3 circular-arc studies. The initial values of G were determined

from the Mach 6 flat-plate data (see Fig. 25). As can be seen from Fig. 30 the average deviation between the theoretical and experimental values of the shape parameter is on the order of 25%. As shown in APPENDIX III, the errors for the Mach 6 data introduced by the use of Eq. 8 are less than 10%, thus indicating that the errors introduced by the lag-length procedure are on the order of 20 to 25% for the Mach 6 data. This indicates the need for additional data for use in extending the lag-length correlation to higher Mach numbers. The data on which the existing correlation is based (see Ref. 1) were obtained in the Mach number range of 2.5 to 3.5. The theoretical values of the displacement thickness (top of Fig. 30) are in agreement with the data; however, the theoretical values of momentum thickness over the downstream portion of the surface (see Fig. 31) are significantly higher than the data. The maximum difference is about 35% of the measured value. This difference is the same order of magnitude as that obtained for the Mach 3 circular-arc studies; but it is in the opposite direction. For both configurations (Mach 3 circular arc and Mach 6 isentropic surface), the maximum discrepancies are within the limits of accuracy for the lag-length calculation procedure developed in Ref. 1. It should be noted, however, that the data on which the lag-length theory is based were obtained in the Mach number range of 2.0 to 3.5. An alternate calculation of the theoretical boundary layer growth over the Mach 6 isentropic compression surface was made by employing the method developed in Ref. 5. This calculation predicted boundary layer separation after 18 deg of isentropic compression, whereas the experimental results showed that the boundary layer did not separate at any point on the isentropic-compression surface having a total turn of 34 deg. Thus, even though there are relatively large differences between the lag-length theory and experiment, the values obtained from the lag-length theory are in better agreement with experiment than other available theories for predicting supersonic turbulent boundary layer growth over cooled walls in adverse pressure gradients.

The theoretical predictions for the upper and lower probable limits of corrected enthalpy thickness are presented in the lower portion of Fig. 31. For the cooled case, the data agree very well with the values

for the lower limit down to the 5.5-deg station and for downstream stations tend to fall between the two limits. For the uncooled case, the data also fall along the lower probable limit to the 5.5-deg station, but are above the upper limit downstream of the 12.8-deg station. Here again, there is a possibility of probe conduction error due to the low bleed flow through the probe in the distorted profiles at the two downstream stations. Complete elimination of this error would probably tend to reduce the ϕ_c in the uncooled case and increase ϕ_c in the cooled case. A statistical analysis of the data has indicated that the total heat flow is greater than the lower probable limit by an amount which is approximately 30% of the difference between the upper and lower probable limits.

CORRELATION OF SKIN-FRICTION AND HEAT-TRANSFER COEFFICIENTS

Calculation of heat transfer in both subsonic and supersonic flows is in general based on a form of Reynolds analogy which relates the Stanton number (heat-transfer coefficient), St, to the skin-friction coefficient, C_f. This relationship can be evaluated with the aid of the Crocco energy integral (see Refs. 34 and 36). In its simplest form the Crocco energy integral can be written as follows:

$$c_p T_T = C_1 + C_2 u \tag{11}$$

in which C_1 and C_2 are evaluated from the boundary conditions at the wall where $T_T = T_W$ and $u = 0$ and in the free stream where $T_T = T_{T_0}$ and $u = u_0$. It should be noted that the Crocco integral was derived for laminar flow and for a Prandtl number of unity; hence its application to the turbulent flow of a gas having a nonunity Prandtl number is

questionable. However, the type of data presented herein (velocity and total-temperature profiles) allows a direct check on the applicability of the Crocco integral to flows of the type studied. Data from one of the Mach 6, cooled, flat-plate profiles are cross plotted in terms of total temperature and velocity in Fig. 32. In this representation the value for the Crocco integral would be a straight line between the wall temperature ratio (at zero velocity) and unity total temperature ratio (at unity velocity ratio). It can be seen from this figure that the measured total temperature deviates from the values for the Crocco integral especially for the higher velocity ratios where it is higher than that predicted by the Crocco integral. These higher total temperatures may be a result of the stepwise temperature distribution (uncooled over initial portion, cooled over rear portion) on the flat plate over which the boundary layer developed. Most of the mass flow in the boundary layer is in the high velocity region; hence, the momentum thickness, θ , and the total enthalpy thickness, ϕ , obtained by integrating the profile data are appreciably different from those predicted on the basis of a Crocco energy integral.

All the flat-plate velocity profiles were plotted on temperature-velocity coordinates in the manner of Fig. 32 and, in general, a straight line drawn between the wall temperature and the data points in the lower velocity region of the boundary layer has the same slope as the data points in that region. It should be noted that the first data point having a non-zero velocity was obtained with the probe touching the wall and hence the measured temperature was in error as a result of heat conduction from the probe to the wall. Consequently, no attempt was made to fair the line through the first data point in the profile. The linear total-temperature relationship over the lower velocity portion of the profile suggested that locally (in the laminar sublayer) a Crocco energy integral is valid and hence the temperature-velocity derivative at the wall is adequately defined and can be employed in evaluating the ratio of the Stanton number to skin-friction

coefficient, St/C_f . It should be noted that a direct evaluation of the heat transfer rate ($k \frac{\partial T_s}{\partial y}\Big|_w$) and wall shearing stress ($\mu \frac{\partial u}{\partial y}\Big|_w$) could not be made from the derivatives of the temperature and velocity with respect to y because a straight-line fairing from the wall condition did not blend with the profile data near the wall.

The following equation was employed in relating the Stanton number to the skin-friction coefficient (see APPENDIX II for derivation of derivative method).

$$\frac{St}{C_f} = \frac{\dfrac{\partial(T_T/T_{T_0})}{\partial(u/u_w)}\Big|_w}{2Pr\left(\dfrac{T_R}{T_{T_0}} - \dfrac{T_w}{T_{T_0}}\right)} \qquad (12)$$

In order to evaluate Eq. 12 the temperature-velocity derivatives at the wall were plotted as a function of the difference between the recovery and measured wall-temperature ratios, as shown in Fig. 33. When plotted in this form the data had a linear relationship with very little scatter and there was no significant difference between the Mach 3 and Mach 6 flat-plate data. A least-squares line originating at the origin was faired through all the data to establish an average slope for evaluating St/C_f by Eq. 12. For a Prandtl number of 0.70 (average value for range of wall temperatures covered) the ratio of Stanton number to skin-friction coefficients from Eq. 12 is 0.95, with a standard deviation of an individual point being about 6%. This value (0.95) is significantly higher than that obtained from the Reynolds-Colburn analogy (Ref. 34) as follows:

$$\frac{St}{C_f} = \frac{1}{2Pr^{2/3}} = 0.635 \text{ FOR } Pr = 0.70 \qquad (13)$$

In order to check the order of magnitude of St/C_f , an alternate method was employed. This method used the integral quantities of

momentum thickness, θ , and total enthalpy thickness, ϕ . It is shown in APPENDIX II that the following equation relates St and C_f with ϕ and θ for flat-plate boundary layer growth over an isothermal surface.

$$\frac{St}{C_f} = \frac{\phi/\theta}{2\left(\frac{T_R}{T_{T_0}} - \frac{T_W}{T_{T_0}}\right)} \tag{14}$$

Since the model employed for the experiments did not have an isothermal surface over the entire length of boundary layer growth (the front portion, about half the total length, was uncooled and resulted in a stepwise temperature distribution), the effective wall temperature (a length-weighed average defined below) was used in evaluating Eq. 14.

$$T'_W = \frac{T_{W_1} L_1 + T_{W_2} L_2}{L_1 + L_2} \tag{15}$$

In this equation the subscript 1 refers to the uncooled portion and the subscript 2 refers to the length of cooled portion up to the measuring station. This approximation for the effective temperature could be improved by incorporating an average skin-friction coefficient (see APPENDIX II); however, the increased accuracy was not justified on the basis that the total enthalpy thickness integral, ϕ , was already believed to be the least accurate quantity in the expression. The ratios of ϕ/θ for all the flat-plate data were plotted as a function of the difference between the recovery and effective wall temperature ratios as shown in Fig. 34. A least-squares straight line was faired through the data and the origin. The standard deviation of a point was about 17%, and again there was no significant difference between the Mach 3 and Mach 6 data. The ratio of St/C_f evaluated by this integral

method was 0.805. Although this value of the ratio of Stanton number to skin-friction coefficient is lower than that obtained by the first (differential) method, it, too, is significantly higher than the theoretical value obtained from Eq. 13. Both methods, however, are subject to errors in the measured total temperature. If the true temperatures were lower than the values used, the ratio of St/C_f computed from the derivative method would be lower and the ratio of St/C_f computed by the integral method would be higher than the values obtained in the present analysis. In order to decrease the ratio of Stanton number to skin-friction coefficient by both methods, the true total temperature would have to be lower than the value used near the wall and higher than the value used near the free stream. The method used to evaluate total temperature (discussed in APPENDIX I) has already favored the data in the direction of lower values of St/C_f over more conventional ways of evaluating total temperature from the temperatures measured with a shielded thermocouple.

A factor which may contribute to the measurement of a high value for St/C_f is the use of a wall which was not cooled from the origin of the boundary layer growth; heat transfer rates greater than the flat-plate value would be expected at the beginning of the cooled portion of a plate having a stepwise temperature distribution. This problem is discussed in Ref. 37. From the data presented in this reference the error in heat-transfer coefficient that would be expected from the first (differential) method would range from 10 to 15%, and the error expected from the second (integral) method would range from 15 to 25%. Thus, errors due to a stepwise temperature distribution can be quite large for the present experiments and can account for the difference between the theoretical value, $St/C_f = 0.635$, and the measured value, $St/C_f = 0.81$, obtained from the integral method; however, these errors do not account for the large difference between the theory and the value obtained by the differential method, $St/C_f = 0.95$, which gave more self-consistent results. The value calculated by the differential method was based on wall derivatives obtained from straight-line fairings on the total temperature-velocity plots (see Fig. 32). More data in the lower velocity region of the

boundary layer is needed to verify that such a linear relationship is valid.

Since the derivative method of evaluating the ratio of Stanton number to skin-friction coefficient for the flat-plate data gives the more consistent results, this method was also employed to evaluate St/C_f for the boundary layer growth in adverse pressure gradients. The data were evaluated at each measuring station on the circular-arc and isentropic-surface models and for each deflection angle of the shock-generator tests. The results are presented in Fig. 35 as a function of the total deflection angle, ψ, through which flow was turned. The flagged symbols for the high deflection angles indicate that St/C_f may be higher than that shown by the data. For these data points, a straight-line fairing on the temperature-velocity plot (see Fig. 32) from the wall did not blend with the data points in the lower part of the profile. The resulting error is believed to be in a direction which reduces the measured values of St/C_f. The data presented in Fig. 35 show that the ratio of St/C_f increases as the total deflection angle (the amount of deceleration) is increased and that the deviation from the flat-plate value is greatest for the most severe pressure gradients (shock generator) and lowest for the mildest pressure gradients (isentropic surface). This increase in St/C_f does not imply, however, that the heat transfer is increasing at these points since the skin-friction coefficient is less than the flat-plate value due to the distorted profile.

REFERENCES

1. McLafferty, G. H., and R. E. Barber: Turbulent Boundary Layer Characteristics in Supersonic Stream Having Adverse Pressure Gradients. UAC Research Laboratories Report R-1285-11, September 1959 (to be published in January-February 1962 issue of Journal of the Aerospace Sciences).

2. Kepler, C. E., J. W. Cnossen, and P. E. Demarest: Hypersonic Inlet Investigations Including Tests to Mach 8.7 and Theoretical Analyses to Mach 15. ASD Technical Report 61-137, June 1961. Confidential. (Unclassified title) *

3. Gadd, G. E.: An Experimental Investigation of Heat Transfer Effects on Boundary Layer Separation in Supersonic Flow, Journal of Fluid Mechanics, Vol. 2, Part 2, March 1957.

4. Seban, R. A., and H. W. Chan: Heat Transfer to Boundary Layers with Pressure Gradients. WADC Technical Report 57-111, May 1958.

5. Reshotko, E., and M. Tucker: Approximate Calculation of the Compressible Turbulent Boundary Layer with Heat Transfer and Arbitrary Pressure Gradient, NACA TN 4154, December 1957.

6. Tetervin, N. and C. C. Lin: A General Integral Form of the Boundary-Layer Equation for Incompressible Flow with an Application to the Calculation of the Separation Point of Turbulent Boundary Layers. NACA Report 1046, 1951.

7. Monaghan, R. J., and J. R. Cooke: The Measurement of Heat-Transfer and Skin Friction at Supersonic Speeds, Part III: Measurements of Over-all Heat-Transfer of the Associated Boundary Layers on a Flat Plate at M = 2.43. RAE Technical Note Aerodynamics 2125, March 1954.

8. Lobb, R. K., E. M. Winkler, and J. Persh: Experimental Investigation of Turbulent Boundary Layers in Hypersonic Flow. Journal of the Aeronautical Sciences, Vol. 22, January 1955.

REFERENCES
(Contd.)

9. Hill, F. K.: Turbulent Boundary-Layer Measurements at Mach numbers from 8 to 10. Physics of Fluids, Vol. 2, No. 6, November-December 1959.

10. Winkler, E. M.: Investigation of Flat-Plate Hypersonic, Turbulent Boundary Layers with Heat Transfer. Journal of Applied Mechanics, September 1961.

11. Van Driest, E. R.: The Turbulent Boundary Layer with Variable Prandtl Number. North American Aviation, Inc., Report No. AL-1914, April 1954.

12. Persh, J.: A Theoretical Investigation of Turbulent Boundary Layer Flow with Heat Transfer at Supersonic and Hypersonic Speeds. NOL NAVORD Report 3854, May 1955.

13. Ackeret, J., F. Feldmann, and N. Rott: Investigations of Compression Shocks and Boundary Layers in Gases Moving at High Speed. NACA TM 1113, January 1947.

14. Fage, A., and R. E. Sargent: Shock Wave and Boundary Layer Phenomena Near a Flat Surface. Proceedings of the Royal Society, Vol. 190, Series A, No. 1020, June 1947.

15. Liepmann, H. W., A. Roshko, and S. D. Dhawan: On Reflection of Shock Waves from Boundary Layers. NACA TN 2334, April 1951.

16. Barry, F. W., A. H. Shapiro, and E. P. Neumann: The Interaction of Shock Waves with Boundary Layers on a Flat Surface. Journal of the Aeronautical Sciences, Vol. 18, No. 4, April 1951.

17. Donaldson, C. duP., and R. H. Lange: A Study of the Pressure Rise Across Shock Waves Required to Separate Laminar and Turbulent Boundary Layers. NACA TN 2770, September 1952.

REFERENCES
(Contd.)

18. Bogdonoff, S. M., C. E. Kepler, and E. Sanlorenzo: A Study of Shock Wave Turbulent Boundary Layer Interaction at M = 3. Princeton University, Report No. 222, July 1953.

19. Kepler, C. E., and S. M. Bogdonoff: Interaction of a Turbulent Boundary Layer with a Step at M = 3. Princeton University, Report No. 238, September 1953.

20. Gadd, G. E., D. W. Holder, and J. D. Regan: An Experimental Investigation of the Interaction Between Shock Waves and Boundary Layers. Proceedings of the Royal Society, Vol. 226, Series A, October 1954.

21. Lange, R. H.: Present Status of Information Relative to the Prediction of Shock-Induced Boundary-Layer Separation. NACA TN 3065, February 1954.

22. Chapman, D. R., D. M. Kuehn, and H. K. Larson: Investigation of Separated Flows in Supersonic and Subsonic Streams with Emphasis on the Effect of Transition. NACA TN 3869, March 1957.

23. Hammitt, A. G., I. E. Vas, and S. Hight: An Analysis of the Effect of Shock Waves on Turbulent Boundary Layers. Princeton University, Report No. 396, AFOSR TN 57-297, July 1957.

24. Tyler, R. D., and A. H. Shapiro: Pressure Rise Required for Separation in Interaction Between Turbulent Boundary Layer and Shock Wave. Journal of the Aeronautical Sciences, Vol. 20, No. 12, December 1953.

25. Crocco, L., and R. F. Probstein: The Peak Pressure Rise Across an Oblique Shock Emerging From a Turbulent Boundary Layer Over a Plane Surface. Princeton University, Report No. 254, March 1954.

26. Mager, A.: Prediction of Shock-Induced Turbulent Boundary Layer Separation. Journal of the Aeronautical Sciences, Vol. 22, No. 3, March 1955.

REFERENCES
(Contd.)

27. Reshotko, E., and M. Tucker: Effect of a Discontinuity on Turbulent Boundary-Layer-Thickness Parameters with Application to Shock-Induced Separation. NACA TN 3454, May 1955.

28. Hammitt, A. G.: An Approximate Theory of Turbulent Boundary Layer Shock Wave Interaction. Princeton University, Report No. 340, AFOSR TN 56-160, April 1956.

29. Kuehn, D. M.: Experimental Investigation of the Pressure Rise Required for the Incipient Separation of Turbulent Boundary Layers in Two Dimensional Supersonic Flow. NASA Memo 1-21-59A, February 1959.

30. Kuehn, D. M.: Turbulent Boundary-Layer Separation Induced by Flares on Cylinders at Zero of Attack. NASA TR R-117, 1961.

31. Ludwieg, H. and W. Tillman: Investigations of the Wall-Shearing Stress in Turbulent Boundary Layers. NACA TM 1285, 1950.

32. Eckert, E. R. G.: Engineering Relations for Friction and Heat Transfer to Surfaces in High Velocity Flow. Journal of the Aeronautical Sciences, Vol. 22, No. 8, August 1955, pp. 585-586.

33. Persh, J. and R. Lee: Tabulation of Compressible Turbulent Boundary Layer Parameters. NAVORD Report 4282, May 1956.

34. Schlichting, H.: Boundary Layer Theory. McGraw-Hill Book Co., New York. 4th Edition, 1960.

35. Tucker, M.: Approximate Turbulent Boundary-Layer Development in Plane Compressible Flow Along Thermally Insulated Surfaces with Application to Supersonic-Tunnel Contour Correction. NACA TN 2045, March 1950.

REFERENCES
(Contd.)

36. Truitt, R. W.: Fundamentals of Aerodynamic Heating. Ronald Press Company, New York, 1960.

37. Conti, R. J.: Heat-Transfer Measurements at a Mach Number of 2 in the Turbulent Boundary Layer on a Flat Plate Having a Stepwise Temperature Distribution. NASA TN D-159, November 1959.

38. Landenburg, R. W., et al: Physical Measurements in Gas Dynamics and Combustion. High Speed Aerodynamic and Jet Propulsion, Vol. IX, Princeton University Press, 1957.

39. New Mach Number Tables for Internal Ram-Jet Flow Analysis. Consolidated Vultee Aircraft Corporation, Ordnance Aerophysics Laboratory. OAL Memorandum 50, April 1952.

*Note: No Classified material extracted from this report.

APPENDIX I

METHOD OF EVALUATING TOTAL TEMPERATURE THROUGH A BOUNDARY LAYER

The temperature measured by a shielded thermocouple probe does not equal the local total temperature of the stream. For a shielded thermocouple probe of the type used herein (see Fig. 5), the velocity of the air past the thermocouple junction is in the very low subsonic speed range and, as a result, the recovery temperature at the junction should be within 1/10 of 1% of the true total temperature. However, most probes of this type indicate considerably lower temperatures. The conventional way of correcting the measured probe temperature is to employ a recovery factor for the probe based on a probe calibration. Most probes have recovery factors varying from 0.94 to 0.98 (see Ref. 38) depending on the method of fabrication. The difference between the true and measured temperatures is commonly cr ıited to radiation effects which has led to the use of multiple shields. However, after an examination of the order of magnitude of the radiation effect in the probes employed herein it was concluded that radiation was not the primary cause of probe temperature errors; the real source of error was felt to be due to conduction from the thermocouple wires to the average temperature of the probe head. If the error is assumed to be due to conduction, the following heat balance can be written:

$$\text{heat into junction} \quad \dot{q} = \bar{S}\,\rho\,\bar{U}\,c_p(T_T - T_M)A_1 \tag{16}$$

$$\text{heat out of junction} \quad q = k\frac{A_2}{\ell_2}(T_M - T_P) \tag{17}$$

where T_T is the local total temperature, T_M the temperature of the junction (measured temperature); T_P the average probe temperature;

A_1, A_2, ℓ_2 are some effective areas and lengths (all unknown) which are introduced to provide the correct units; and the bars ($\bar{}$) denote average conditions. The quantities that vary during a boundary layer survey are the temperatures and the mass flow ($\bar{\rho}\bar{u}$) through the probe. When a supersonic boundary layer is surveyed the ratio of pitot to external static pressure is usually large enough (except right next to the wall) to choke the bleed hole. Hence the mass flow through the probe can be expressed as:

$$\rho u A_3 = \rho^* u^* A^* = \frac{\bar{m}^* P_p A^*}{\sqrt{T_T}} \tag{18}$$

where the starred conditions (*) refer to the sonic conditions at the bleed hole and $\bar{m}^*$ is a Mach number function tabulated in Ref. 39. By substituting Eq. 18 into Eq. 16 and equating Eqs. 16 and 17 the following expression is obtained:

$$\bar{St}\, \bar{m}^* \frac{P_p}{\sqrt{T_T}} \frac{A^*}{A_3} c_p (T_T - T_M) A_1 = k \frac{A_2}{\ell_2} (T_M - T_p) \tag{19}$$

By combining all the unknown constants into one new constant, B'',

$$\frac{P_p}{\sqrt{T_T}} (T_T - T_M) = B'' (T_M - T_p) \tag{20}$$

Since we are looking for small temperature differences, the variation

of $\sqrt{T_T}$ can be neglected leaving the following:

$$P_p(T_T - T_M) = B(T_M - T_p) \tag{21}$$

where B must be determined from an experimental calibration.

A probe calibration test was performed at Mach 6 with the probe located in the free stream where $T_T = T_{T_0} \approx 860\,R$. The mass flow through the probe was controlled by varying the tunnel stagnation pressure which in turn varied the pitot pressure. The results of this calibration are shown in Fig. 36. These tests showed that the measured temperature decreased (temperature error increased) as the mass flow (proportional to pitot pressure) decreased. Furthermore, the measured variation in the temperature error could be predicted from the relationship given in Eq. 21. Also shown in this figure is the temperature error that would be predicted by the conventional technique of assigning a constant recovery factor ($\eta_R = .94$) to the probe. It can be seen that the temperature error determined by the conventional method would be low by a significant amount. Conversely, correcting the measured probe temperature by assigning a constant recovery factor to the probe would result in significant errors in the calculated total temperature.

The method of correcting the measured temperature employed Eq. 21 with the constant B evaluated in the free stream. The average probe temperature, T_p , was assumed to be the laminar recovery temperature on the probe head. Thus:

$$T_p = T_T \left(\frac{1 + \eta_R \frac{\gamma-1}{2} M^2}{1 + \frac{\gamma-1}{2} M^2} \right) \tag{22}$$

where η_R is the laminar recovery factor.

Substituting Eq. 22 into Eq. 21

$$P_p(T_T - T_M) = B\left[T_M - T_T\left(\frac{1+\eta_R\frac{\gamma-1}{2}M^2}{1+\frac{\gamma-1}{2}M^2}\right)\right] \tag{23}$$

Rearranging

$$T_T\left[P_p + B\left(\frac{1+\eta_R\frac{\gamma-1}{2}M^2}{1+\frac{\gamma-1}{2}M^2}\right)\right] = T_M(P_p + B) \tag{24}$$

After nondimensionalizing and rearranging

$$\frac{T_T}{T_{T_0}} = \frac{T_M}{T_{T_0}}\left[\frac{\frac{P_p}{P_{T_0}} + B'}{\frac{P_p}{P_{T_0}} + B'\left(\frac{1+\eta_R\frac{\gamma-1}{2}M^2}{1+\frac{\gamma-1}{2}M^2}\right)}\right] \tag{25}$$

Where B' is the new constant after nondimensionalizing.

A comparison of the present method (Eq. 25) with the conventional method (η_R = const) of computing the total temperature variations through a typical cooled boundary layer at Mach 6 is shown in Fig. 37. Both methods correct the measured temperature at the edge of the boundary layer to the free-stream total temperature and both methods produce very little correction near the wall (correction is zero when velocity is zero); however, between the wall and edge of the boundary

layer the present method results in a higher total temperature. In the integration of the total enthalpy thickness, ϕ, (see Data Reduction Procedure) it is the temperature difference $(1-T_T/T_{T_0})$ which enters into the calculation. At the outer edge of the boundary layer the temperature difference computed by the present method is about half of the temperature difference computed with a constant recovery factor. Consequently the value of ϕ computed by the present method is considerably less than would be computed by the assumption of a constant probe recovery factor. This method of reducing data leads to a more conservative (lower) estimate of the ratio of Stanton number to skin-friction coefficient as discussed in the section entitled CORRELATION OF SKIN-FRICTION AND HEAT-TRANSFER COEFFICIENTS. The current evaluation of the probe temperature correction is felt to be an improvement on the state-of-the-art in temperature measurement; however, further refinements are still necessary to improve the accuracy of temperature measurements when quantities involving small temperature differences (such as ϕ) are to be calculated.

APPENDIX II

DEVELOPMENT OF DIFFERENTIAL AND INTEGRAL METHODS OF CORRELATING SKIN-FRICTION AND HEAT-TRANSFER COEFFICIENTS

Differential Method

The following heat-transfer and skin-friction equations relate the conditions at the wall to the free-stream conditions:

$$St\rho_0 u_0 c_p (T_R - T_w) = \dot{q} = k \left.\frac{\partial T_s}{\partial y}\right|_w \tag{26}$$

$$C_f \tfrac{1}{2} \rho_0 u_0^2 = \tau_w = \mu \left.\frac{\partial u}{\partial y}\right|_w \tag{27}$$

where the subscript w refers to conditions evaluated at the wall. By dividing Eq. 26 by Eq. 27 and rearranging the following form is obtained.

$$\frac{St}{C_f} = \frac{u_0}{2\left(\frac{\mu c_p}{k}\right)(T_R - T_w)} \cdot \left.\frac{\partial T_s}{\partial u}\right|_w \tag{28}$$

Employing the energy equation in the following form,

$$T_s = T_T - \frac{1}{2c_p} u^2 \tag{29}$$

differentiating,

$$\frac{\partial T_S}{\partial u} = \frac{\partial T_T}{\partial u} - \frac{u}{c_p} \tag{30}$$

and evaluating at the wall where $u = 0$, the following result is obtained:

$$\left.\frac{\partial T_S}{\partial u}\right|_w = \left.\frac{\partial T_T}{\partial u}\right|_w \tag{31}$$

By substituting Eq. 31 into Eq. 28 and nondimensionalizing, the following form is obtained:

$$\frac{St}{C_f} = \frac{\left.\dfrac{\partial (T_T/T_{T_0})}{\partial (u/u_0)}\right|_w}{2\,Pr\left(\dfrac{T_R}{T_{T_0}} - \dfrac{T_W}{T_{T_0}}\right)} \tag{32}$$

where $Pr = \mu c_p / k$

Eq. 32 can now be employed to evaluate St/C_f from the experimental data.

Integral Method

The following equations for flat-plate boundary layer growth relate the boundary layer momentum thickness and total enthalpy thickness to the skin-friction coefficient and Stanton number (heat-transfer coefficient).

$$\rho_0 u_0 c_p T_{T_0} \phi = \int_0^x St \rho_0 u_0 c_p (T_R - T_W)\, dx \tag{33}$$

$$\rho_0 u_0^2 \theta = \int_0^x C_f \tfrac{1}{2} \rho_0 u_0^2 \, dx \tag{34}$$

By dividing Eq. 33 by Eq. 34 and rearranging, the following form is obtained.

$$\frac{\phi}{\theta} = \frac{2\int_0^x St\left(\frac{T_R}{T_{T_0}} - \frac{T_W}{T_{T_0}}\right) dx}{\int_0^x C_f \, dx} \tag{35}$$

If an isothermal surface (T_W = const.) is considered, and, if St/C_f = const, Eq. 35 can be written in the following form.

$$\frac{\phi}{\theta} = \frac{2\left(\frac{T_R}{T_{T_0}} - \frac{T_W}{T_{T_0}}\right) \frac{St}{C_f} \int_0^x C_f \, dx}{\int_0^x C_f \, dx} \tag{36}$$

Then, even though C_f varies along the surface, the integrals cancel leaving the following relationship:

$$\frac{St}{C_f} = \frac{\phi/\theta}{2\left(\frac{T_R}{T_{T_0}} - \frac{T_W}{T_{T_0}}\right)} \tag{37}$$

For the case of a nonisothermal wall which has a stepwise temperature distribution, Eq. 37 can be written in the same manner by subsituting

an effective wall temperature, T'_w , for T_w where T'_w is defined by:

$$T'_w = \frac{\bar{C}_{f_1} T_{w_1} L_1 + \bar{C}_{f_2} T_{w_2} L_2}{\bar{C}_{f_1} L_1 + \bar{C}_{f_2} L_2} \tag{38}$$

In this equation the subscript 1 refers to the conditions over the front portion and the subscript 2 refers to the conditions over the rear portion, and $\bar{C}_f$ is the average skin-friction coefficient over the respective portions of the plate. For simplicity in evaluating the data, $\bar{C}_{f_1}$, was assumed equal to $\bar{C}_{f_2}$.

APPENDIX III

EVALUATION OF THE VALIDITY OF THE ASSUMPTION FOR THE REDUCED SHAPE PARAMETER USED IN THE ANALYTICAL INVESTIGATION

The method of analysis used to predict the growth of a cooled supersonic turbulent boundary layer in the presence of an adverse pressure gradient was based on the lag-length procedure of Ref. 1 which was developed for flow over an insulated surface. In order to modify this procedure to account for the effect of wall cooling, it was necessary to evaluate the change in the boundary layer shape parameter due to wall cooling. In order to provide this information, an assumption was made relating the shape parameter, G, of a cooled boundary layer in an adverse pressure gradient to the shape parameter of an uncooled (adiabatic wall) boundary layer in an adverse pressure gradient. This assumption was described analytically by Eq. 8 in the section entitled ANALYTICAL INVESTIGATION. This equation may be re-written as follows:

$$\left(\frac{G_{COOLED}}{G_{ADIABATIC}}\right)_{\substack{ADVERSE\\PRESSURE\\GRADIENT}} = \left(\frac{G_{COOLED}}{G_{ADIABATIC}}\right)_{FLAT\ PLATE} \qquad (39)$$

The ratio of the cooled to adiabatic shape parameter for a flat-plate boundary layer was evaluated from the data obtained during the flat-plate tests. The flat-plate value was obtained from a direct plotting of the data presented in Figs. 10 and 25. The ratio $G_{COOLED}/G_{ADIABATIC}$ for both the Mach 3 and 6 flat-plate data is plotted as a function of the ratio of wall temperature to recovery temperature in Fig. 38. Both sets of data fall along a single line with an r.m.s. scatter of 1.4% and virtually all the data lie within two standard deviations (2.8%) of the line.

The validity of Eq. 39 may be evaluated by comparing the ratio of $G_{COOLED}/G_{ADIABATIC}$ for both the curved-surface data and the flat-plate data. If the data from both types of tests exhibit the same trends (when plotted as a function of wall temperature ratio), it may then be concluded that the assumption of Eq. 39 is a good first approximation to the physical phenomena. However, none of the data were obtained with adiabatic wall conditions due to heat transfer from the tunnel to the room. Therefore, before making the above-mentioned comparison, it was necessary to evaluate the reduced shape parameter for the adiabatic wall conditions.

Two different methods were employed to evaluate the adiabatic wall values of G at each station on the curved surface models. These two methods, the averaging method and the extrapolation method, are compared in Fig. 39 for the 12 deg station on the Mach 3 circular-arc model. The greatest deviation between these two methods occurs for the data obtained at this station. The adiabatic wall value obtained by the averaging method was evaluated by employing Eq. 39 and inverting the calculation procedure to determine, for each data point, the value of $G_{ADIABATIC}$ which is consistent with the calculation procedure. These values are shown by the open triangular symbols in the figures. The average of these values, shown by the solid triangular symbol, was used to determine the value of $G_{COOLED}/G_{ADIABATIC}$. The adiabatic wall value obtained by the extrapolation method was evaluated by fairing a curve through the data and extrapolating this curve to the adiabatic value of the wall temperature ratio. This value is shown by the solid square symbol. This method of obtaining the adiabatic value gives most weight to the data point at the highest value of the wall temperature, whereas the averaging method weights all points evenly.

The results of calculations of $G_{COOLED}/G_{ADIABATIC}$ for the Mach 3 circular-arc data and Mach 6 isentropic surface data are shown in Figs. 40 and 41. In these figures the dashed curves are the same as faired data curves from Figs. 20 and 30. As shown in Fig. 40, the averaging method results in several values for the reduced shape parameter for the adiabatic surface condition at each station. These values were

evenly weighted to obtain the mean curves for the adiabatic shape parameter. These curves are shown on the figure for both the Mach 3 and Mach 6 curved surfaces. The shaded region about the mean adiabatic wall curve is shown to indicate the maximum accuracy to be expected on the basis of the 2.8% scatter of the flat-plate shape parameters shown in Fig. 38. Most of the calculated values of adiabatic shape parameter lie within or very near the shaded bands. Since it is more difficult to measure the boundary layer profiles on the curved surface models, it is to be expected that this data should be less accurate than the flat-plate data. The results of the calculations using the extrapolation method are shown in Fig. 41. The values of $G_{ADIABATIC}$ obtained in this manner always fall above the data curves whereas the values of $G_{ADIABATIC}$ obtained by the averaging method sometime fall below the faired curve through the uncooled data, see Fig. 40.

The values of the adiabatic shape parameter at each station on the curved surface models were then employed to obtain the ratio of $G_{COOLED}/G_{ADIABATIC}$ for each data point. This ratio for both methods is plotted in Fig. 42 as a function of the ratio of wall temperature to recovery temperature. The theoretical curve used in Eq. 8 (obtained from the flat-plate data shown in Fig. 38) is also shown in Fig. 42. The ratios computed using the averaging method shown in the upper half of Fig. 42, scatter about the theoretical curve with an r.m.s. deviation of 3.5%. The 2.8% band which contained the flat-plate data of Fig. 38 is also shown on this figure for comparison. The maximum deviation from this line is 8.6% (or 2.5 standard deviations) and occurs for the Mach 3 data with no coolant flow. The r.m.s. deviation of 3.5% is the order of accuracy to be expected from the experimental measurements of boundary layer profiles in an adverse pressure gradient.

The ratios computed using the extrapolation method, shown in the lower half of Fig. 42, exhibit a large deviation from the theoretical value at the low values of the temperature ratio, but show small deviations at the high values of the wall temperature ratio due to the manner in which these points were weighted. When using this method the data at a given station fair to a value of 1.0 at a wall temperature ratio

of 1.0; hence the values of $G_{COOLED}/G_{ADIABATIC}$ at high wall temperature ratios are forced to exhibit a relatively low scatter. For this reason an r.m.s. deviation of all the data would not represent the overall accuracy of Eq. 39 and hence σ r.m.s. is not shown. In general, the ratios for the Mach 3 data fall below the theoretical curve, whereas the ratios for the Mach 6 data scatter about the theoretical curve. The maximum deviation of this ratio for the Mach 3 data occur at the 12 and 18 deg stations. Examination of the data presented in Figs. 20 and 41 shows that the values of this ratio are strongly influenced by the two data points obtained with no wall cooling (high temperature ratios). If the value of these two data points were assumed to be 5% lower than shown, the correlation obtained for the Mach 3 data would be in agreement with the correlation obtained by the averaging method.

The correlation obtained by the averaging method indicates that Eq. 39 can be employed to calculate shape parameters within the limit of accuracy of experimental data. The correlation obtained by the extrapolation method indicates that Eq. 39 will predict the correct trends but that the errors introduced may be larger than expected from experimental data and may be of the same order of magnitude as the theoretical correction for wall cooling.

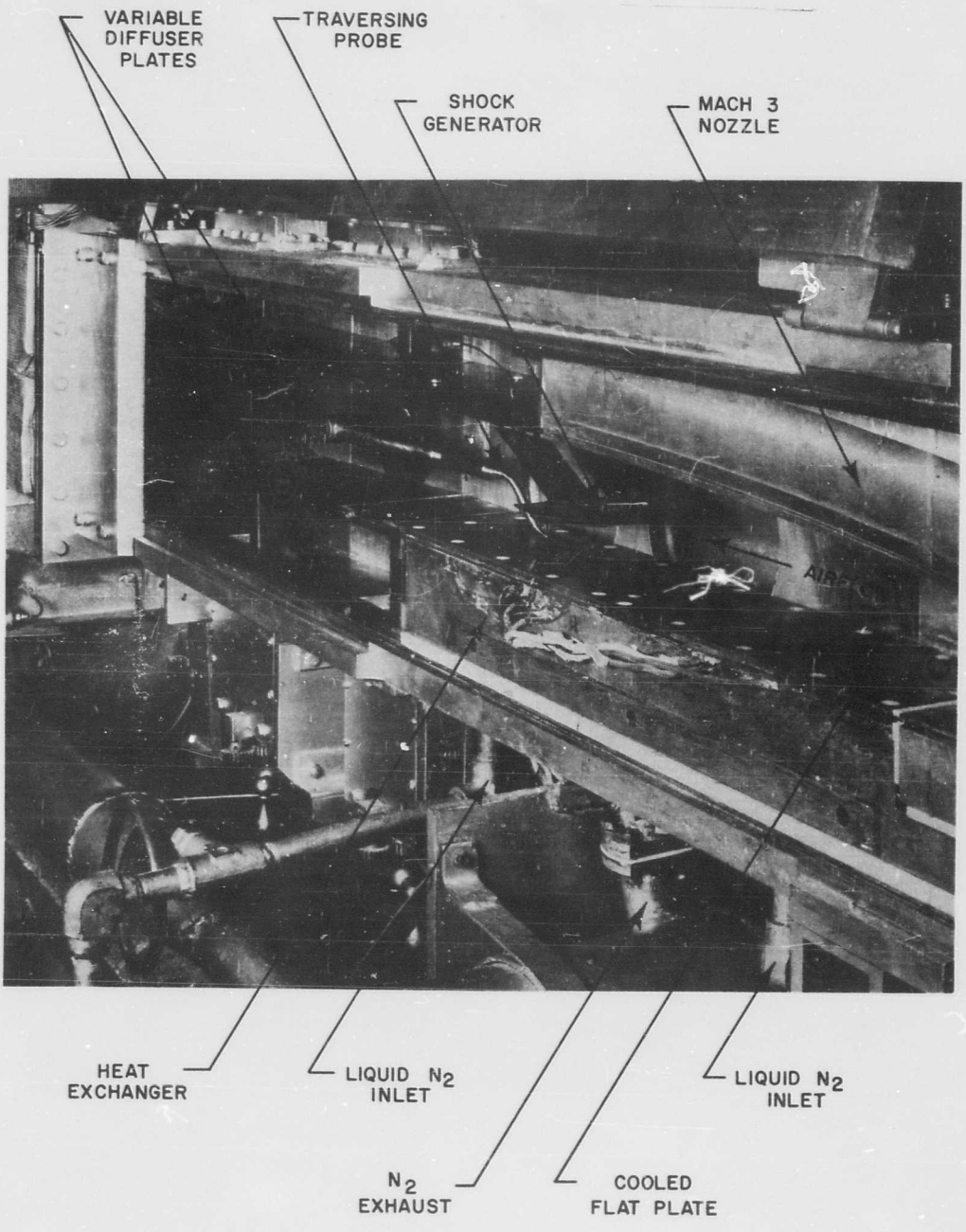

FIGURE 1 PHOTOGRAPH OF TUNNEL WITH MACH 3 NOZZLE, COOLED FLAT PLATE, AND SHOCK GENERATOR INSTALLED

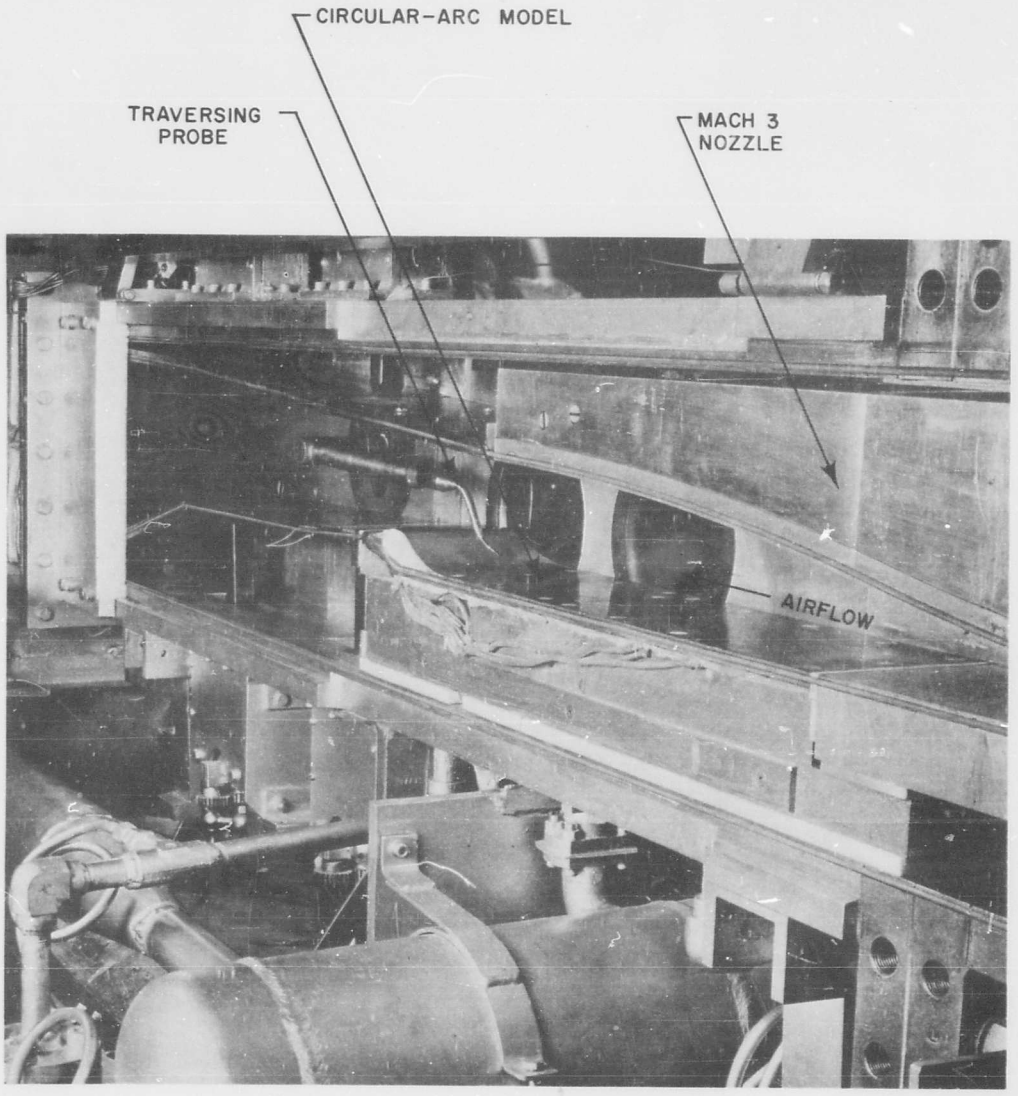

FIGURE 2 PHOTOGRAPH OF TUNNEL WITH MACH 3 NOZZLE AND COOLED CIRCULAR-ARC MODEL INSTALLED

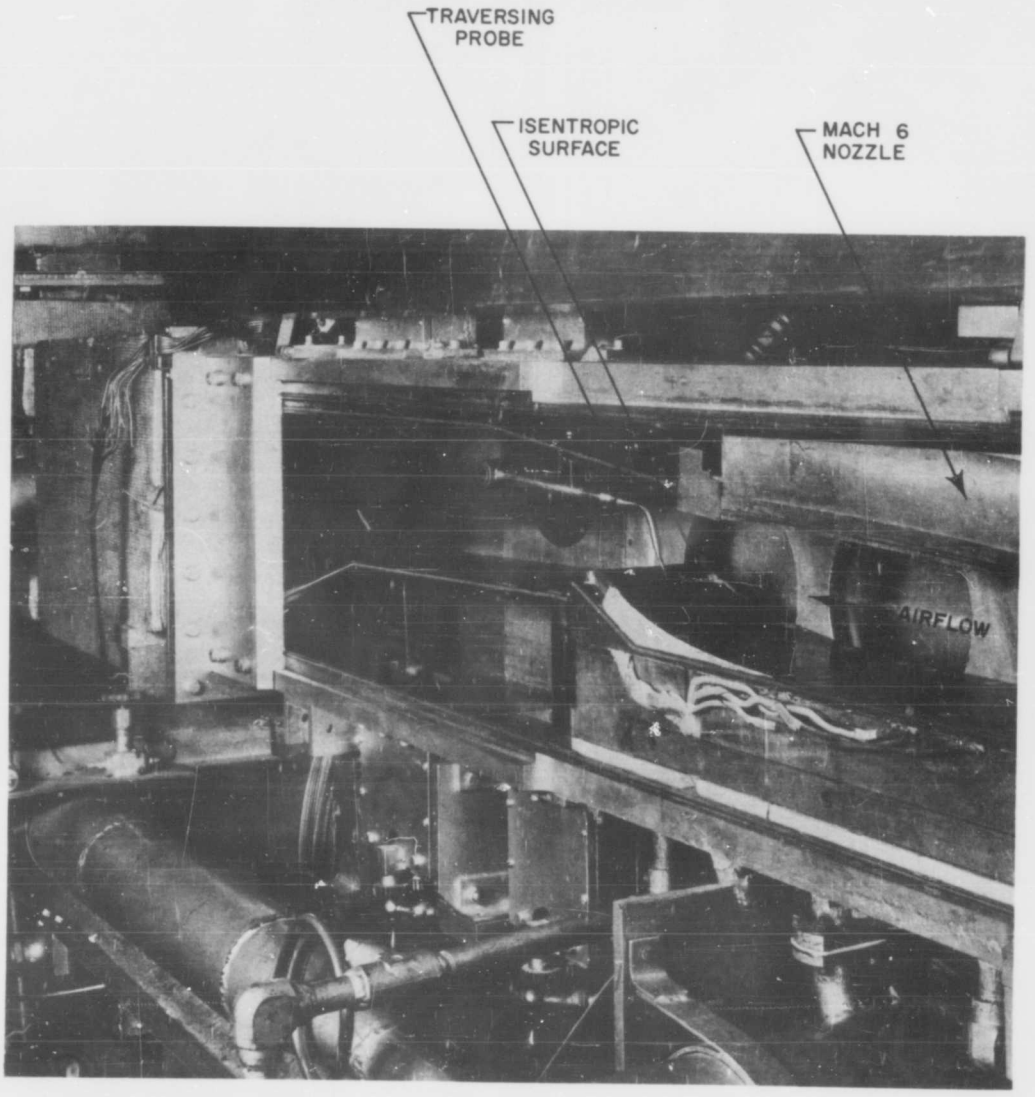

FIGURE 3 PHOTOGRAPH OF TUNNEL WITH MACH 6 NOZZLE AND COOLED ISENTROPIC-SURFACE MODEL INSTALLED

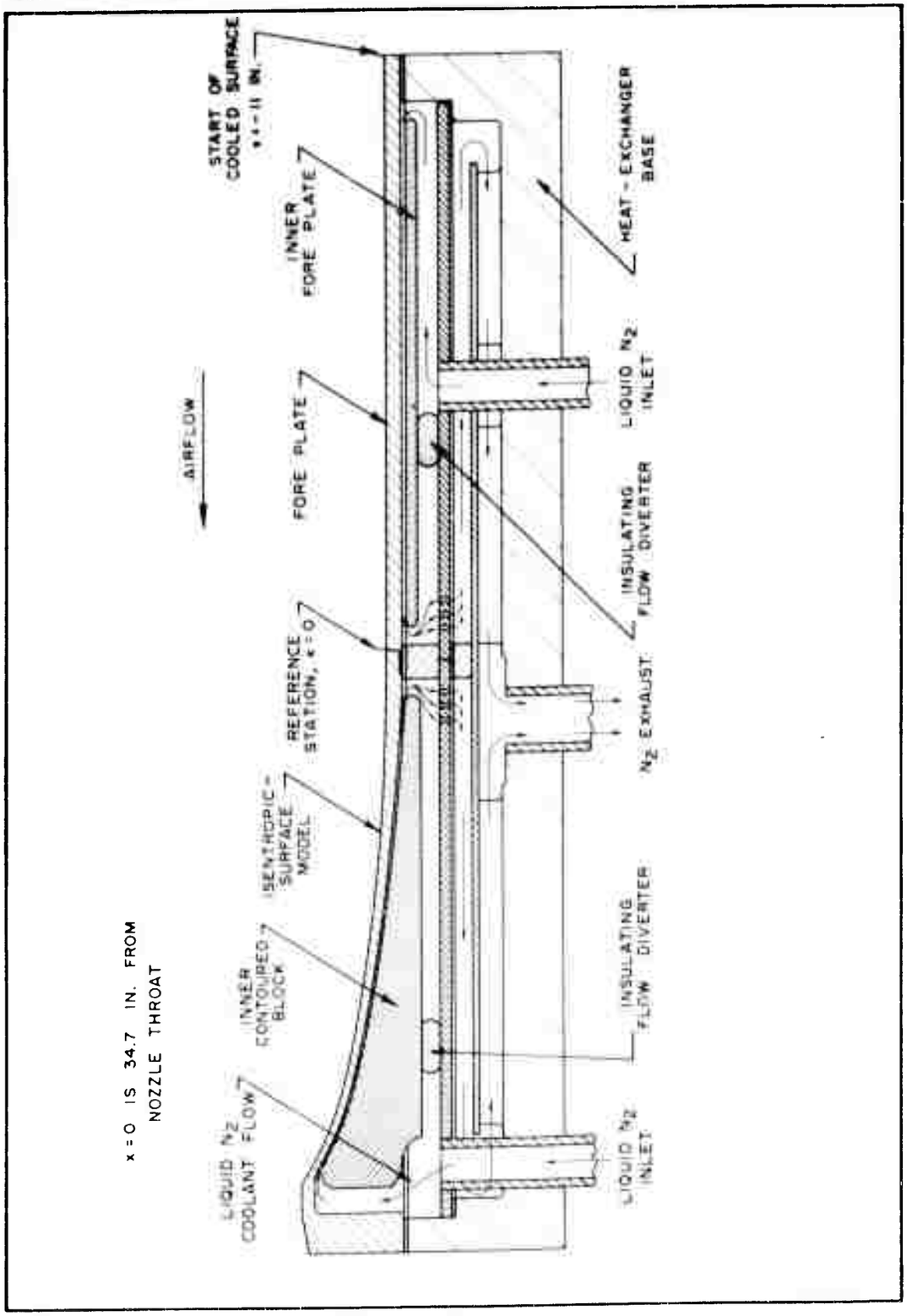

FIGURE 4 SKETCH OF HEAT-EXCHANGER ASSEMBLY WITH ISENTROPIC-SURFACE MODEL INSTALLED

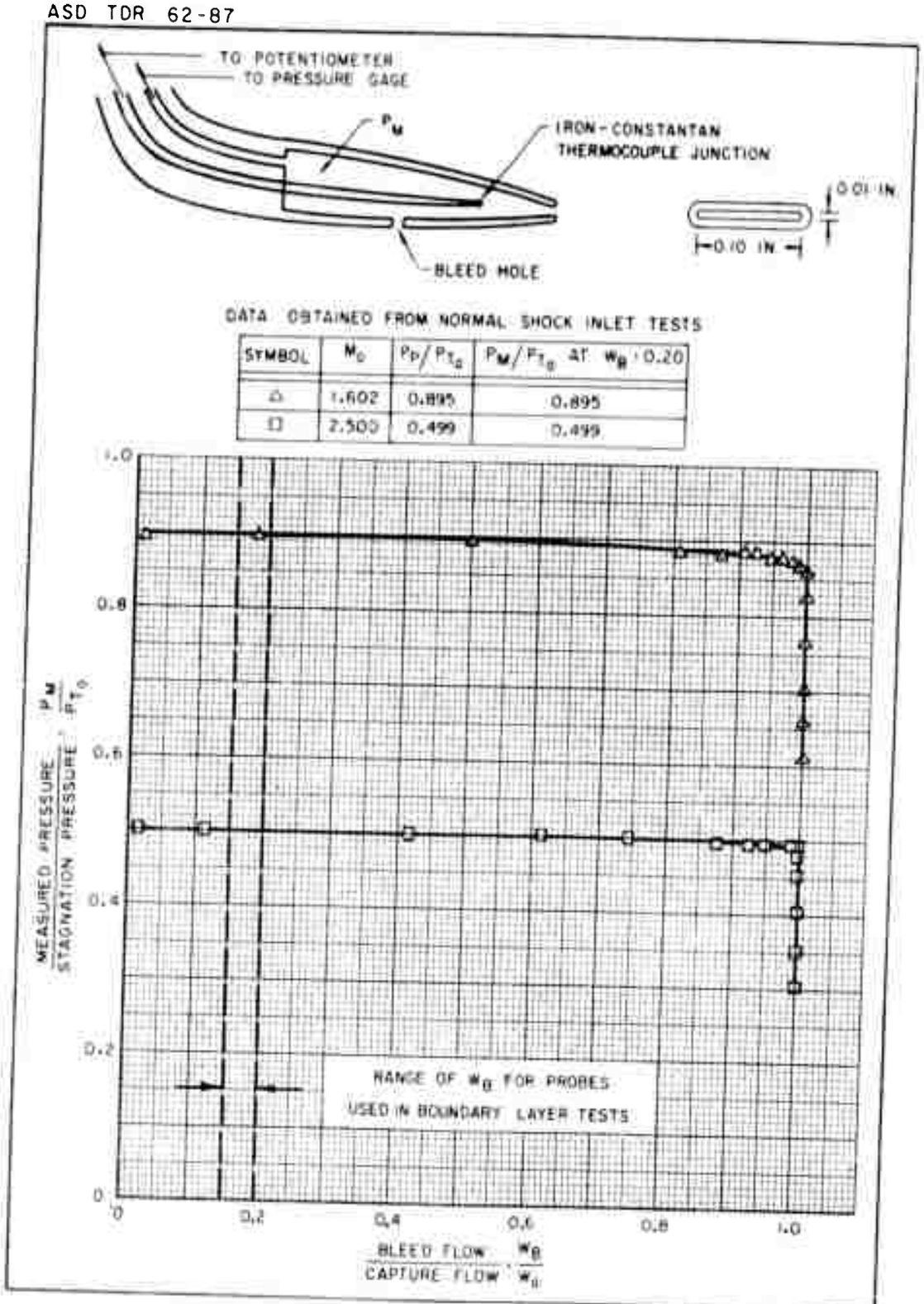

FIGURE 5: SKETCH OF COMBINATION PRESSURE-TEMPERATURE PROBE AND TYPICAL VARIATION OF MEASURED PRESSURE WITH BLEED FLOW

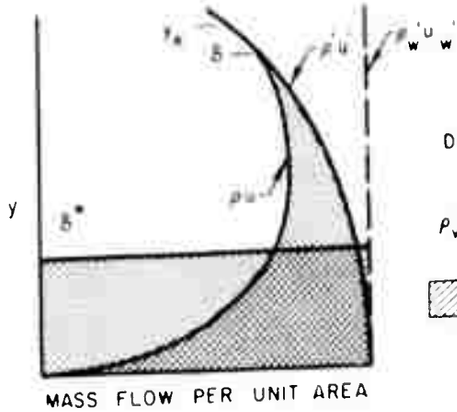

MASS

DISPLACEMENT THICKNESS, δ^*

$$\rho_w u'_w \delta^* = \int_0^\delta \rho' u' \, dy - \int_0^\delta \rho u \, dy$$

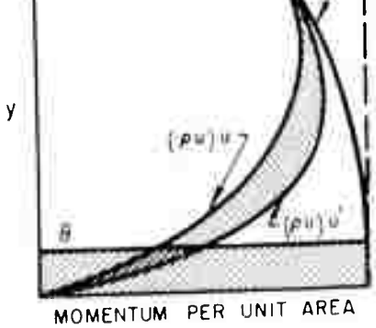

MOMENTUM

MOMENTUM THICKNESS, θ

$$\rho'_w u'^2_w \theta = \int_0^\delta (\rho u) u' \, dy - \int_0^\delta (\rho u) u \, dy$$

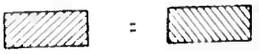

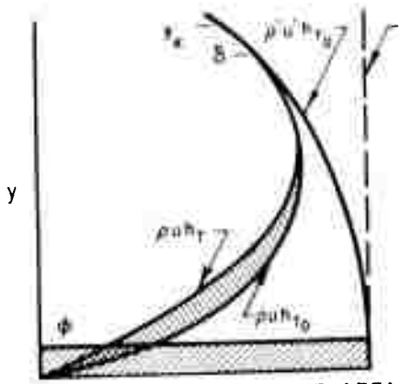

ENERGY

TOTAL ENTHALPY THICKNESS, ϕ

$$\rho'_w u'_w h_{T_0} \phi = \int_0^\delta \rho u h_{T_0} \, dy - \int_0^\delta \rho u h_T \, dy$$

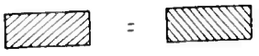

FIGURE 6: INTEGRAL REPRESENTATIONS OF δ^*, θ, AND ϕ FOR A BOUNDARY LAYER HAVING A NORMAL STATIC PRESSURE GRADIENT

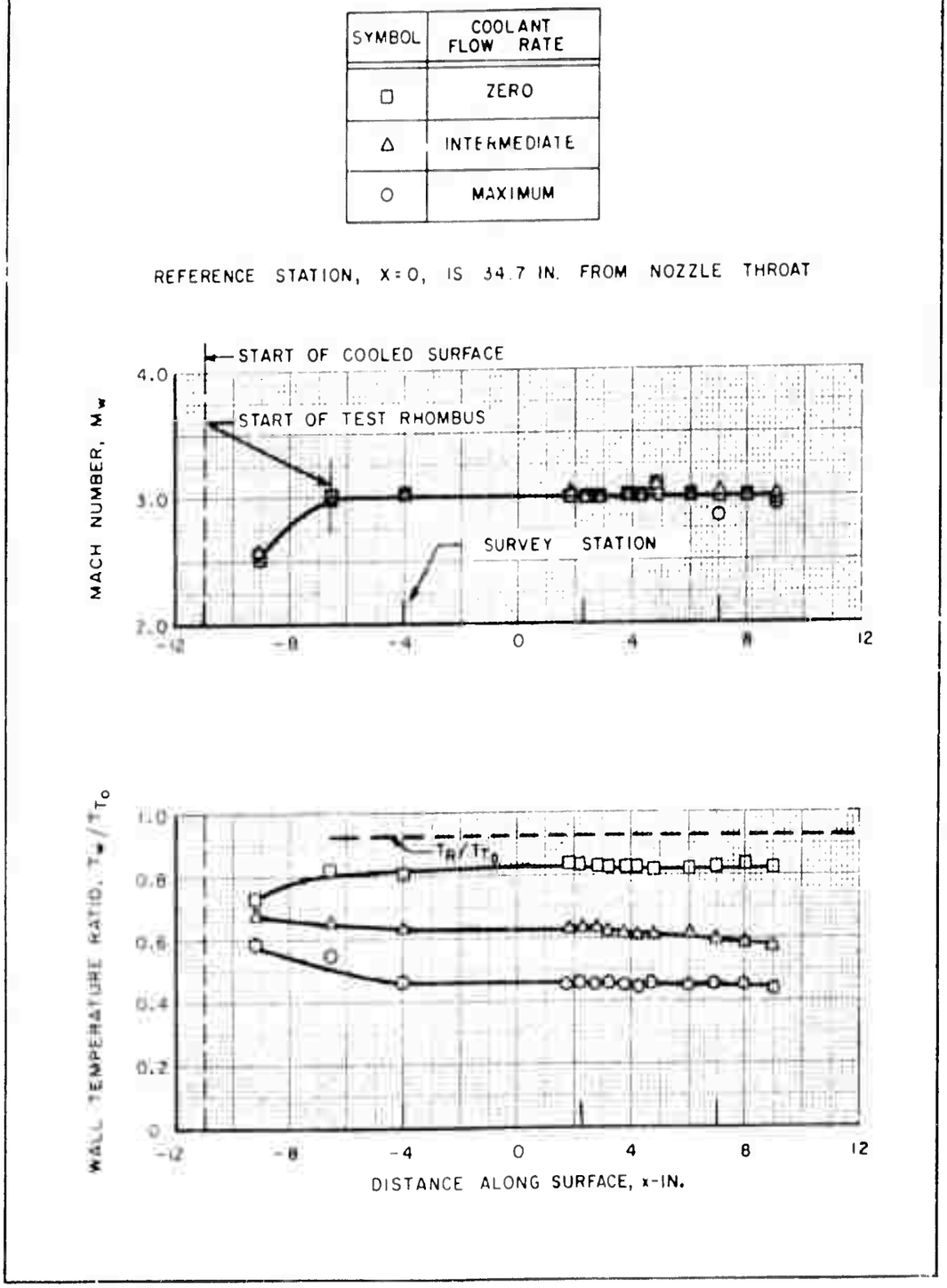

FIGURE 7: MACH NUMBER AND WALL TEMPERATURE DISTRIBUTIONS ON FLAT PLATE WITH MACH 3 NOZZLE INSTALLED

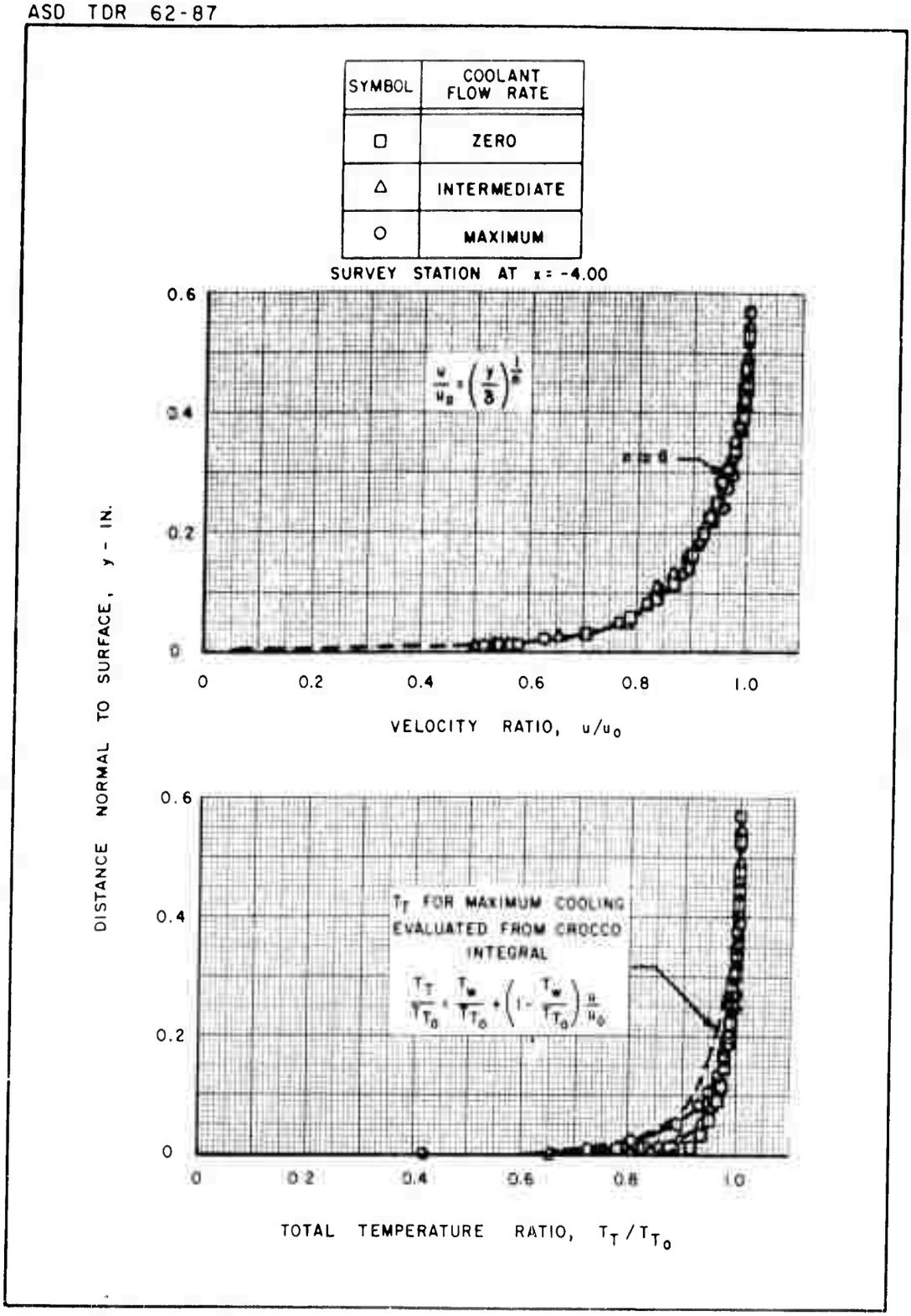

FIGURE 8: REPRESENTATIVE VELOCITY AND TOTAL TEMPERATURE PROFILES ON FLAT PLATE AT MACH 3

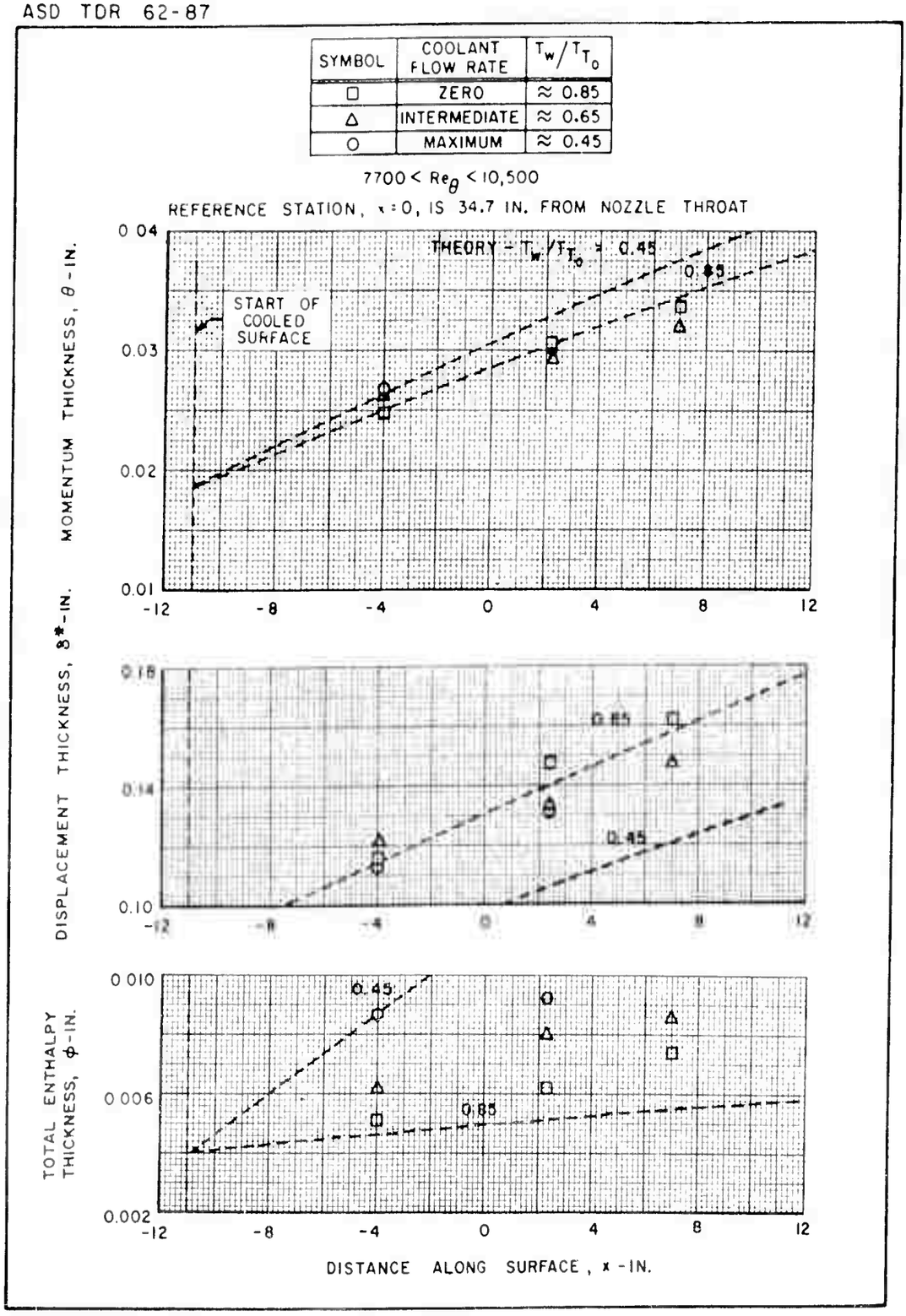

FIGURE 9: VARIATION OF θ, δ^*, AND ϕ ALONG FLAT PLATE AT MACH 3

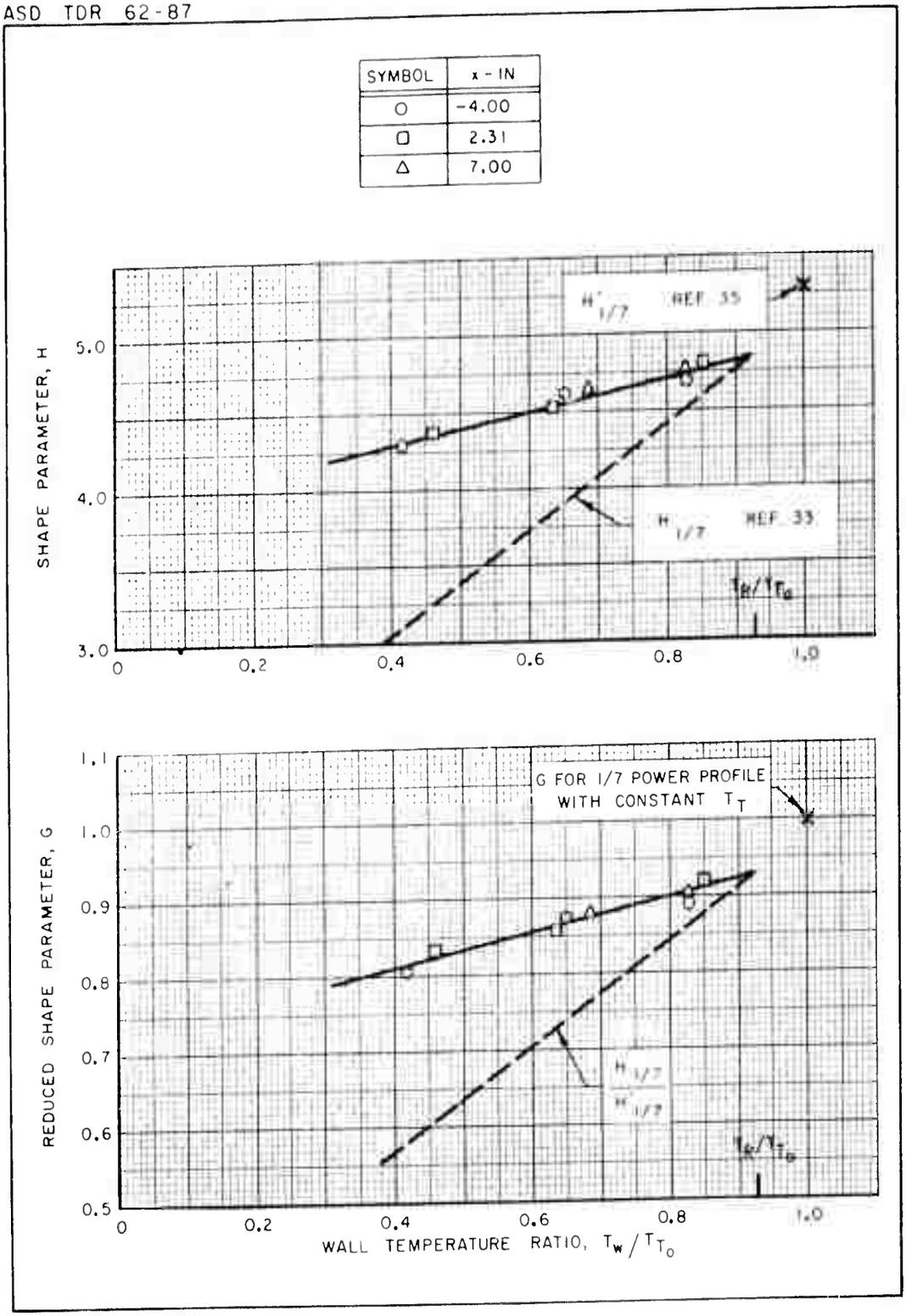

FIGURE 10: EFFECT OF WALL TEMPERATURE ON BOUNDARY LAYER SHAPE PARAMETERS ON FLAT PLATE AT MACH 3

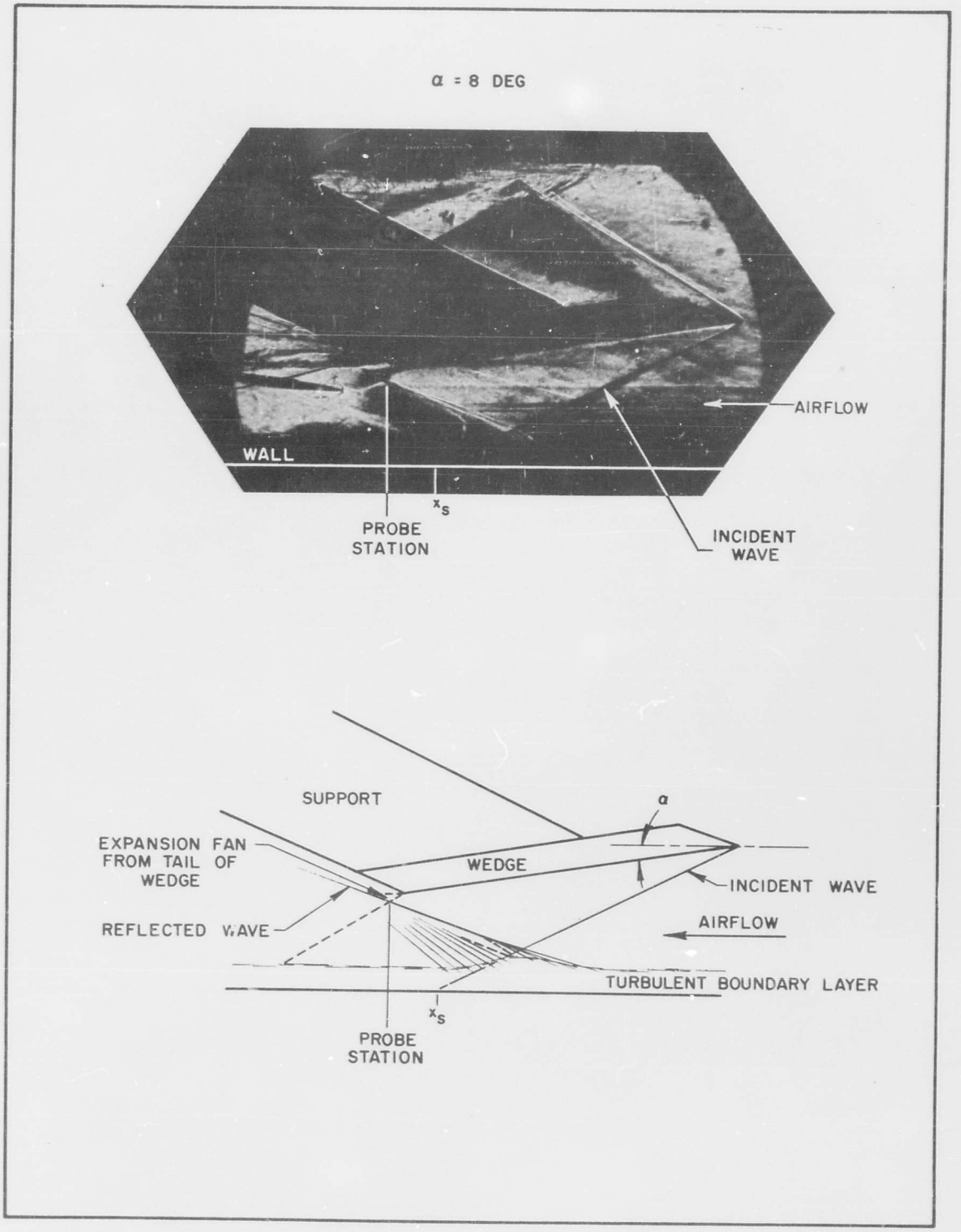

FIGURE 11 SCHLIEREN PHOTOGRAPH AND SKETCH OF SHOCK-REFLECTION INTERACTION AT MACH 3

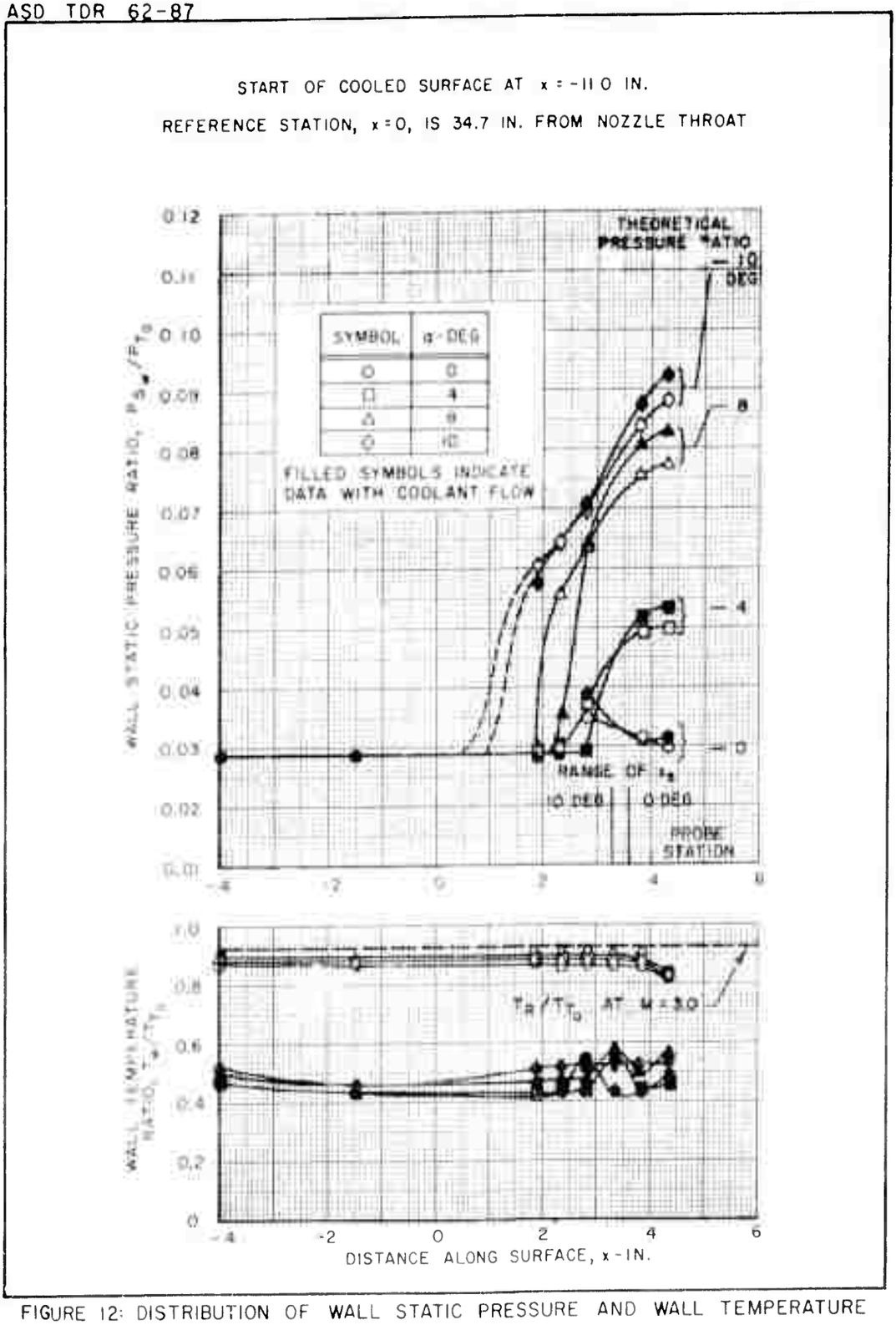

FIGURE 12: DISTRIBUTION OF WALL STATIC PRESSURE AND WALL TEMPERATURE THROUGH SHOCK-REFLECTION INTERACTION AT MACH 3

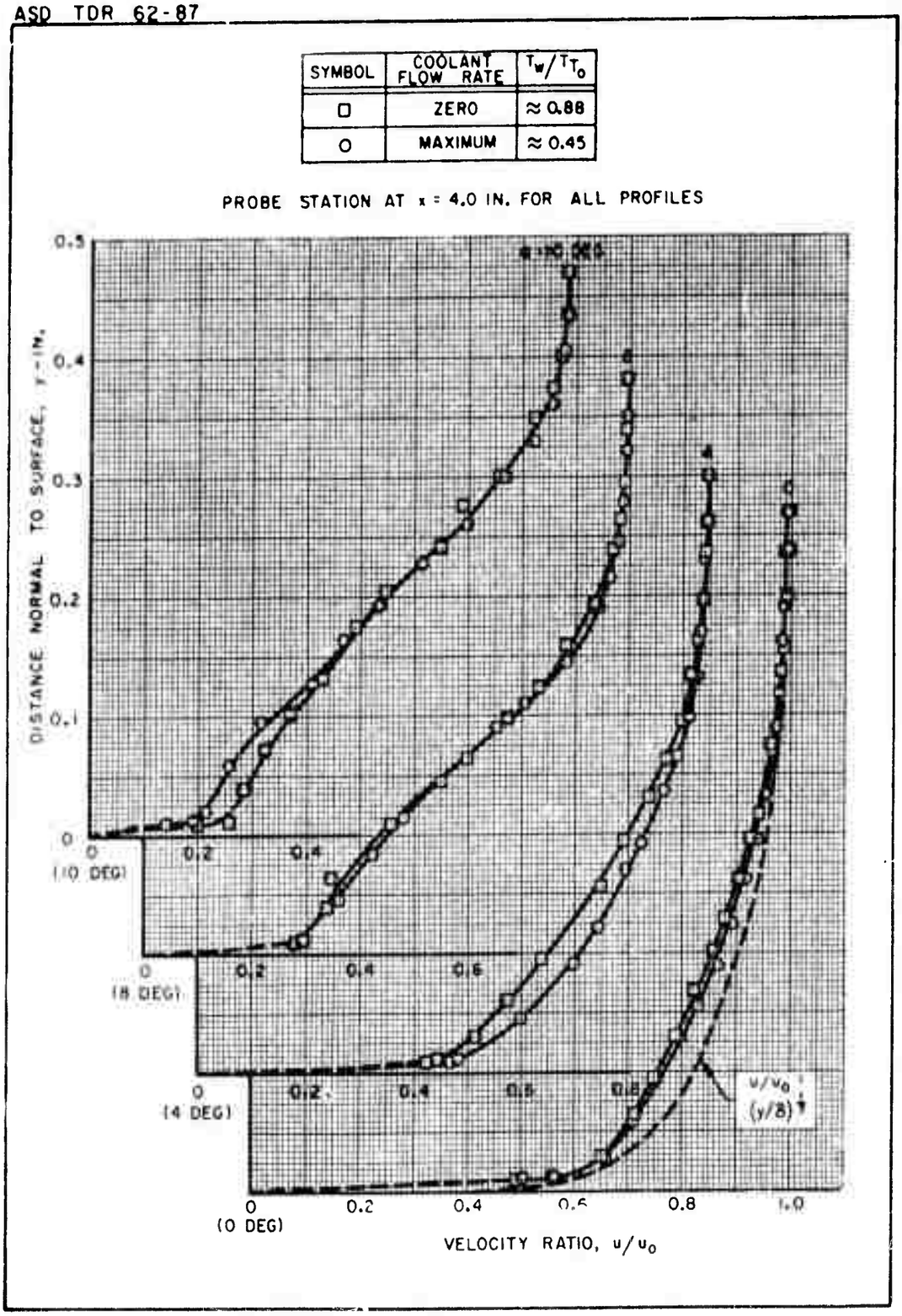

FIGURE 13: VELOCITY PROFILES DOWNSTREAM OF SHOCK-REFLECTION INTERACTION AT MACH 3

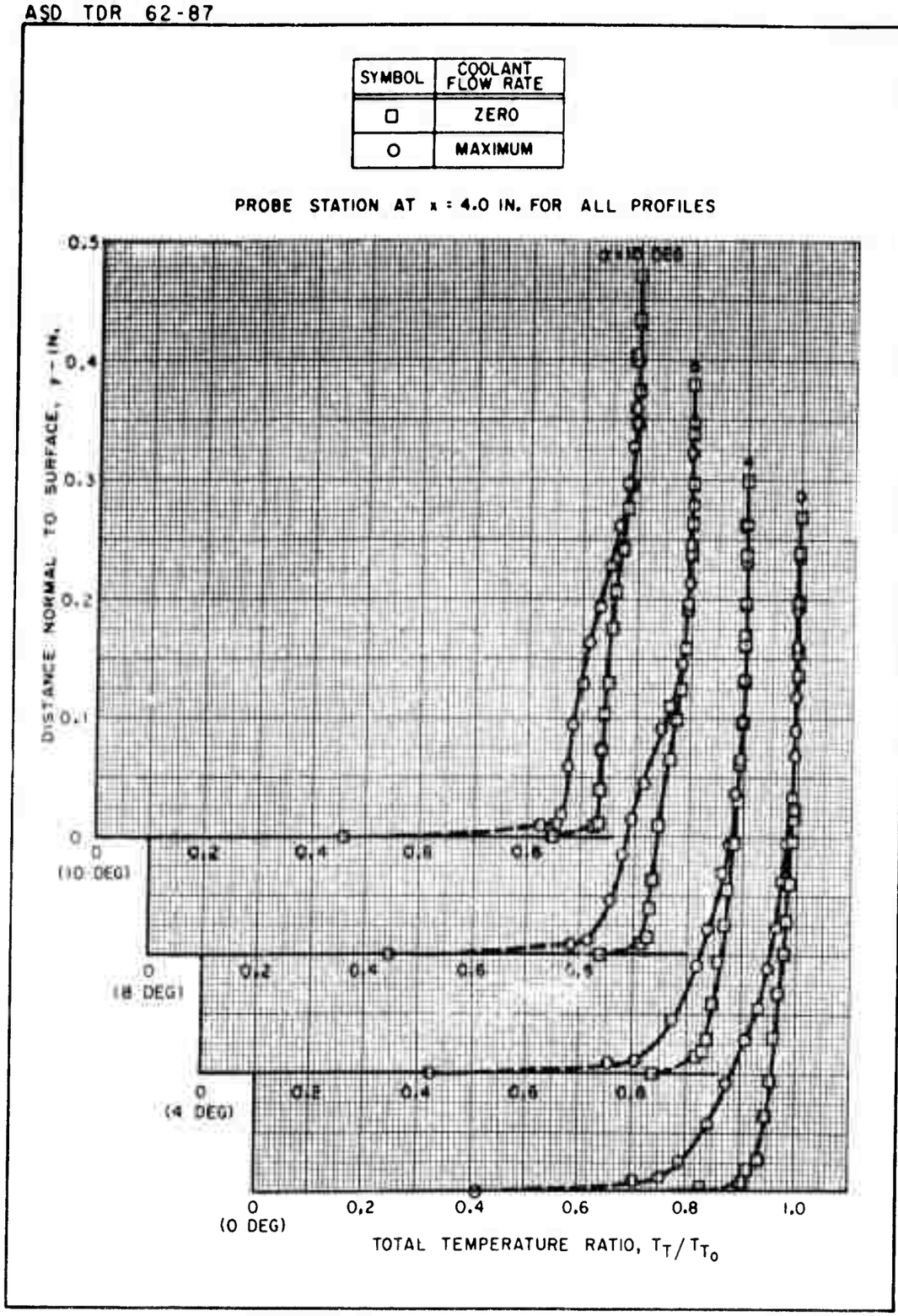

FIGURE 14: TOTAL TEMPERATURE PROFILES DOWNSTREAM OF SHOCK - REFLECTION INTERACTION AT MACH 3

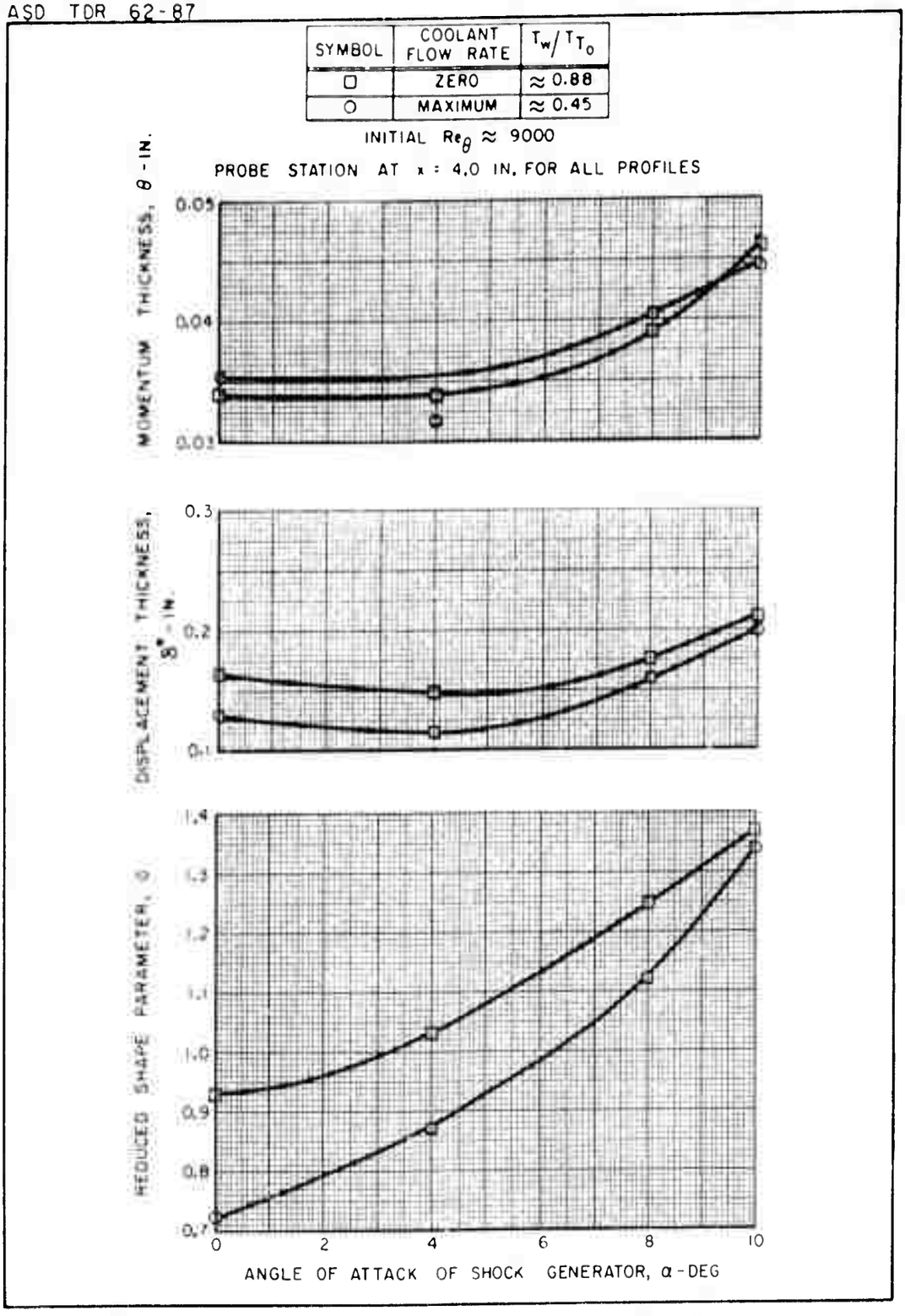

FIGURE 15: VARIATION OF θ, δ^*, AND G WITH INCIDENT SHOCK STRENGTH FOR SHOCK-REFLECTION INTERACTION AT MACH 3

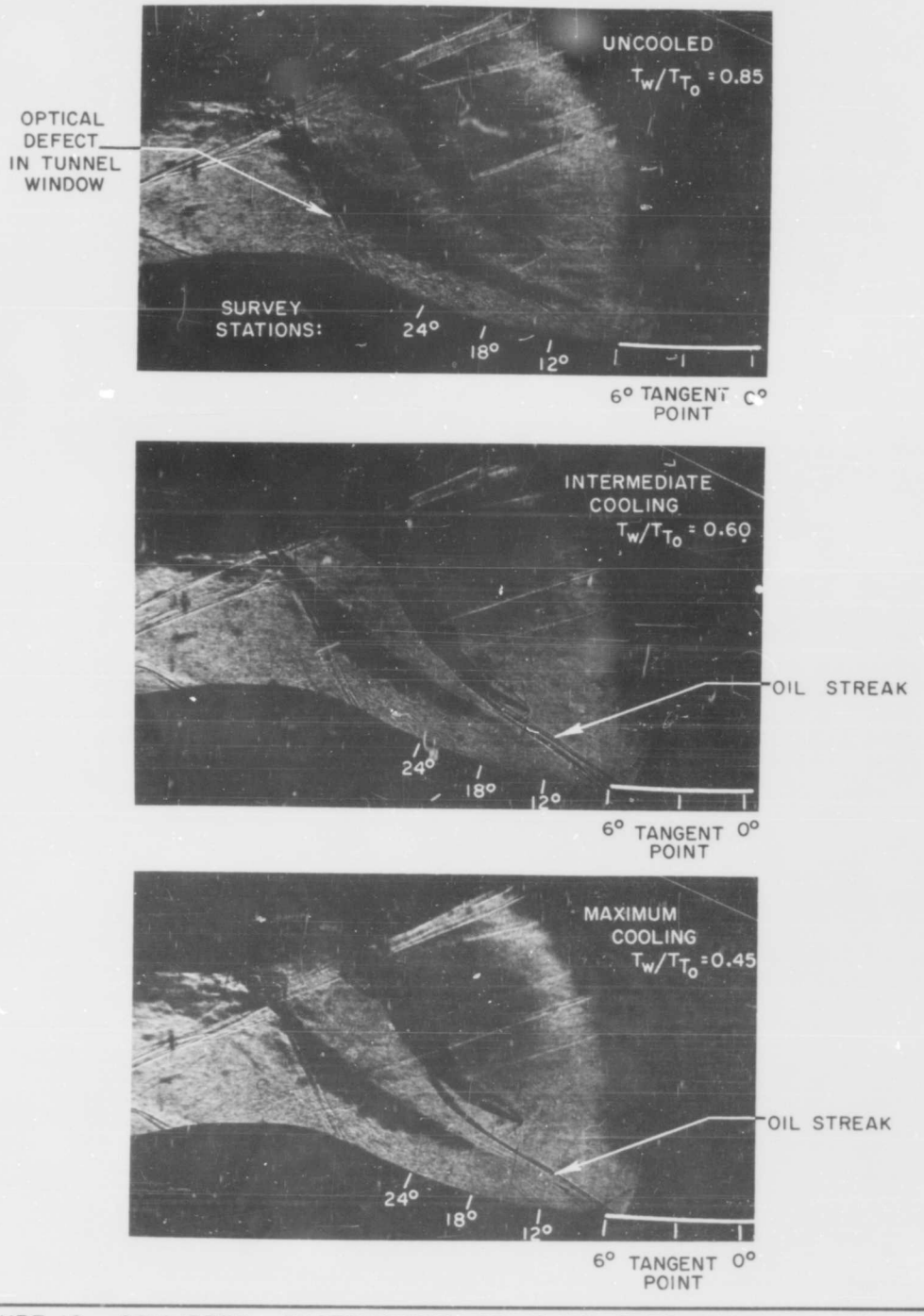

FIGURE 16 SCHLIEREN PHOTOGRAPHS OF FLOW OVER CIRCULAR-ARC MODEL AT MACH 3

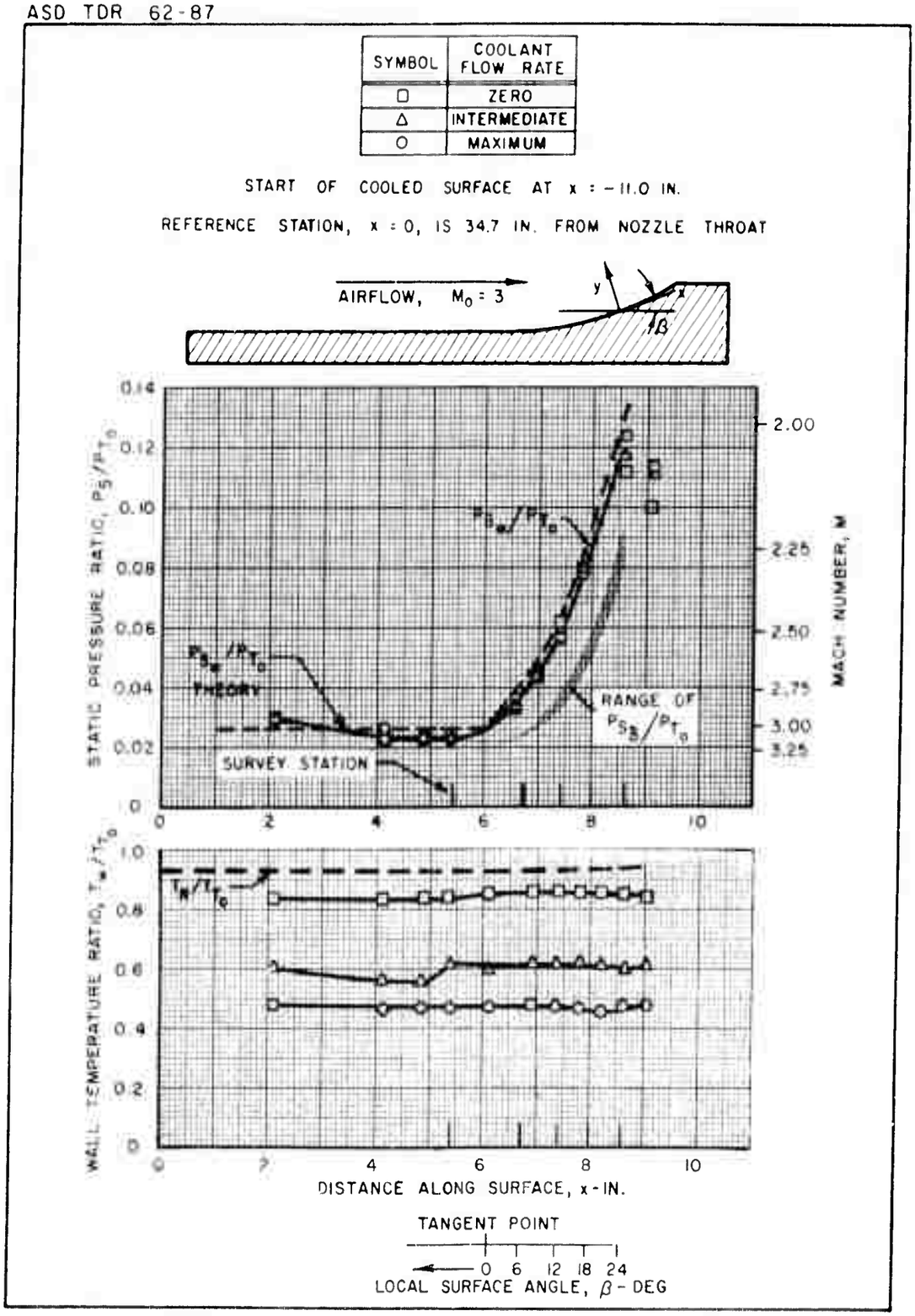

FIGURE 17: DISTRIBUTION OF WALL STATIC PRESSURE AND WALL TEMPERATURE ON CIRCULAR-ARC MODEL AT MACH 3

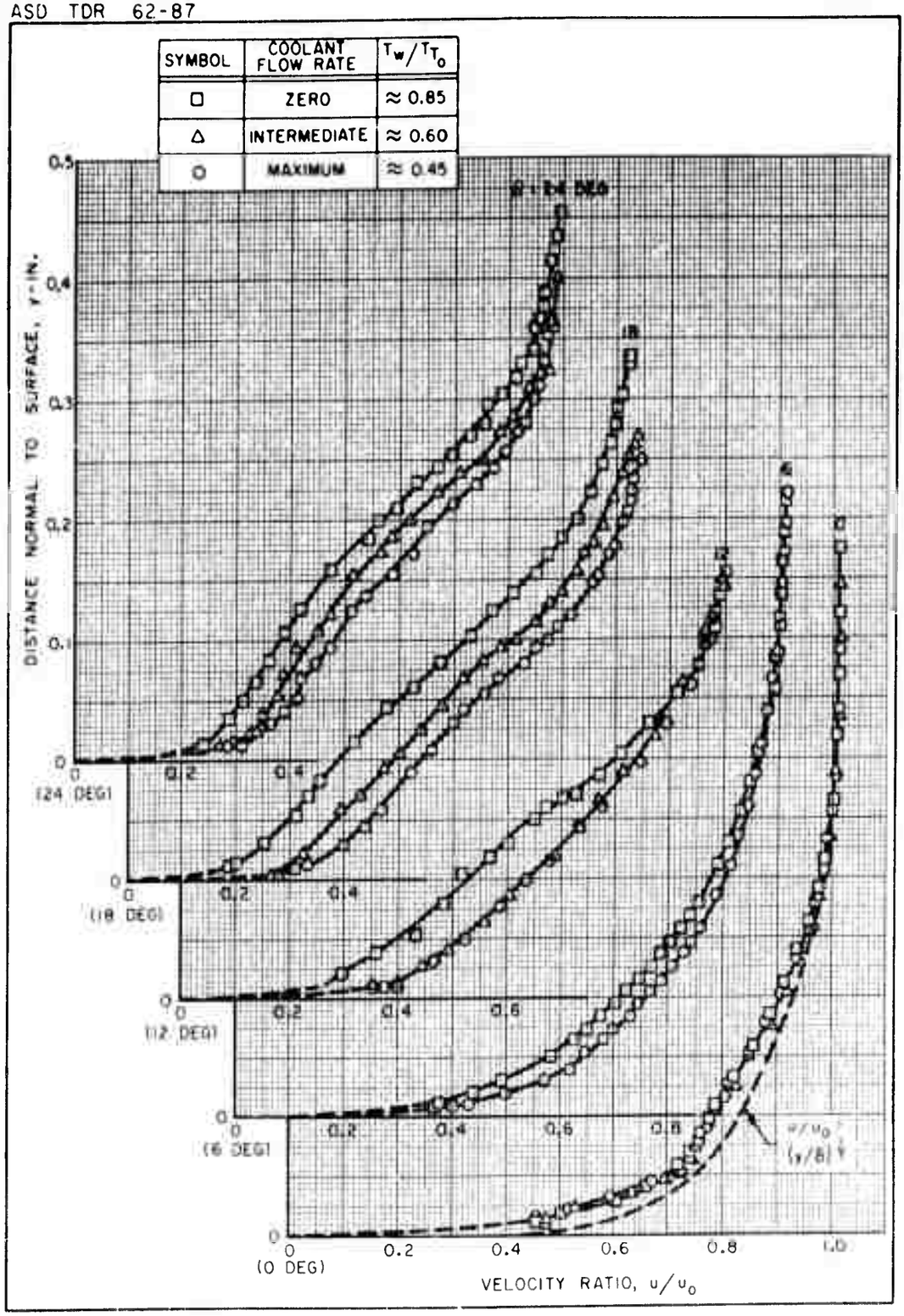

FIGURE 18: VELOCITY PROFILES ON CIRCULAR-ARC MODEL AT MACH 3

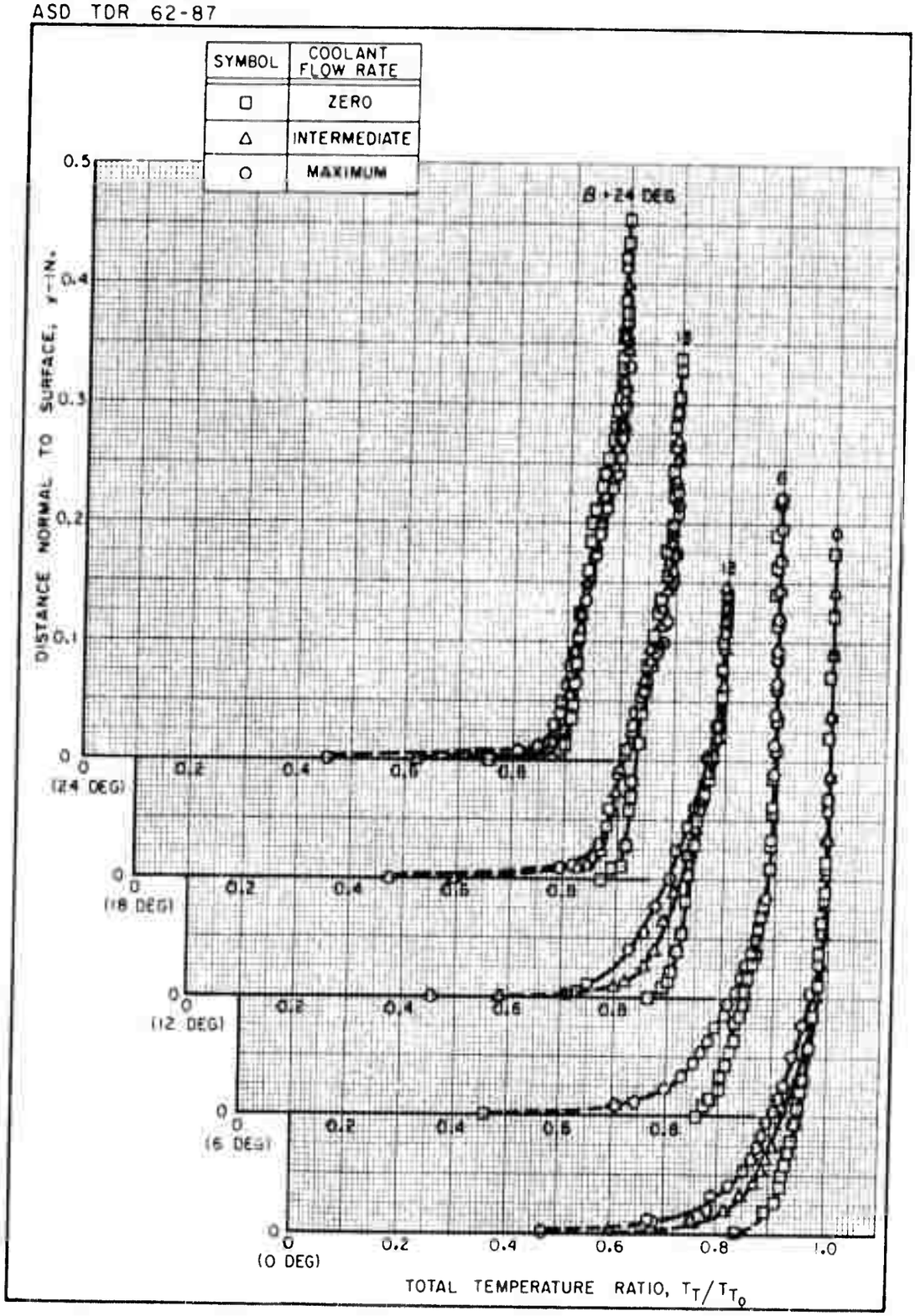

FIGURE 19: TOTAL TEMPERATURE PROFILES ON CIRCULAR-ARC MODEL AT MACH 3

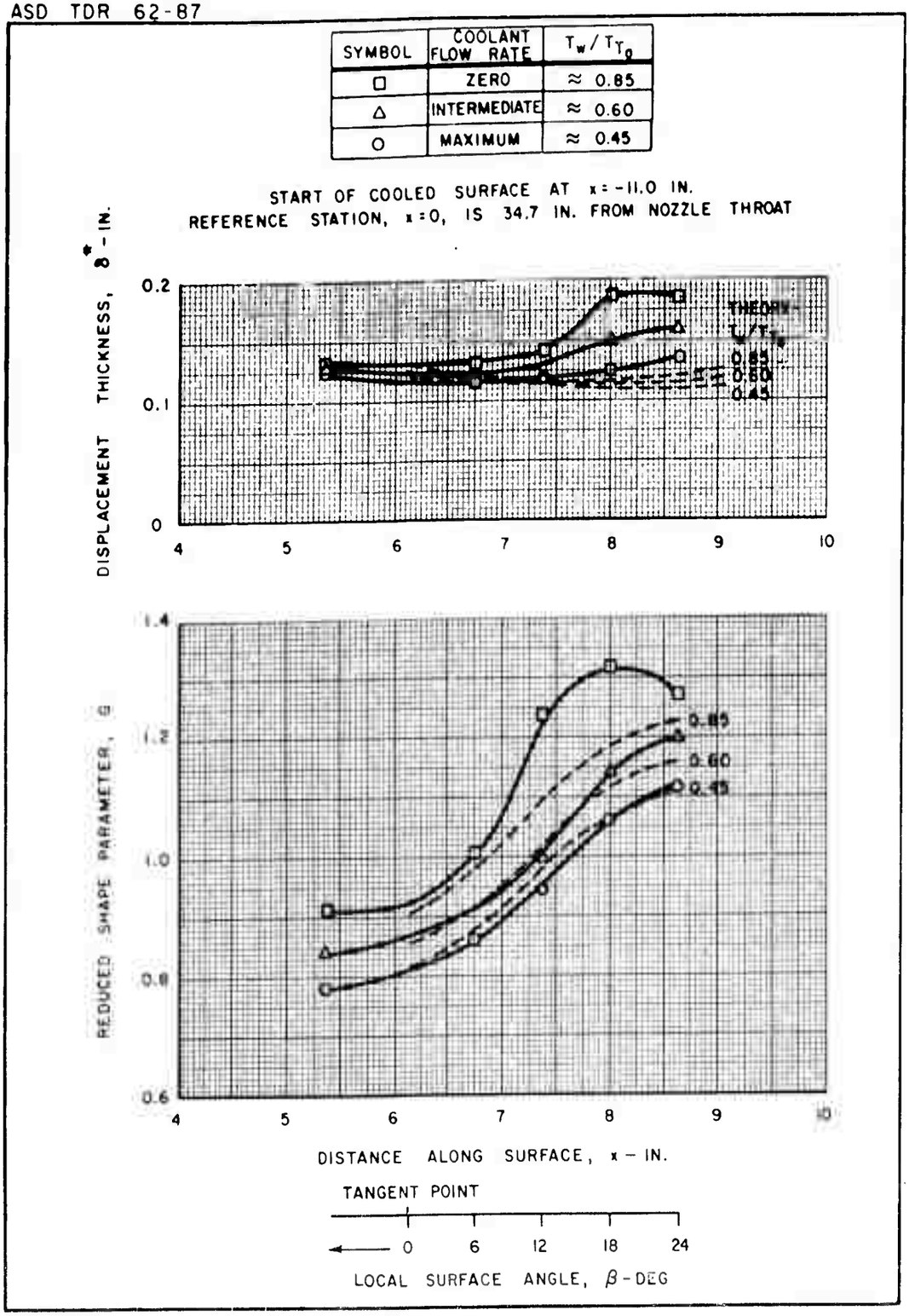

FIGURE 20: VARIATION OF δ^* AND G ALONG CIRCULAR-ARC MODEL AT MACH 3

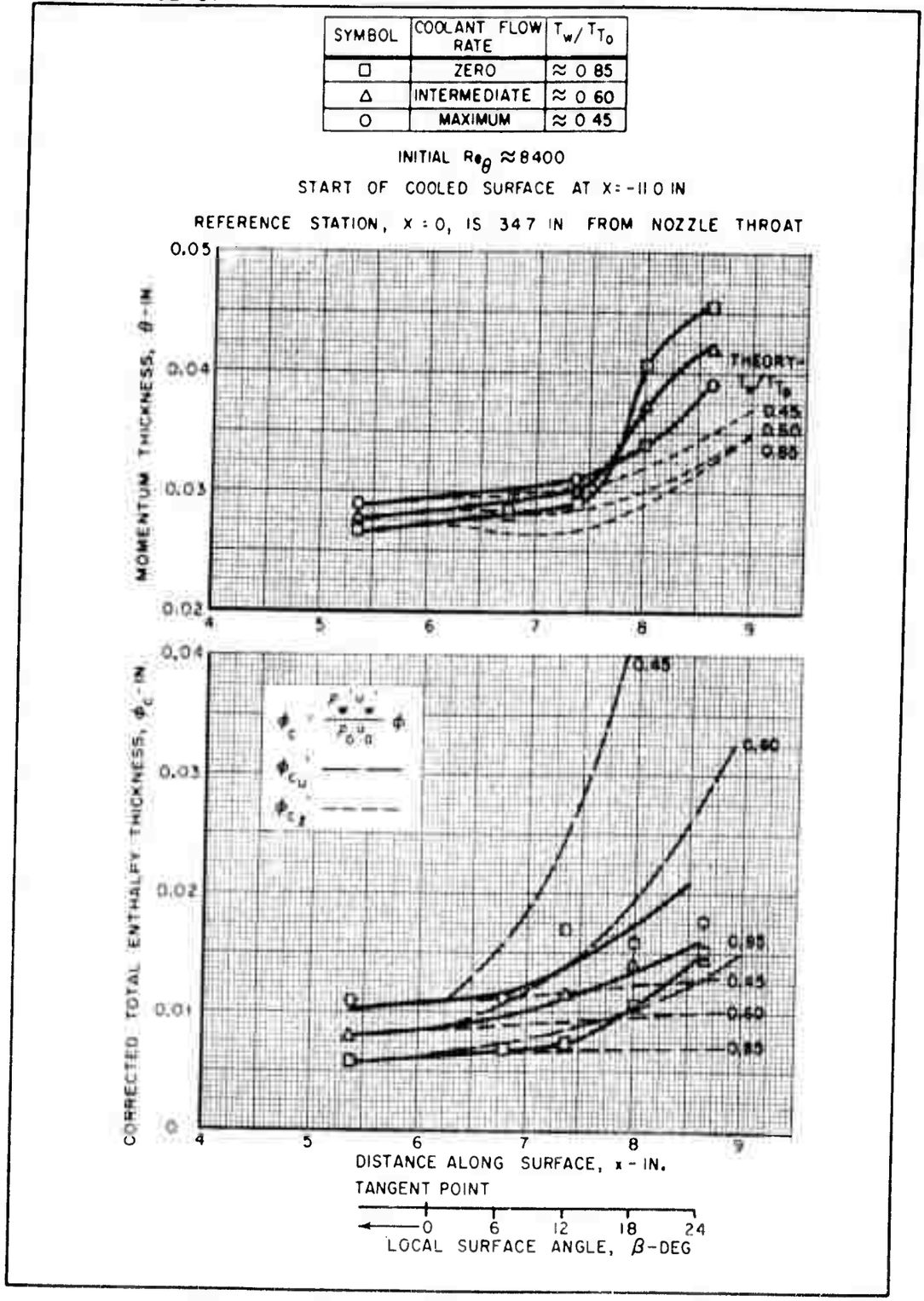

FIGURE 21: VARIATION OF θ AND ϕ_c ALONG CIRCULAR-ARC MODEL AT MACH 3

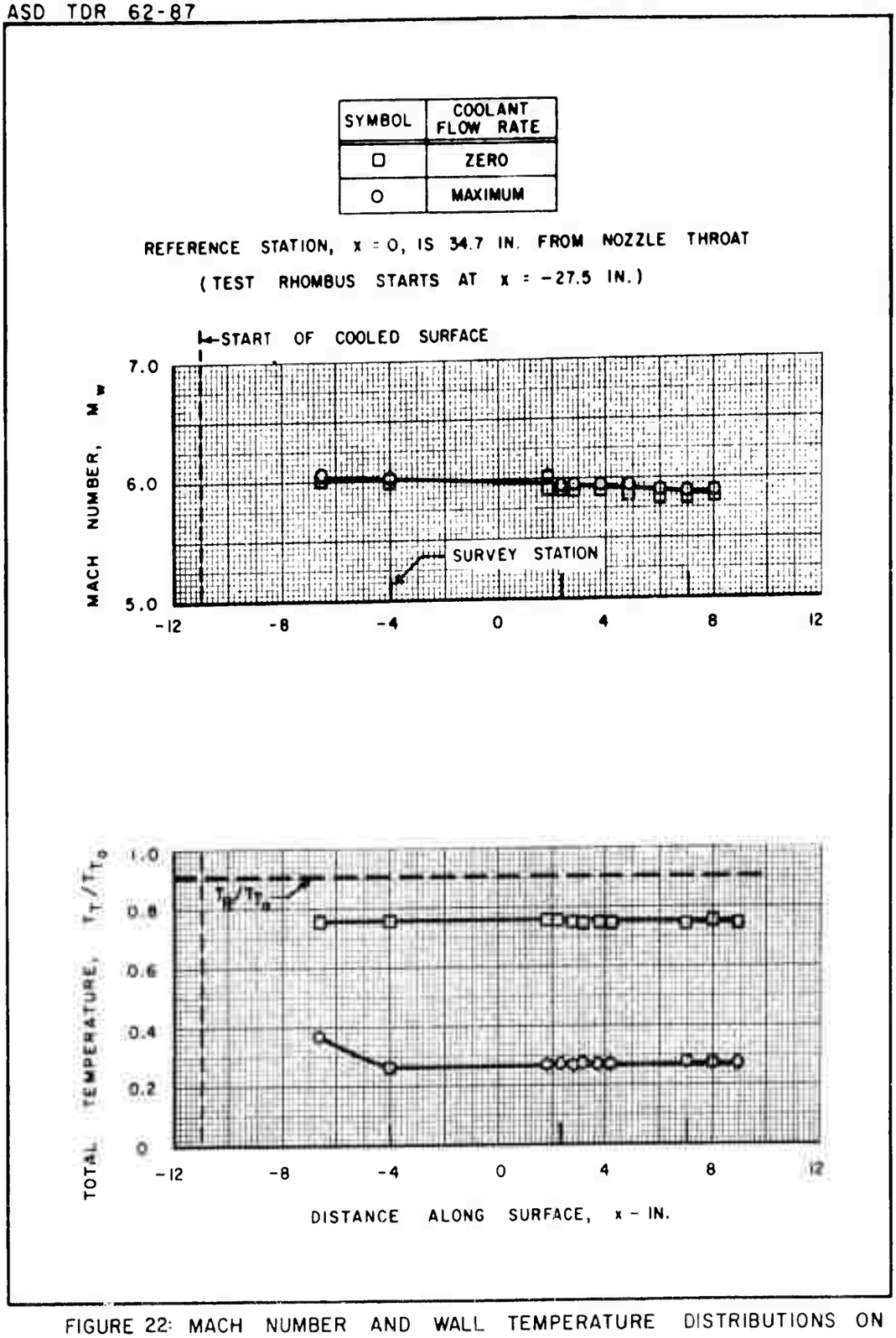

FIGURE 22: MACH NUMBER AND WALL TEMPERATURE DISTRIBUTIONS ON FLAT PLATE WITH MACH 6 NOZZLE INSTALLED

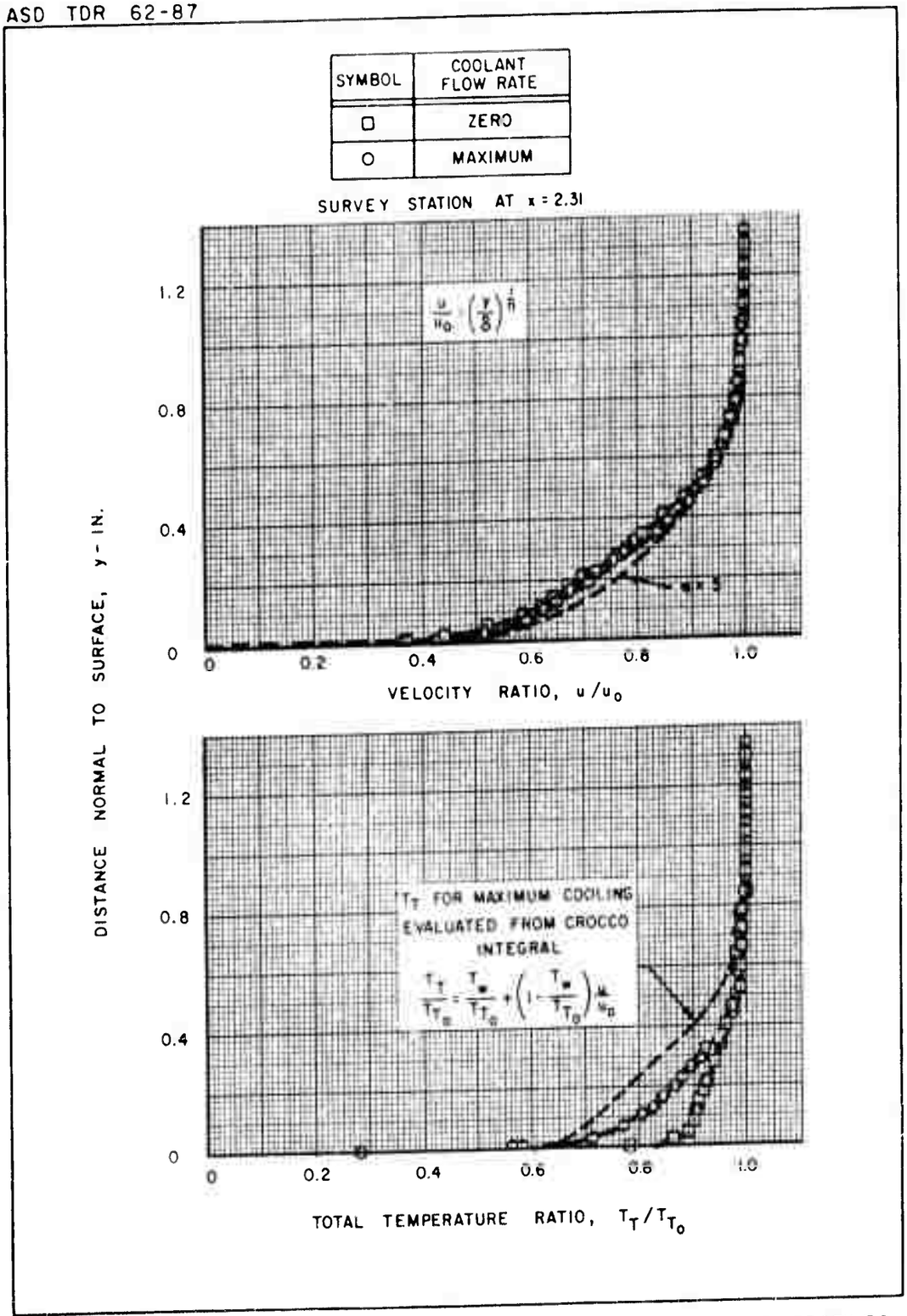

FIGURE 23: REPRESENTATIVE VELOCITY AND TOTAL TEMPERATURE PROFILES ON FLAT PLATE AT MACH 6

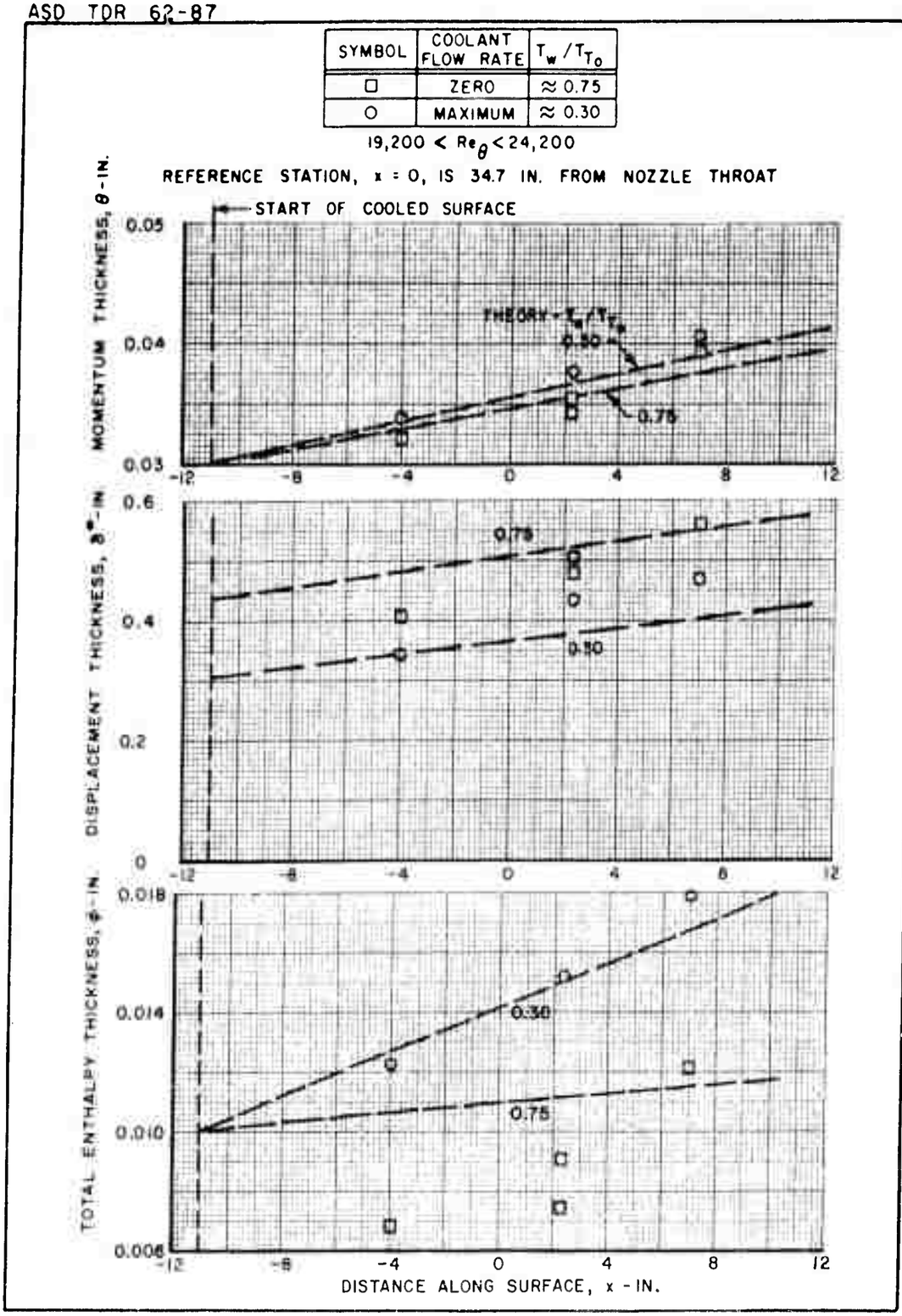

FIGURE 24: VARIATION OF θ, δ^*, AND ϕ ALONG FLAT PLATE AT MACH 6

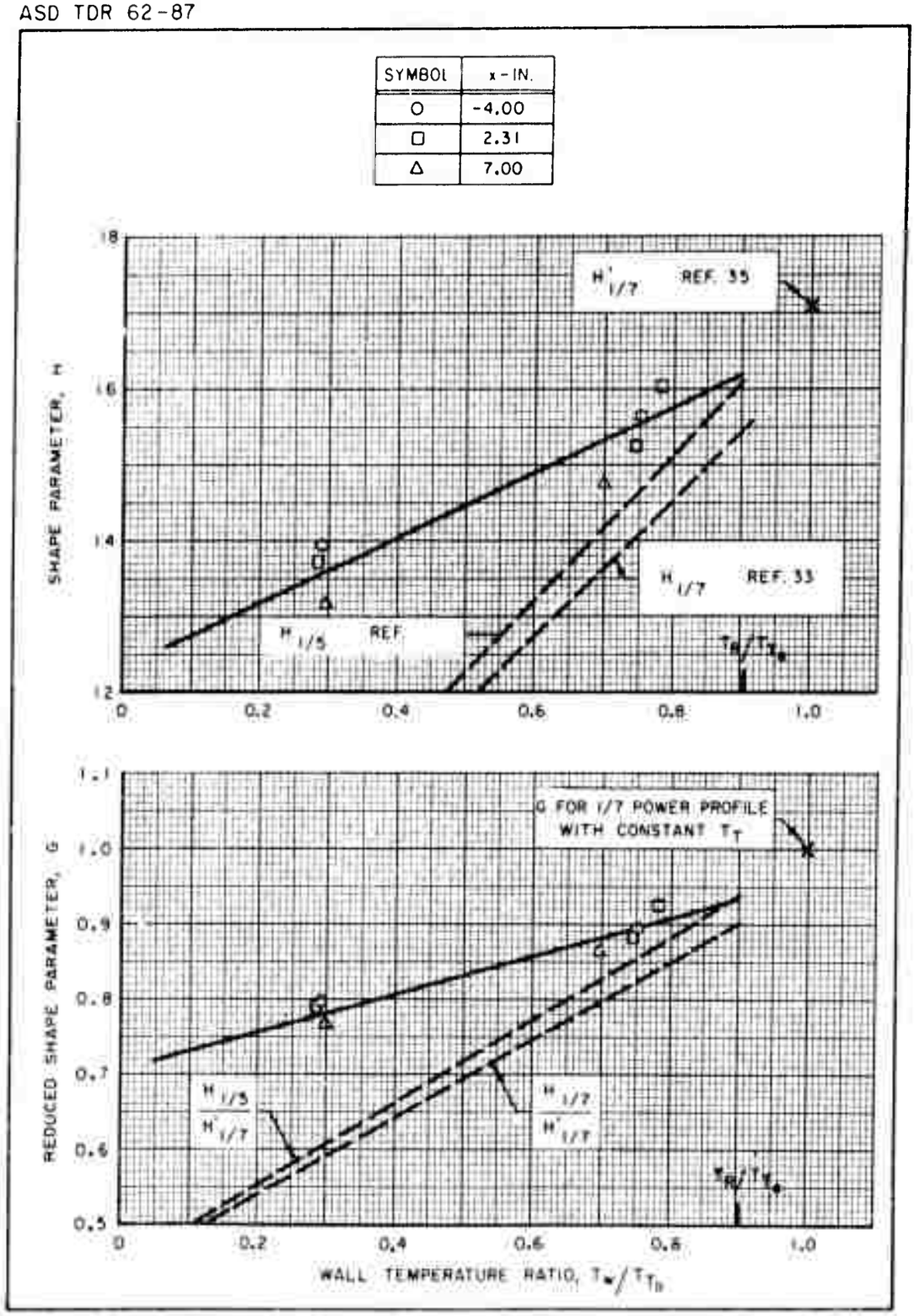

FIGURE 25: EFFECT OF WALL TEMPERATURE ON BOUNDARY LAYER SHAPE PARAMETERS ON FLAT PLATE AT MACH 6

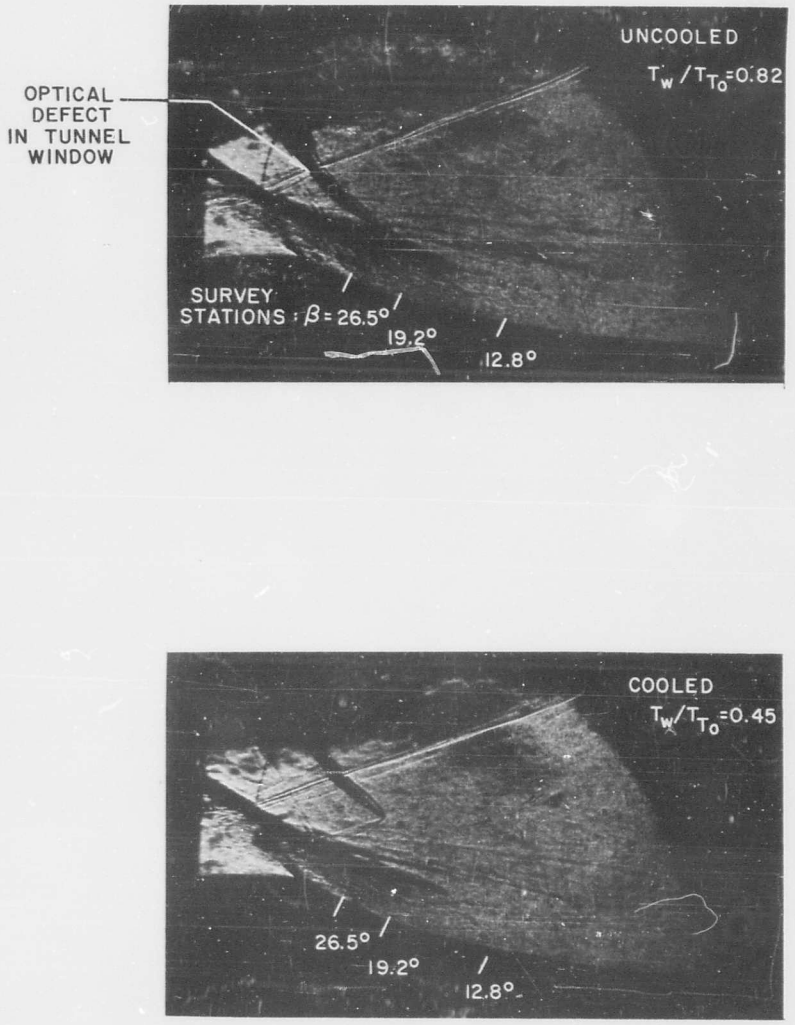

FIGURE 26 SCHLIEREN PHOTOGRAPHS OF FLOW OVER ISENTROPIC-SURFACE MODEL AT MACH 6

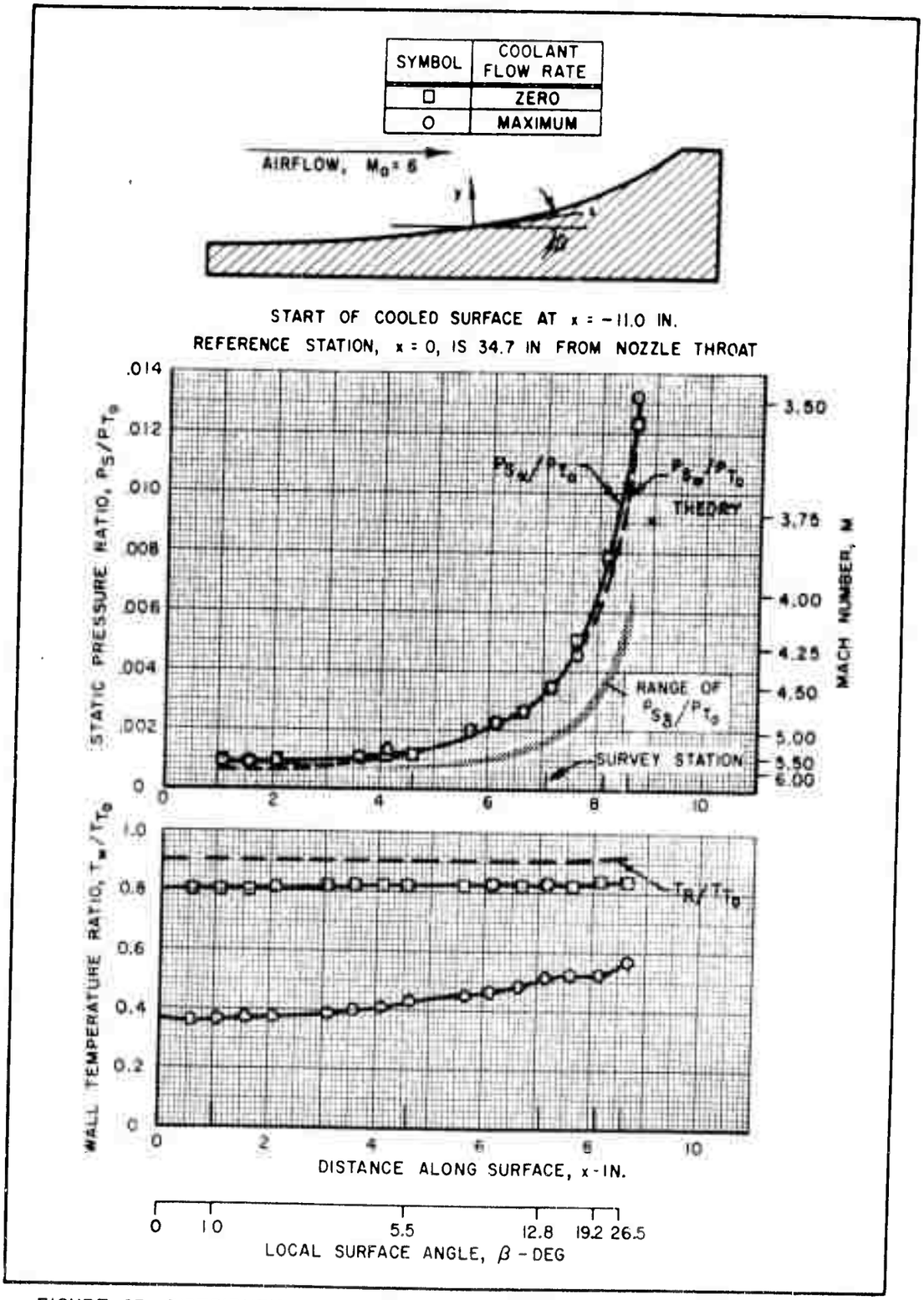

FIGURE 27: DISTRIBUTION OF WALL STATIC PRESSURE AND WALL TEMPERATURE ON ISENTROPIC-SURFACE MODEL AT MACH 6

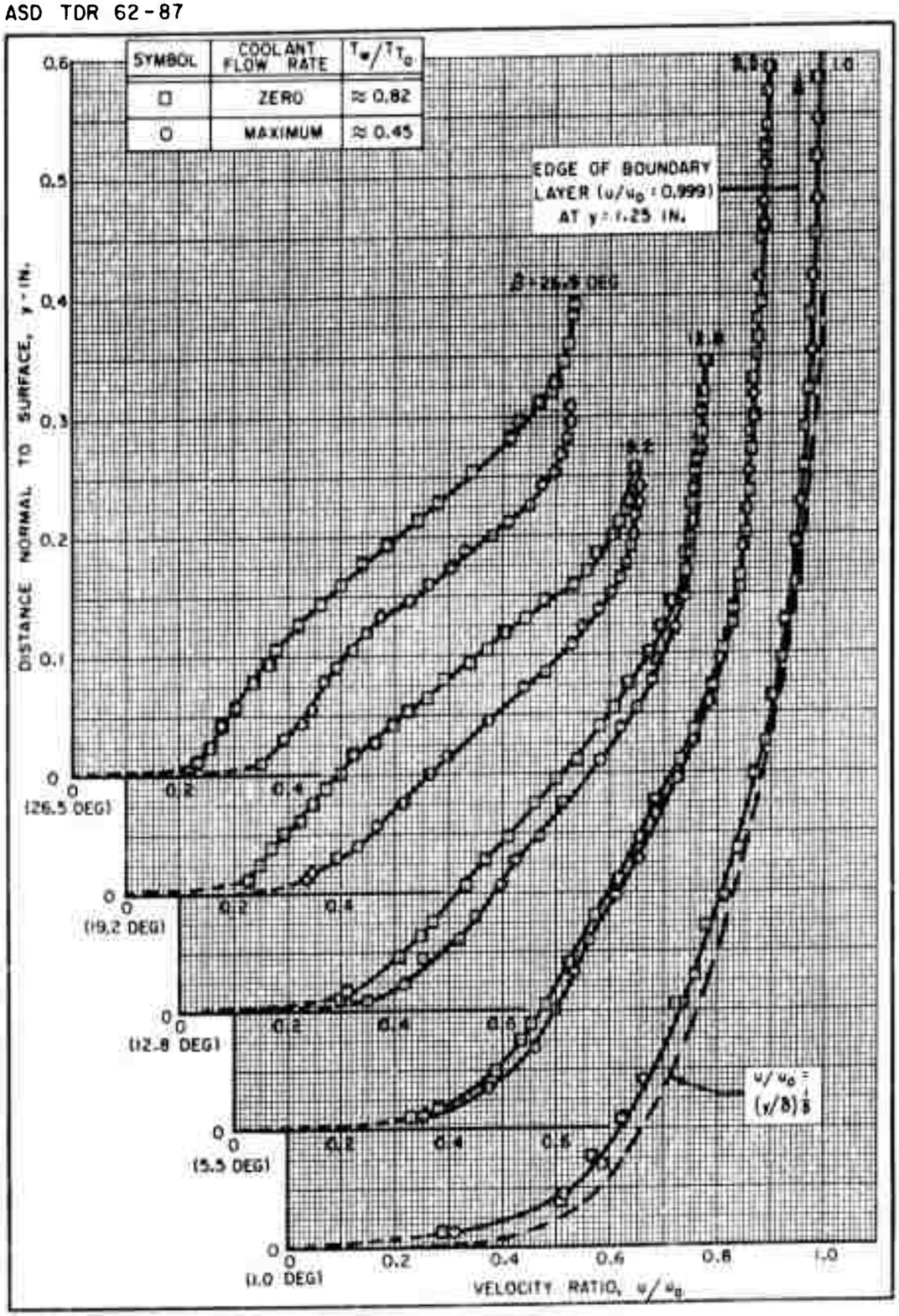

FIGURE 28: VELOCITY PROFILES ON ISENTROPIC-SURFACE MODEL AT MACH 6

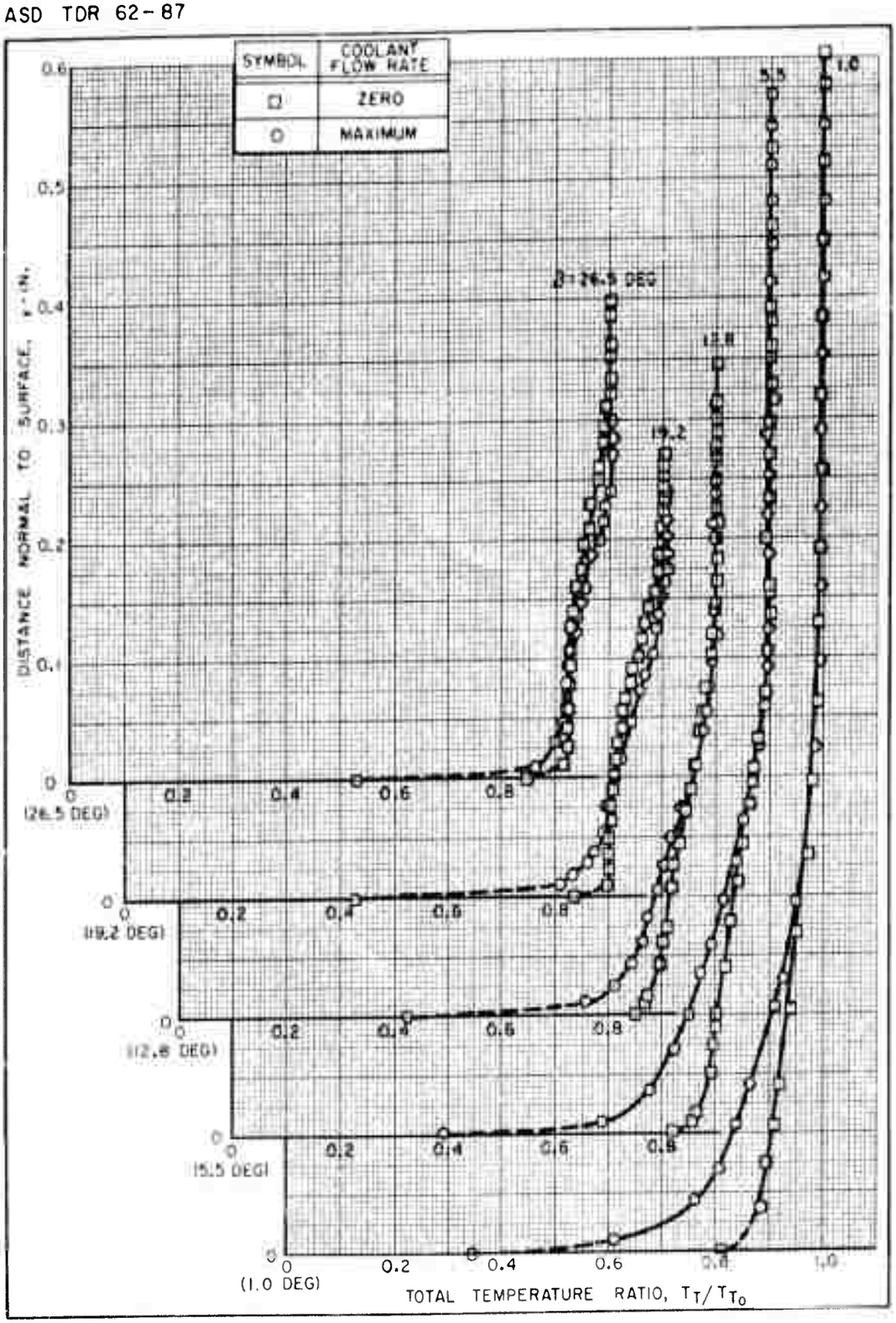

FIGURE 29: TOTAL TEMPERATURE PROFILES ON ISENTROPIC-SURFACE MODEL AT MACH 6

SYMBOL	COOLANT FLOW RATE	T_w/T_{T_0}
□	ZERO	≈ 0.82
○	MAXIMUM	≈ 0.45

START OF COOLED SURFACE AT x = -11.0 IN.

REFERENCE STATION, x = 0, IS 34.7 IN. FROM NOZZLE THROAT

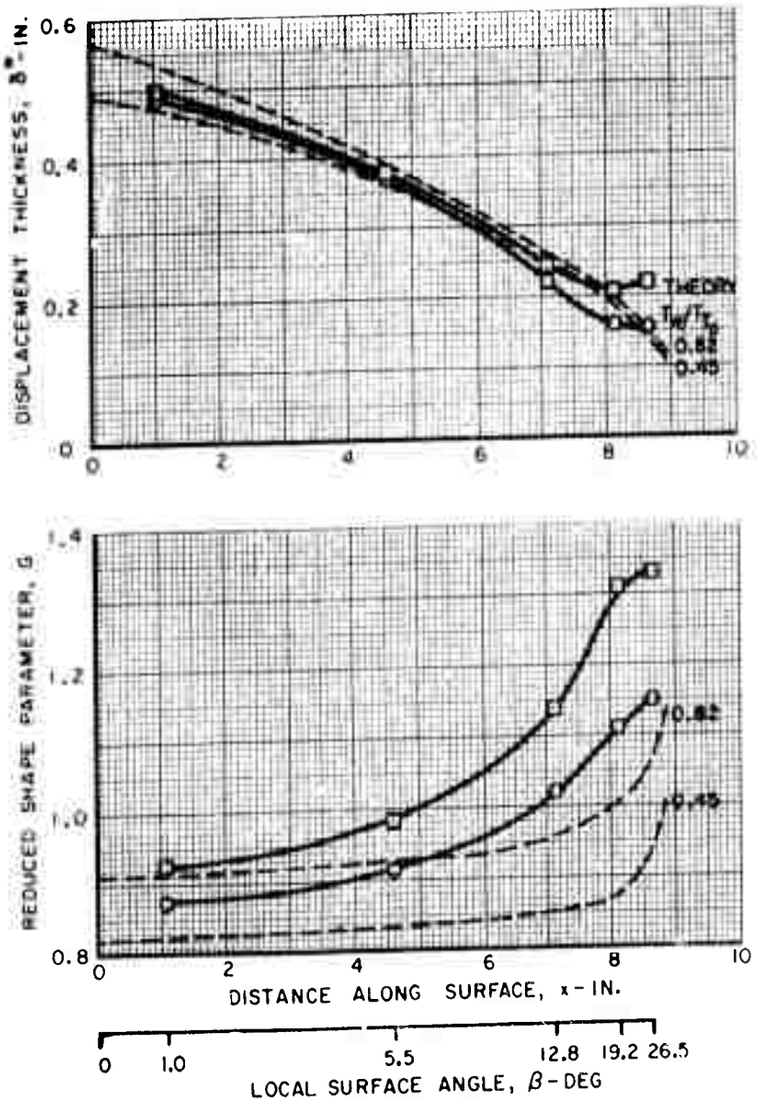

FIGURE 30: VARIATION OF δ^* AND G ALONG ISENTROPIC - SURFACE MODEL AT MACH 6

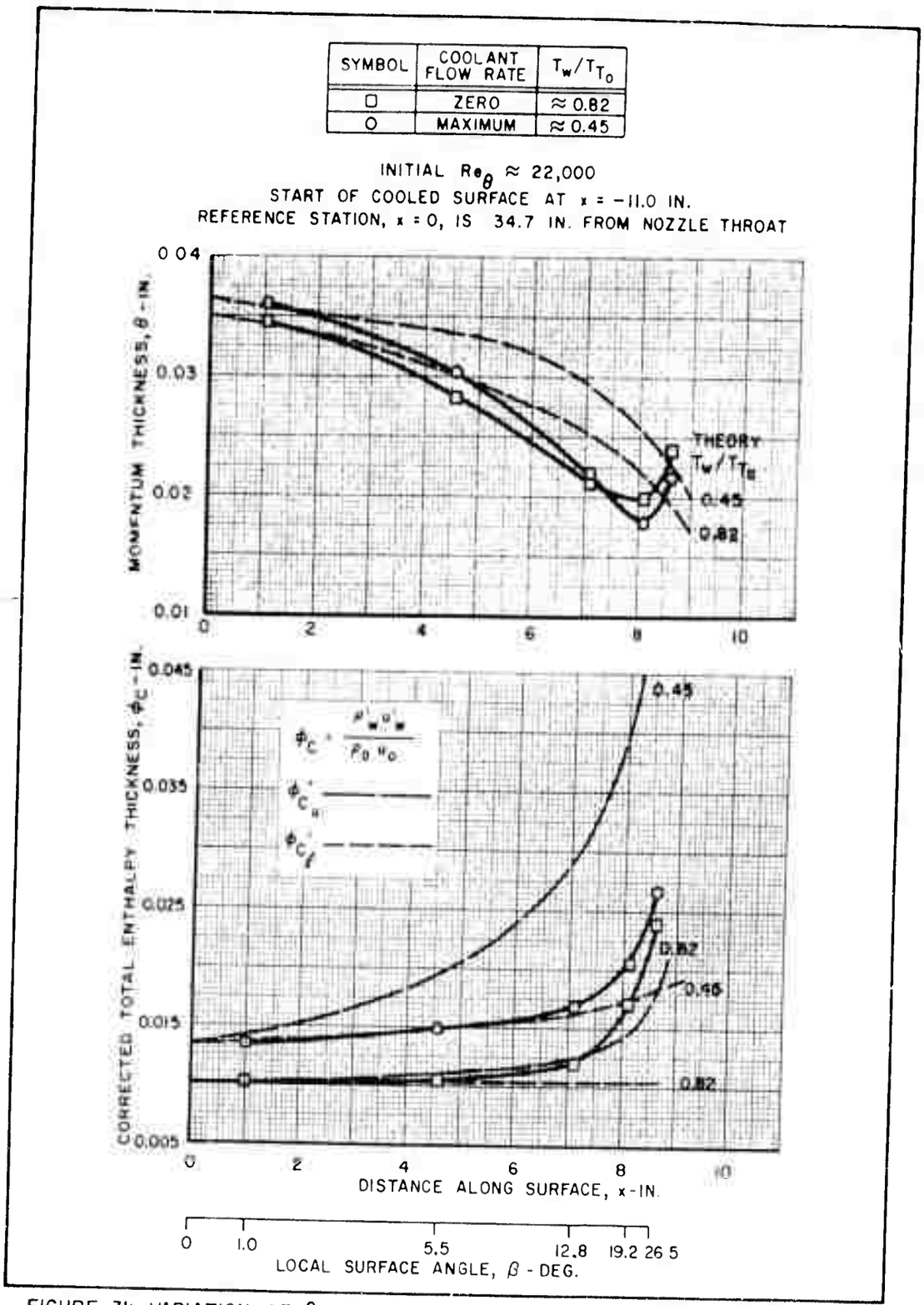

FIGURE 31: VARIATION OF θ AND ϕ_C ALONG ISENTROPIC - SURFACE MODEL AT MACH 6

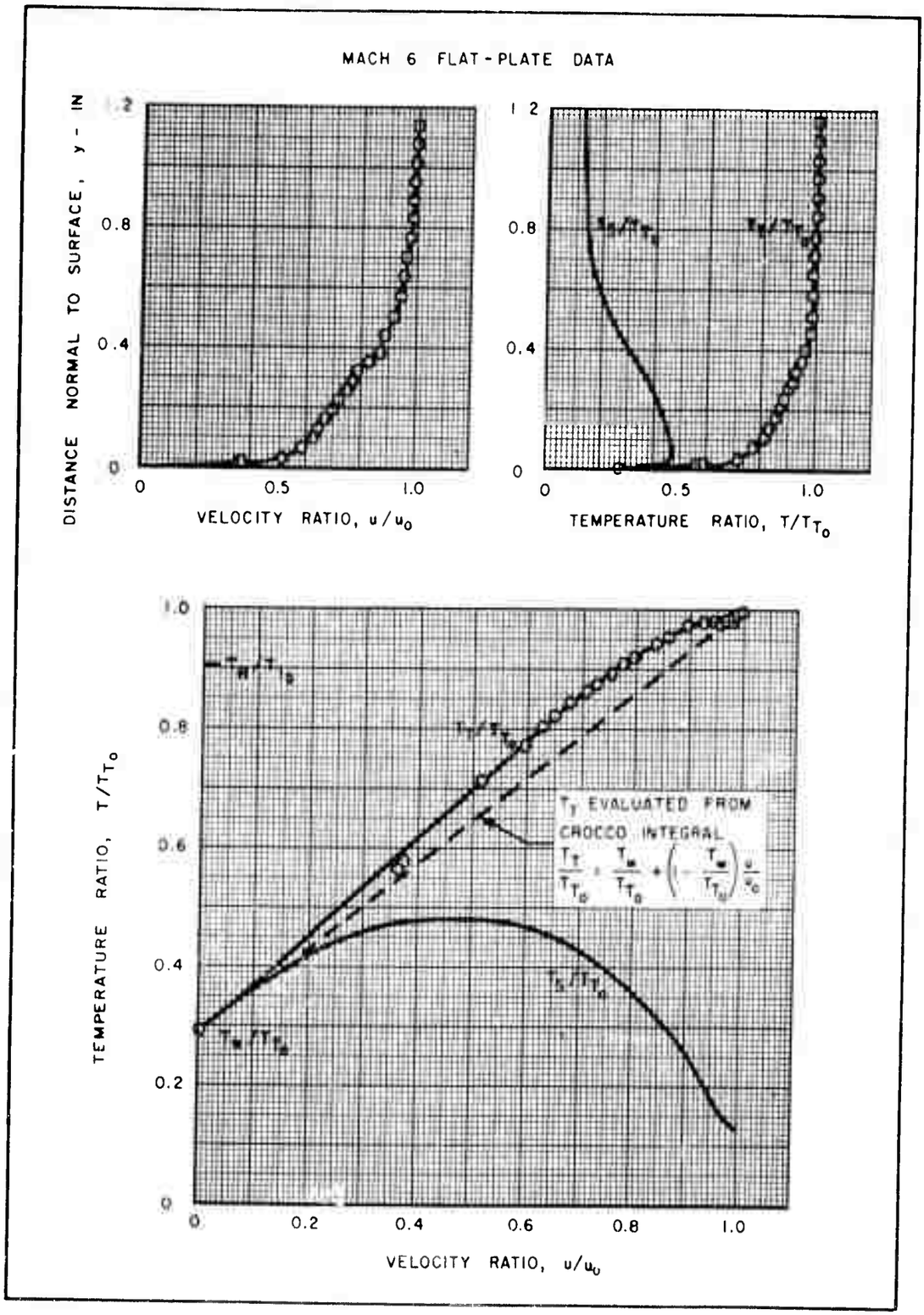

FIGURE 32: TYPICAL VARIATION OF TOTAL AND STATIC TEMPERATURES WITH VELOCITY FOR A COOLED BOUNDARY LAYER

$$\frac{St}{C_f} = \frac{\left.\dfrac{\partial (T_T/T_{T_0})}{\partial (u/u'_w)}\right|_w}{2\,Pr\,(T_R/T_{T_0} - T_w/T_{T_0})} = 0.950$$

$Pr = 0.70$

○ MACH 3 FLAT-PLATE DATA

□ MACH 6 FLAT-PLATE DATA

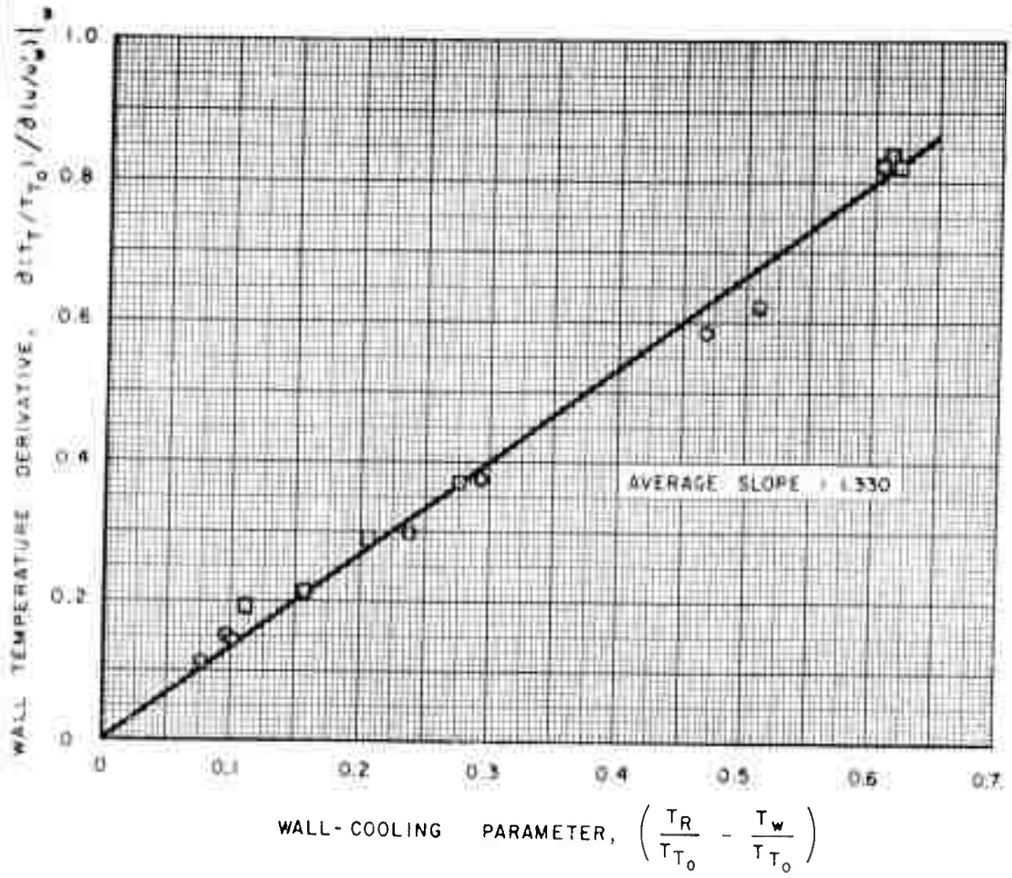

FIGURE 33: DERIVATIVE METHOD OF EVALUATING RATIO OF STANTON NUMBER TO SKIN-FRICTION COEFFICIENT FOR FLAT-PLATE DATA

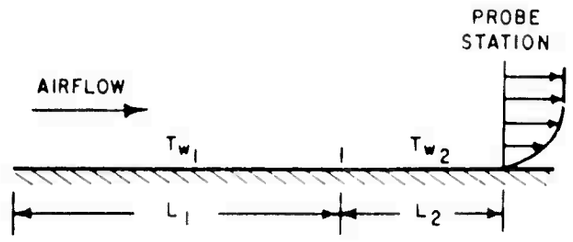

FOR FLAT PLATE HAVING STEPWISE TEMPERATURE DISTRIBUTION THE EFFECTIVE WALL TEMPERATURE, T_w', IS DEFINED BY THE FOLLOWING RELATION:

$$T_w' = \frac{T_{w_1} L_1 + T_{w_2} L_2}{L_1 + L_2}$$

$$\frac{St}{C_f} = \frac{\phi/\theta}{2(T_R/T_{T_0} - T_w'/T_{T_0})} = 0.805$$

○ MACH 3 FLAT-PLATE DATA
□ MACH 6 FLAT-PLATE DATA

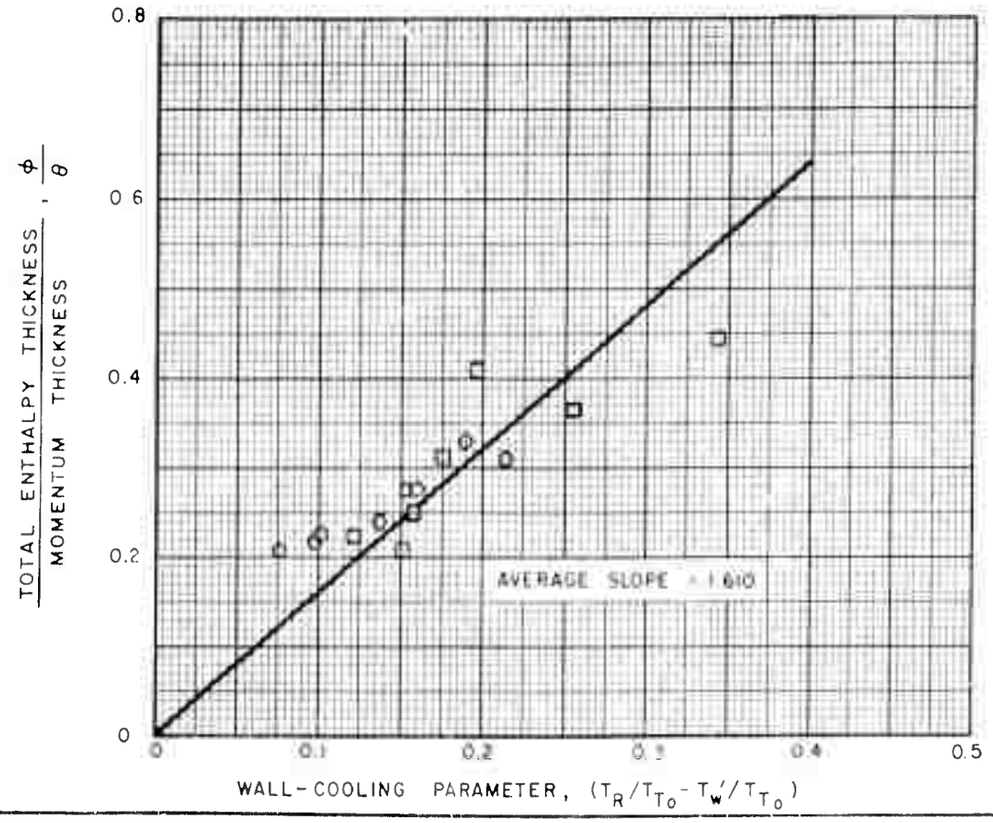

FIGURE 34: INTEGRAL METHOD OF EVALUATING RATIO OF STANTON NUMBER TO SKIN-FRICTION COEFFICIENT FOR FLAT-PLATE DATA

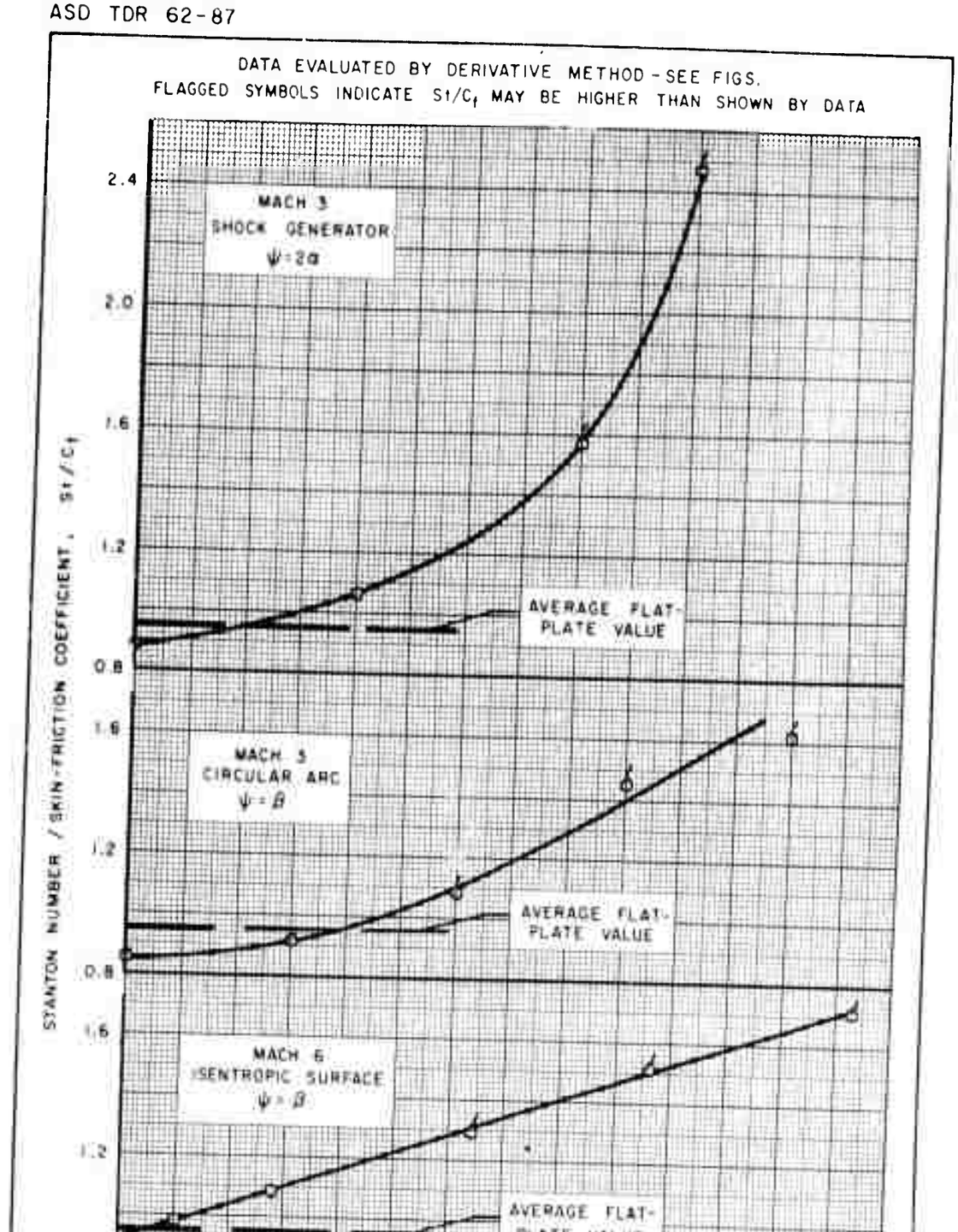

FIGURE 35: EFFECT OF ADVERSE PRESSURE GRADIENT ON RATIO OF STANTON NUMBER TO SKIN-FRICTION COEFFICIENT

ASSUMED RELATION FOR CORRECTING PROBE CONDUCTION ERROR:

$$P_P (T_T - T_M) = B(T_M - T_P)$$

WHERE:

B = CONSTANT DETERMINED FROM MEASURED TEMPERATURE WITH MAXIMUM FLOW THROUGH PROBE

T_P = TEMPERATURE OF PROBE WITH ZERO BLEED FLOW

$$T_T = T_{T_0} \approx 860 \text{ R}$$

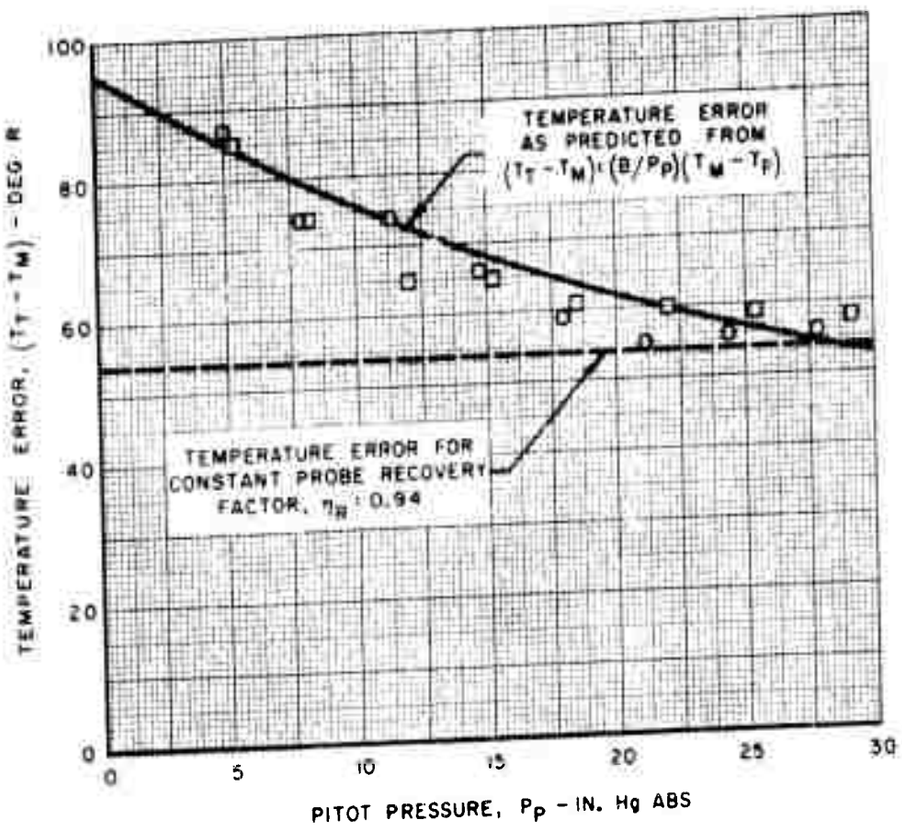

FIGURE 36: EFFECT OF PRESSURE LEVEL ON MEASURED PROBE TEMPERATURE AT MACH 6

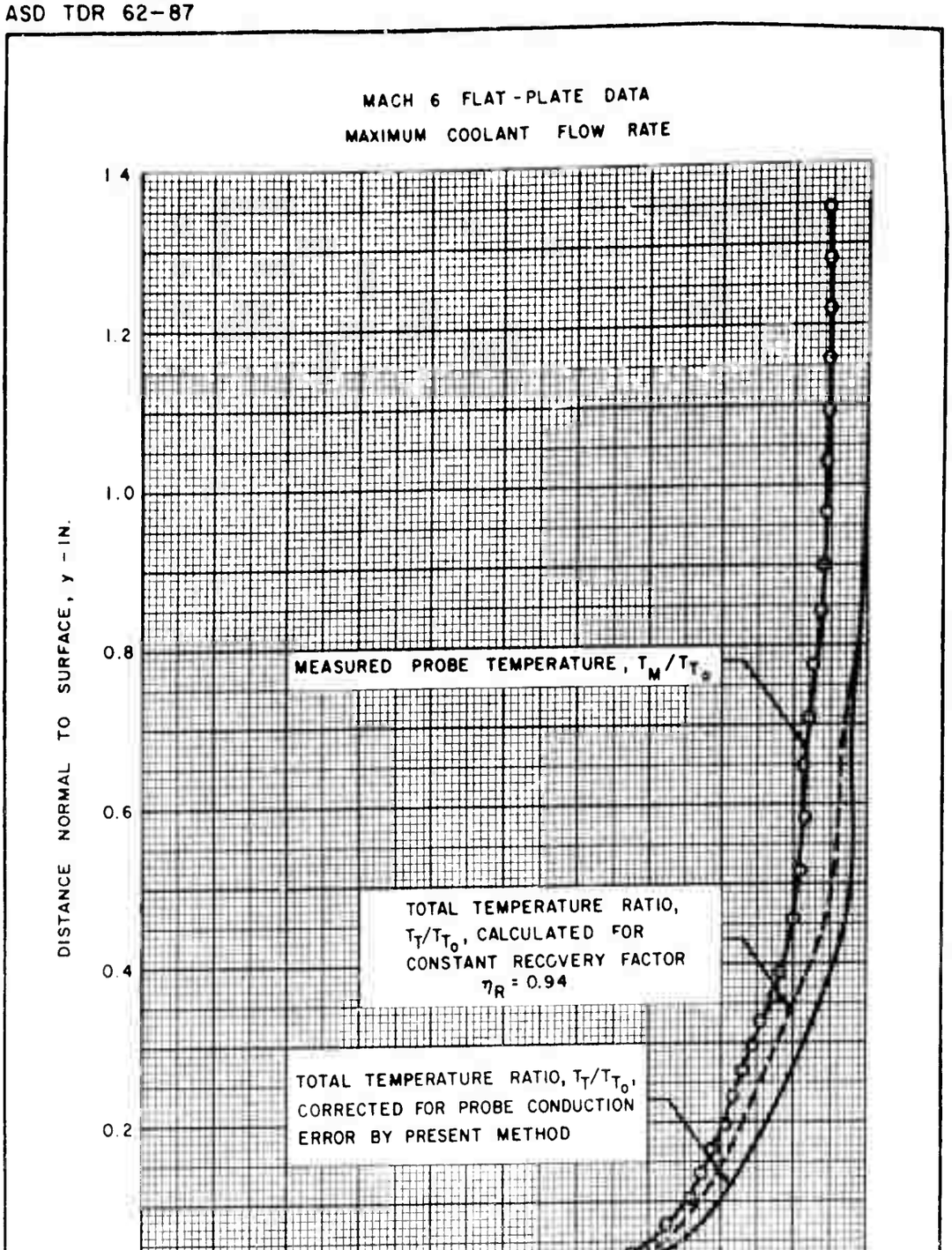

FIGURE 37: COMPARISON OF METHODS FOR EVALUATING TOTAL TEMPERATURES THROUGH A BOUNDARY LAYER

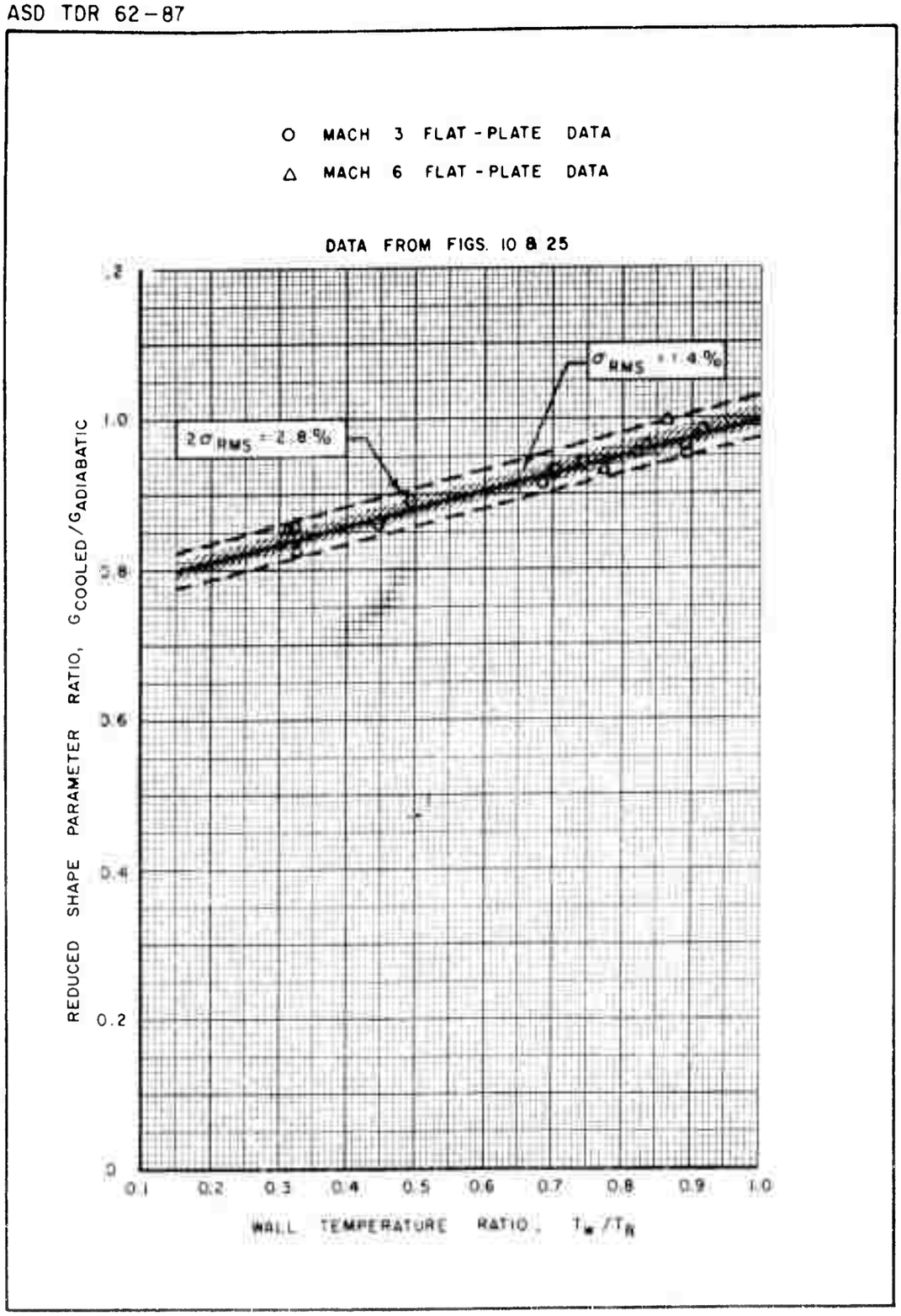

FIGURE 38: REDUCED SHAPE PARAMETERS ON FLAT PLATE AT FREE-STREAM MACH NUMBERS OF 3 AND 6

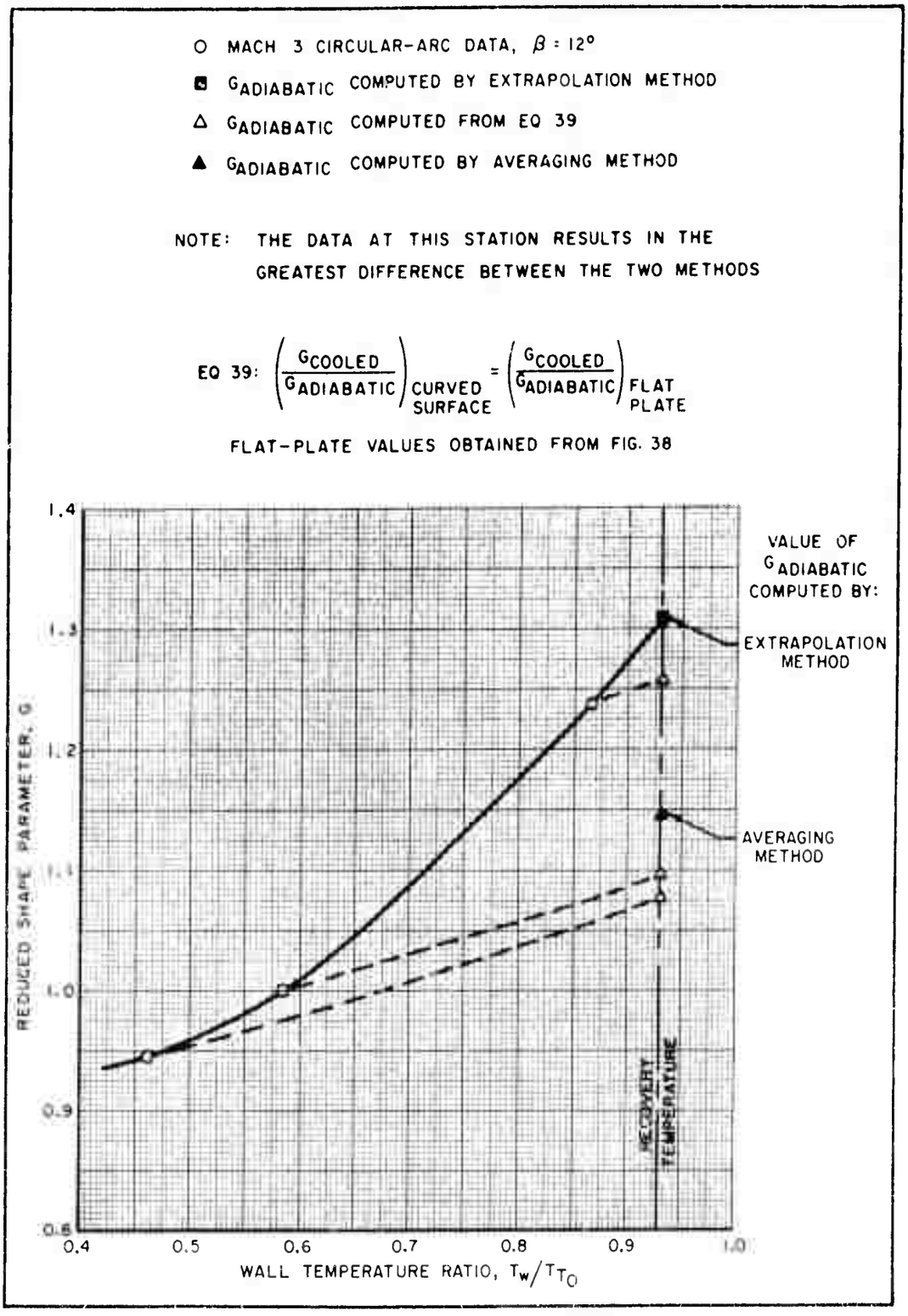

FIGURE 39: COMPARISON OF EXTRAPOLATION AND AVERAGING METHODS OF OBTAINING $G_{ADIABATIC}$

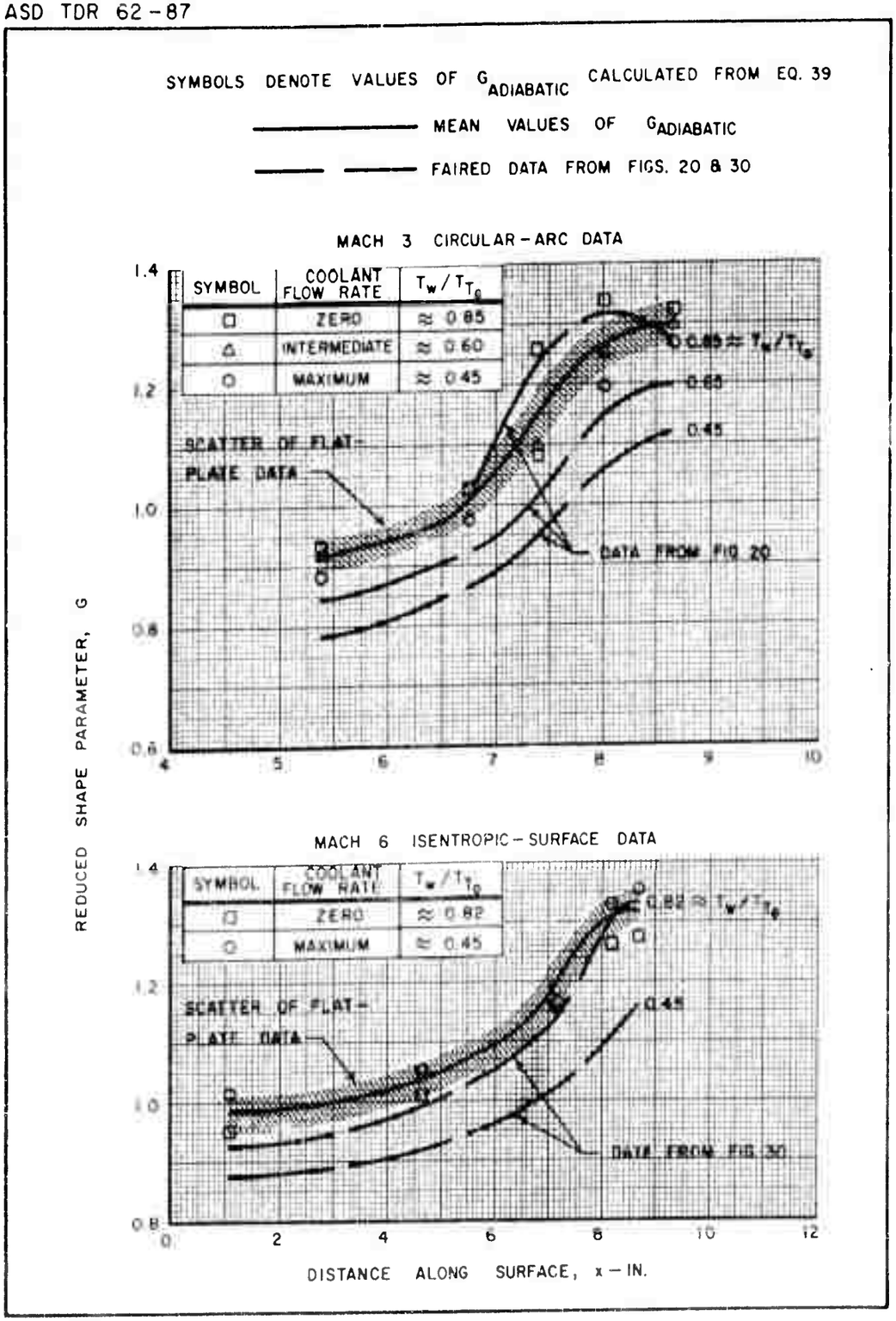

FIGURE 40 : ADIABATIC SHAPE PARAMETER EVALUATED BY AVERAGING METHOD

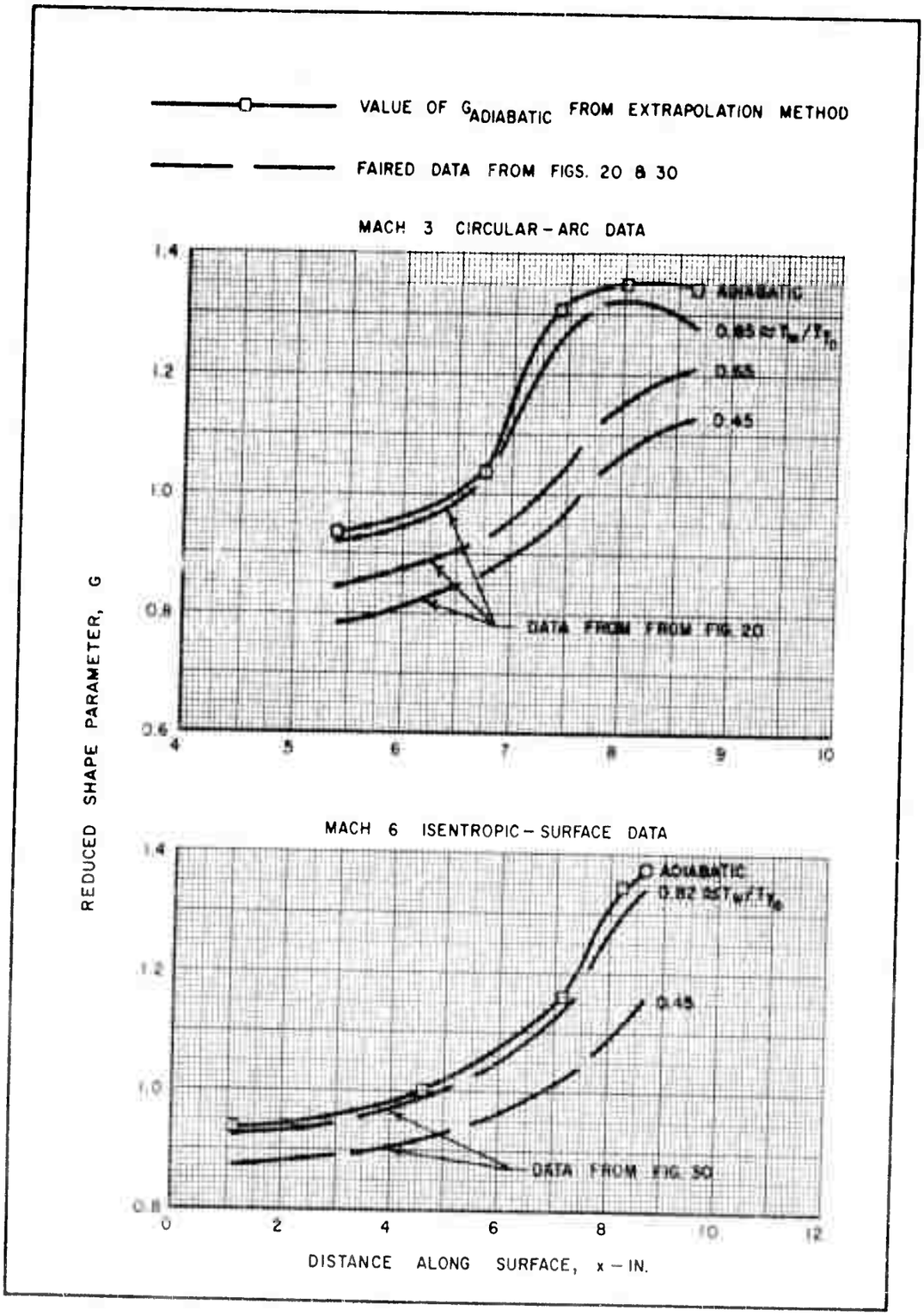

FIGURE 41: ADIABATIC SHAPE PARAMETER EVALUATED BY EXTRAPOLATION METHOD

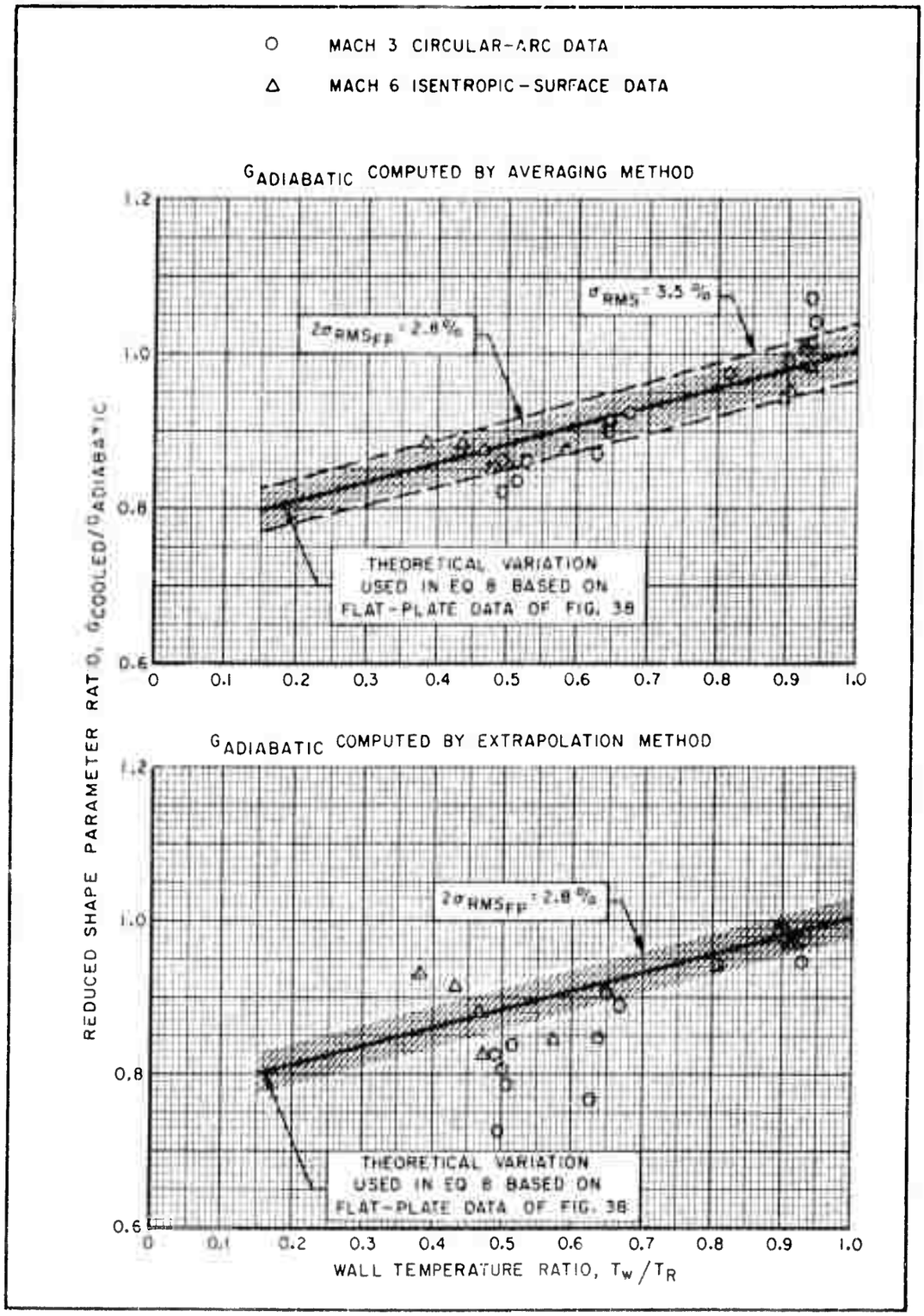

FIGURE 42: CORRELATION OF SHAPE PARAMETERS FOR CURVED SURFACE MODELS

Aeronautical Systems Division, Dir/Aeromechanics, Flight Dynamics Laboratory, Wright-Patterson Air Force Base, Ohio. Rpt No. ASD-TDR-62-87, SUPERSONIC TURBULENT BOUNDARY LAYER GROWTH OVER COOLED WALLS IN ADVERSE PRESSURE GRADIENTS. Final report, Oct 1962, 94p incl illus., 39 refs.

Unclassified Report

The characteristics of supersonic turbulent boundary layers on cooled surfaces having adverse pressure gradients were investigated to provide design information for hypersonic inlets. Tests were conducted at Mach numbers of 3 and 6 with values of wall temperature as low as 30% of the adiabatic recovery

(over)

temperature. Velocity and temperature profiles through the boundary layer were obtained and the integral boundary layer parameters were evaluated along the surface. An analytical investigation was also conducted to provide a basis for evaluating the experimental results.
It was found that cooled, turbulent boundary layers in adverse pressure gradients are thinner and less distorted than uncooled boundary layers, that the ratio of Stanton number to skin-friction coefficient is higher than the flat-plate value, and that the total amount of heat removed is greater than that predicted by integrating local heat transfer rates based on flat-plate conditions along the surface.

1. Turbulent boundary layer
2. Heat transfer
   I. AFSC Project 1366 Task 136605
   II. Contract AF33 (616)-6800
   III. United Aircraft Corp, Research Laboratories, East Hartford, Conn.
   IV. C. E. Kepler R. L. O'Brien
   V. Not aval fr OTS
   VI. In ASTIA collection

Aeronautical Systems Division, Dir/Aeromechanics, Flight Dynamics Laboratory, Wright-Patterson Air Force Base, Ohio. Rpt No. ASD-TDR-62-87, SUPERSONIC TURBULENT BOUNDARY LAYER GROWTH OVER COOLED WALLS IN ADVERSE PRESSURE GRADIENTS. Final report, Oct 1962, 94p incl illus., 39 refs.

Unclassified Report

The characteristics of supersonic turbulent boundary layers on cooled surfaces having adverse pressure gradients were investigated to provide design information for hypersonic inlets. Tests were conducted at Mach numbers of 3 and 6 with values of wall temperature as low as 30% of the adiabatic recovery

(over)

temperature. Velocity and temperature profiles through the boundary layer were obtained and the integral boundary layer parameters were evaluated along the surface. An analytical investigation was also conducted to provide a basis for evaluating the experimental results.
It was found that cooled, turbulent boundary layers in adverse pressure gradients are thinner and less distorted than uncooled boundary layers, that the ratio of Stanton number to skin-friction coefficient is higher than the flat-plate value, and that the total amount of heat removed is greater than that predicted by integrating local heat transfer rates based on flat-plate conditions along the surface.

1. Turbulent boundary layer
2. Heat transfer
   I. AFSC Project 1366 Task 136605
   II. Contract AF33 (616)-6800
   III. United Aircraft Corp, Research Laboratories, East Hartford, Conn.
   IV. C. E. Kepler R. L. O'Brien
   V. Not aval fr OTS
   VI. In ASTIA collection

Aeronautical Systems Division, Dir/Aeromechanics, Flight Dynamics Laboratory, Wright-Patterson Air Force Base, Ohio. Rpt No. ASD-TDR-62-87, SUPERSONIC TURBULENT BOUNDARY LAYER GROWTH OVER COOLED WALLS IN ADVERSE PRESSURE GRADIENTS. Final report, Oct 1962, 94p incl illus., 39 refs.

Unclassified Report

The characteristics of supersonic turbulent boundary layers on cooled surfaces having adverse pressure gradients were investigated to provide design information for hypersonic inlets. Tests were conducted at Mach numbers of 3 and 6 with values of wall temperature as low as 30% of the adiabatic recovery

1. Turbulent boundary layer
2. Heat transfer
   I. AFSC Project 1366 Task 136605
   II. Contract AF33 (616)-6800
   III. United Aircraft Corp, Research Laboratories, East Hartford, Conn.
   IV. C. E. Kepler R. L. O'Brien
   V. Not aval fr OTS
   VI. In ASTIA collection

Aeronautical Systems Division, Dir/Aeromechanics, Flight Dynamics Laboratory, Wright-Patterson Air Force Base, Ohio. Rpt No. ASD-TDR-62-87, SUPERSONIC TURBULENT BOUNDARY LAYER GROWTH OVER COOLED WALLS IN ADVERSE PRESSURE GRADIENTS. Final report, Oct 1962, 94p incl illus., 39 refs.

Unclassified Report

The characteristics of supersonic turbulent boundary layers on cooled surfaces having adverse pressure gradients were investigated to provide design information for hypersonic inlets. Tests were conducted at Mach numbers of 3 and 6 with values of wall temperature as low as 30% of the adiabatic recovery

1. Turbulent boundary layer
2. Heat transfer
   I. AFSC Project 1366 Task 136605
   II. Contract AF33 (616)-6800
   III. United Aircraft Corp, Research Laboratories, East Hartford, Conn.
   IV. C. E. Kepler R. L. O'Brien
   V. Not aval fr OTS
   VI. In ASTIA collection

UNCLASSIFIED